ELASTIC PROPERTY PREDICTION OF SHORT FIBER COMPOSITES USING A UNIFORM MESH FINITE ELEMENT METHOD

A Thesis
presented to
the Faculty of the Graduate School
University of Missouri - Columbia

In Partial Fulfillment
of the Requirements for the Degree

Master of Science

---

by
ELIJAH CASELMAN

Dr. Douglas E. Smith, Thesis Supervisor

DECEMBER 2007

The undersigned, appointed by the Dean of the Graduate School, have examined the thesis entitled

ELASTIC PROPERTY PREDICTION OF SHORT FIBER COMPOSITES USING A UNIFORM MESH FINITE ELEMENT METHOD

presented by Elijah Caselman

a candidate for the degree of Master of Science

and hereby certify that in their opinion it is worthy of acceptance.

Advisor: _____
Dr. Douglas E. Smith

Readers: _____
Dr. P. Frank Pai

_____
Dr. V.S. Gopalaratnam

_____
Dr. David A. Jack

ACKNOWLEDGEMENTS

I would like to thank my advisor Dr. Douglas E. Smith for his continuous guidance and encouragement throughout my graduate study. I would like to thank my thesis committee members Dr. P. Frank Pai, Dr. V.S. Gopalaratnam, and Dr. David A. Jack for their criticism and advice. I would also like to thank David for all of the help and enthusiasm he provided while at the University of Missouri. Finally, I would like to thank my family. They have always been a continuous source of love and support and without them none of this would have been possible.

ELASTIC PROPERTY PREDICTION OF SHORT FIBER COMPOSITES USING A UNIFORM MESH FINITE ELEMENT METHOD

Elijah Caselman

Dr. Douglas E. Smith, Thesis Supervisor

ABSTRACT

This thesis presents a uniform mesh finite element method to determine the elastic material non-isotropic properties of fiber reinforced composite materials. This method employs a uniform array of custom three dimensional displacement based elements that use an increased number of Gauss points in the elemental stiffness calculation in order to define the fiber boundaries. The material properties at each Gauss point are dependent upon whether the Gauss point lies within a fiber or matrix. A correction factor is developed to account for differences in strain in the fiber and matrix and thus provide increased accuracy for "hybrid" elements. This method allows for a significant reduction in the number of degrees of freedom in the model, resulting in dramatically reduced memory requirements and computational time. The use of a uniform mesh also greatly simplifies the meshing procedure and is ideal for implementing periodic boundary conditions.

The method is compared with continuous and a short single fiber finite element models found in literature. The method is also used to provide property predictions for a model consisting of 100 misaligned short fibers randomly placed using a Monte Carlo algorithm. The predictions are compared with a constant strain orientation averaging scheme using both the Halpin-Tsai and Tandon-Weng micromechanical models. The method is shown to be in good agreement with the results from literature.

TABLE OF CONTENTS

LIST OF TABLES

LIST OF FIGURES

CHAPTER 1

INTRODUCTION

Composite materials have become increasingly important in engineering due to their higher strength and stiffness to weight ratios when compared with traditional engineering materials. These enhanced properties are the result of combining two or more materials. A typical composite consists of a continuous phase known as the matrix and interdispersed inclusions known as fibers. The matrix binds the fibers together and provides durability for the overall composite while the fibers provide the stiffness and strength and carry the structural load.

Three different fiber geometries are often used: discontinuous fibers, continuous fibers, and woven fibers. Discontinuous fibers are charaterized by their aspect ratio, or ratio of length to diameter. Fibers with aspect ratios less than 100 are known as short fibers and fibers with aspect ratios greater than 100 are known as long fibers. Discontinuous fiber composites are widely used because they can be manufactured into very complex parts using injection molding, compression molding, and extrusion techniques [3]. Continuous fibers are gathered together into tapes or tows and aligned in one direction. This allows for greater fiber volume fractions to be achieved thus providing greater in-plane property enhancement over discontinuous fibers. The fiber tows can also be interlaced and interlocked in two- and three-dimensions to form woven composites. Woven composites offer enhanced in- and out-of-plane strength and stiffness [3]. However, these composites are more difficult and expensive to manufacture and can only be used for parts with low complexity.

The effective properties of fibrous composite materials are dependent upon several factors which include:

- The material properties of the fiber and matrix
- The ratio of the fiber length to fiber diameter, or aspect ratio
- The ratio of the fiber volume to the total volume of the composite, or volume fraction
- The spatial arrangement of the fibers
- The orientation of the fibers

Unfortunately, the various manufacturing processes inevitably result in composites with fibers of varying length, complex or random fiber arrangements, and varying fiber orientations. Therefore, reliable yet cost effective methods for determining the effective properties of composite materials are of utmost importance to the composite industry. Determining the effective properties of discontinuous fiber composites, more specifically short fiber composites, will be the focus of this research.

1.1 Organization of Thesis

Chapter One provides an introduction to composite materials and provides the research objective of this thesis. A review of the analytical and numerical methods currently used to predict elastic properties of short fiber composites is given in Chapter Two. The development and implementation of the uniform mesh finite element method is provided in Chapter Three. Chapter Four oulines the procedure for finding

the effective elastic properties from the finite element results and provides validation of the method with conventional finite elements. In Chapter Five, the method is compared with single fiber continuous and short fiber finite elements models found in literature. The method is then used to predict the elastic properties of a model consisting of 100 short fibers and compared with an orientation averaging scheme using both the Halpin-Tsai and Tandon-Weng micromechanical models in Chapter Six. Finally, Chapter Seven provides conclusions and recommendations for future work.

CHAPTER 2

LITERATURE REVIEW

Due to the variability in the effective properties of fibrous composites, property prediction methods have drawn considerable attention in literature over the past several decades. The methods can be divided into two main categories: analytical and numerical. The analytical methods are often employed due to their ease of use but these methods are limited in their application due to their underlying simplifying assumptions. Numerical methods have seen increasing use with the increase in computational power. These methods are much more flexible in their application, but require increased preparation and are limited by the amount of computer memory available. An overview of the strengths and weaknesses of these methods is given below.

2.1 Analytical Property Prediction

Numerous micromechanical models have been developed to predict the elastic properties of aligned short fiber composites [4]. All of the micromechanical models have the same basic assumptions [4]:

- The fibers and matrix are linear elastic, the matrix is isotropic and the fibers are either isotropic or transversely isotropic.
- The fibers are axisymmetric, identical in shape and size, and fully aligned.
- The fibers and matrix are well bonded at their interface.

Although these assumptions allow many of the micromechanical models to be expressed in very concise, easy to use formats, they are not consistent with "real" materials. It is impossible to obtain fully aligned samples and real composites always exhibit a degree of misalignment and variability in fiber aspect ratio. However, due to their popularity, several of the most common micromechanical models will be presented.

2.1.1 Halpin-Tsai Model

The Halpin-Tsai [5] model is one of the most widely used micromechanical models for the prediction of elastic properties in short fiber composites. This model (as shown in equations 4.30-4.33 and table 4.1) is based on the self-consistent approach of Hill [6] and the solutions of Hermans [7]. Halpin and Tsai [5] made a few additional assumptions to reduce Hermans solutions for the elastic constants which provides a simpler analytical form. The appeal of the Halpin-Tsai equations is that only one equation is needed to find all the composite moduli and the longitudinal Poisson's ratio is simply found from the rule of mixtures. The Halpin-Tsai equations are semi-empirical in that one of the parameters (ζ) was found by fitting the equations to numerical results. The Halpin-Tsai equations provide reasonable results for E_{11} and G_{12} at low volume fractions, but underpredicts these properties at higher volume fractions. Hewitt and Malherbe [8] suggested ζ should be a function of volume fraction in order to obtain better results for G_{12}. They proposed a new equation for ζ based on comparisons with two-dimensional finite element results for G_{12}. Lewis and Nielson [9] modified the Halpin-Tsai equations to achieve better results for the elastic moduli at

higher volume fractions by taking into account the maximum volume fraction. A new function was added so that the shear modulus prediction approaches infinity as the volume fraction approaches the maximum volume fraction. The Lewis-Nielson modification has been shown to provide better results for E_{11} at higher volume fractions for short fibers [10]. The Halpin-Tsai equations have been found to provide a very poor prediction for the transverse Poisson's ratio, sometimes giving predictions 2 to 3 times higher than numerical and experimental results [4, 11].

2.1.2 Mori-Tanka Model

The Mori-Tanaka model [12] is based on the work of Eshelby [13] who developed a solution for a single ellipsoidal inclusion in an infinite matrix. The Eshelby solution is therefore only accurate for very dilute volume fractions. Mori and Tanaka extended the ideas of Eshelby to include interactions between fibers, thus providing more accurate results at higher volume fractions. The Mori-Tanaka model assumes the fiber in a concentrated composite experiences the average strain of the matrix. Tandon and Weng [14]used the Mori-Tanaka approach to develop equations for a complete set of elastic constants (as shown in equations 4.35-4.53). Tandon and Weng's equations included a coupling between the bulk modulus K_{23} and longitudinal Poisson's ratio ν_{12} which must be solved iteratively. Tucker and Liang solved this problem by providing an alternative equation for ν_{12} to avoid the iteration process [4]. Several authors have found that the Tandon-Weng model provides the most accurate predictions for short fiber composites [4,11,15]. In particular, the Tandon-Weng model provides a considerably more accurate prediction for the transverse Poisson's ratio than the Halpin-Tsai

model. The model has been found to be very accurate for low volume fractions and high aspect ratios, but the accuracy decreases as the volume fraction and ratio of the fiber Young's modulus to the matrix Young's modulus (E_f/E_m) increases [16]

2.1.3 Bounding Models

The bounding models make assumptions on either the stress or strain field and the unknown field is found through variational principles. As the name suggests, the bounding models only provide upper and lower bounds for the stiffness of the composite. Two of the earliest bounding models are the Voigt and Reuss bounds [4]. The Voigt model assumes the fiber and matrix both experience the same uniform strain. The calculated stiffness with this assumption represents an upper bound and the actual stiffness must be less than or equal to the Voigt result. The Reuss model assumes the fiber and matrix both experience the same uniform stress. The results of this model represent a lower bound and the actual stiffness with be greater than or equal to the Reuss result. The Voigt and Reuss models are known to only provide isotropic results which is not representative of continuous or short fiber composites. Also, if the matrix and fiber have very different stiffnesses, the Voigt and Reuss results will be far apart and give little information about the stiffness of the composite.

Hashin and Shtrikman [17] developed bounding model for heterogeneous materials using a different variational principle. Their results provide both a lower and upper bound on the composite stiffness. They introduced the idea of a reference material, and by choosing either the matrix or the fiber as the reference material, both bounds can be found. The Hashin-Shtrickman model provides tighter bounds than the Voigt

and Reuss models. There method was extended by Walpole to include anistropic materials and Willis [18] extended the results of Walpole to short fiber composites. The Mori-Tanaka result is equivalent to the Hashin-Shtrickman-Willis lower bound and can also be used to obtain the Hashin-Shtrickman-Willis upper bound by assuming the fiber is the continuous phase and the matrix is the dispersed phase. Lielens et al. [19] noted that the results should be equivalent to the Hashin-Shtrickman-Willis lower bound, or Mori-Tanaka approach, at low volume fractions and approach the upper bound at high volume fractions. Lielens et al. developed a new model to interpolate between the Hashin-Shtrickman-Willis bounds thus providing better results over the entire range of volume fractions.

2.1.4 Orientation Averaging

When a misaligned long fiber introduces anisotropy, the orientation of the fiber must be accounted for in the averaging process [20]. Two step fiber orientation averaging schemes for calculating the properties of short fiber composites have been proposed by Ward [21], Advani and Tucker [20] and Camacho et al. [22]. The first step in the orientation averaging procedure is to reduce the composite into a set of units, or aggregates, with aligned fibers and having the same volume fraction as the composite. Each aggregate is then homogenized using one of the micromechanical models described above, and the average properties of the aggregate are found. In the second step, the individual aggregates are homogenized by applying an orientation average to account for the spatial orientation of each aggregate, to obtain a single anisotropic material. The orientation averaging only takes into account the orientation of the

fibers but neglects the spatial separation between the fibers. The orientation average is applied assuming a distribution for the stress and strain between the aggregates. If the Voigt assumption of constant strain is assumed, then a summation of the stiffness constants is performed. The Voigt assumption is used in the procedures of Advani and Tucker [20] and Camacho et al. [22]. A Reuss assumption of constant stress between the aggregates can also be used and a summation of the compliance constants is performed. Ward [21] provides results using both assumptions. A Mori-Tanaka assumption of mean strain over the aggregate has also been used by Lielens et. al. [19]. However, Lielens et. al. [19] found that using the Mori-Tanaka assumption can result in stiffnesses above the Voigt upper bound when the fibers are stiffer than the matrix and result in stiffnesses below the Reuss lower bound when the matrix is stiffer. As a result, Lielens et. al. also suggested using the Voigt assumption. The use of the Voigt assumption has been validated by Lusti et. al. [15] and Hine et. al. [23] in that they found the Voigt assumption provides much better results than the Reuss assumption when comparting orientation averaging results with misaligned finite element models.

The orientation averaging procedure has also been extended to textile composites. In the fabric geometry model (FGM) by dividing the composite into layers. Each layer is modeled as a unidirectional lamina and the layer is homogenized using a continuous fiber micromechanical model. Therefore, the fabric is broken up into layers of varying orientation. By assuming constant strain between the layers, an orientation average is performed and the effective stiffness is found as the weighted sum of the layers [24,25]. The FGM has been shown to give reasonable results for the in-plane elastic constants for woven and braided composites but greatly overpredicts

the moduli for knitted fiber composites [26, 27]. The main difference between woven and knitted composites is knitted fiber composites contain curled fiber yarns which reduce the property enhancements of the fibers. Gommers et al. [26] and Huysmans et al. [28] have accounted for the fiber curvature by dividing the fibers tows into segments and each segment is treated as an inclusion. An equivalent aspect ratio is found from the curvature of the fiber tow and used for all the inclusions. The segments are then homogenized using a Mori-Tanaka micromechanical model. Gommers et al. [26] successfully used a modified Mori-Tanaka assumption for the orientation averaging procedure to ensure the effective stiffnesses remain within the Voigt and Reuss bounds.

2.2 Numerical Property Prediction

Numerical methods, such as the finite element and boundary element methods, have also been extensively used in literature to predict the elastic properties of short fiber composites. Numerical models provide a way to accurately predict the properties of short fiber composites with complicated geometries and avoid the limiting assumptions of the micromechanical models. However, modeling a composite with many short fibers using numerical methods presents several problems. The numerical methods require the discretization of the fibers and matrix through a meshing process. However, due to the complexity of the model, it is very difficult to obtain a reliable mesh. The meshing process can often result in a poor quality mesh in which the aspect ratio of the elements is much greater than one. This can lead to convergence issues during the solution process. Also, tetrahedral elements must be used due to their flexible geometry. However, tetrahedral elements are a constant strain element and

in order to obtain a physically accurate solution, a very fine mesh must be used. This presents a second problem with numerical models, that of computational power. As the number of elements increases, so does the number of degrees of freedom of the system thus requiring more computer memory to solve the finite element or boundary element equations. These two methods have seen extensive use in literature and are reviewed below.

2.2.1 Finite Element Method

The finite element is particularly susceptible to computer memory limitations because this method requires the entire volume of the constituents to be discretized. Therefore, many techniques have been developed in order to reduce the size of the numerical model. One such technique is the use of a unit cell or representative volume element (RVE). This technique views the overall composite as a periodic array of RVE's and each RVE is chosen such that it has the same fiber volume fraction as the composite. Finite elements are then used to find the elastic properties of the RVE and these are assumed to be equivalent to the effective properties of the composite. For simplicity, single fiber RVE's have been used in the past [1, 4, 29, 30] but these models inherently make the same assumptions as the micromechanical models: uniform fiber geometry and aspect ratio; fully aligned fibers of uniform spatial separation. Therefore, these models cannot accurately predict the elastic properties of real materials.

The minimum number of inclusions needed in an RVE to accurately model a real composite has been investigated by numerous authors [31–36]. They have found that by averaging the results for a number of random spatial fiber arrangements, a

surprisingly small RVE can accurately predict the effective properties of discontinuous composite. RVE's with approximately 30 fibers produced mean values within a couple of percent of the true value. However, the standard deviation using 30 fibers is relatively large and by increasing the number of fibers even further, more accurate means with lower standard deviations were obtained. Hine et. al. [34] concluded that RVE's with approximately 100 fibers produced very accurate mean values with very little standard deviation.

Advances in computational power have led to increased use of multiple inclusion RVE's. The multiple inclusion finite element procedure of Gusev [32,33] has been used extensively in recent literature [11,15,16,23,34,37,38]. The approach of Gusev begins by placing the desired number of inclusions in the periodic unit cell. The coordinates of the centroid are then randomly translated using a Monte Carlo algorithm. The Monte Carlo procedure continues until no overlap occurs between the inclusions. This procedure has been used successfully for spherical inclusions and aligned short fibers. However, for misaligned fibers it becomes nearly impossible to randomly place them in a periodic unit cell, even at low volume fractions. Lusti et.al. [15] modified the packing procedure for misaligned fibers by increasing the size of the unit cell until the volume fraction was around 0.1%. The unit cell was then step-wise compressed during the Monte Carlo procedure until the desired volume fraction was achieved while keeping the fiber orientations constant. Once the inclusions have been placed, a custom periodic morphology adaptive quality mesh generator is used to mesh the geometry with constant strain tetrahedral elements.

The effect of the fiber length distribution (FLD) on the effective elastic properties

of aligned short fiber composites has been investigated by Hine et al. [34]. The fiber lengths of 27,500 fibers of an injection moulded composite were measured. A model consisting of 100 fibers was assigned fiber length values by seeding a Monte Carlo procedure with the measured FLD data. The results of this model were then compared with models consisting of constant fiber lengths equal to the weight and number average of the real FLD, the rms average, and the skewed number average. Hine et al. [34] concluded that the number average length provides accurate results over a range of aspect ratios and could be used in place of the FLD.

A similar approach was used by Gusev et al. [11] to determine the effects of the fiber diameter distribution (FDD) and spatial orientation on the elastic properties of a unidirectional short fiber composite. The experimental elastic constants of the unidirectional composite were found using an ultrasonic velocity method. Image analysis was used to find the fiber diameters from a transverse cross-section of the composite. The data was then used to seed a Monte Carlo algorithm for assigning the fiber diameters to the model. They also used three different packing arrangements: randomly packed, hexagonal array, and a square array. They concluded that the fiber diameter distribution had little effect on the elastic properties but the spatial arrangement of the fibers did effect the transverse Young's modulus, Poisson's ratio, and shear modulus (E_{22},G_{23},ν_{23}). The randomly packed models resulted in the most accurate predictions, thus validating the randomness of actual composites. The results were also compared with micromechanical models and it was determined that the micromechanical models do not provide reliable predictions for the transverse properties due to their inability to account for the spatial distribution of the fibers.

Textile composites also possess a very complex microstructure consisting of multiple structural and scale levels: fibers ($10^{-5}m$), tows/yarns ($10^{-3}m$), fabrics ($10^{-1}m$), composites ($10^{0}m$) [39]. These multiple levels complicate the modeling procedure of textile composites because information from smaller scales must be incorporated into larger scale models. The mesostructure, or fabric, can often be very complex and difficult to define let alone model. Textile composites are further complicated by contact between the fiber tows and the nonlinear behavior of the constituents. The meshing and computational issues of short fiber composites are also major factors in modeling textile composites.

Several methods have been developed to simplify the meshing procedure and reduce the number of elements in the finite element model. Whitcomb and coworkers [40, 41] have used a local/global method in which separate meshes are used for local and global analyses. For the global analysis a very coarse mesh is used along with homogenized properties to obtain global displacement and forces. A local analysis is then performed in a region of interest and a fine mesh is used to model a unit cell containing the woven microstructure. The displacements and forces computed from the global model are applied to the mesh of the local model as boundary conditions. However, the two meshes do not contain the same number of nodes, therefore it is difficult to properly apply the globally obtained displacements and forces to the local model.

Cox et al. [42] developed a binary model which used one-dimensional line elements to represent the tow properties. The one-dimensional elements were fixed

within three-dimensional elements, known as "effective medium" elements, that represented the matrix-dominated properties. The line elements were used to obtain an approximation of the curved tow paths and the effects of tow waviness on the elastic properties were investigated.

Zeng et al. [43] simplified the meshing process by dividing the RVE into a regular array of subcells. Gauss quadrature was used to solve the elemental stiffness matrix and the fiber geometry was defined by varying the material properties at each Gauss point. If the Gauss point was in the fiber volume, then the fiber material property matrix was used, otherwise the matrix material property matrix was used. Effective property results were compared with available literature with limited success, in that the out of plane modulus was found to be stiffer than that from literature. A similar method will be used and expanded upon in this research for the analysis of short fibers.

In order to deal with the multiple length scales, a homogenization method is often employed [44, 45]. The microstructure, or fiber tows, consist of thousands of continuous fibers bound together with a polymer matrix. This homogenization method first homogenizes the microstructure by obtaining the effective properties of a continuous fiber unit cell through the finite element method. The homogenized properties of the microstructure are then used in the analysis of the mesostructure. A finite element model of an RVE containing the fabric architecture is then used to homogenize the mesostructure. Peng and Cao [45] used this technique to obtain the nonlinear elastic moduli of a plain weave composite as a function of elemental strains.

2.2.2 Boundary Element Method

The boundary element method has been extensively used because it only requires the boundaries or surfaces of the constituents to be discretized. This greatly simplifies the meshing process as well as reduces the number of elements and corresponding degrees of freedom [46]. By decreasing the degrees of freedom, larger models can be solved before memory limitations are reached. Over a decade ago, Papathanasiou and Ingber [10, 46, 47] successfully modeled short fiber composites with up to 200 fibers using the boundary element method and parallel supercomputer. They were able to analyze the effects of fiber orientation and spatial arrangement on the elastic properties of short fiber composites which could not be analyzed by micromechanical models and single fiber finite element models. They concluded that single fiber models and micromechancial models provide good approximations at low volume fractions, but become increasingly less accurate at higher volume fractions [10, 47] due to increased fiber interaction. They also were able to show that aligned fibers provide a significant increase in the longitudinal modulus over randomly aligned fibers [46]. Unfortunately, Papathanasiou and Ingber did not use the periodic RVE approach when generating random fibers, and as a result, interactions with the edge of the container often occured resulting in artificial fiber alignment. They were also limited to composites with an incompressible matrix and rigid fibers in order to simplify the boundary integral calculations of the BEM.

A new method for solving the boundary integral equations, known as the fast multipole method or FMM (see, e.g. Nashimura [48]), has been developed that greatly

accelerates the solution time and efficiency of the BEM method. As a result the solution time for a BEM problem has been reduced from $O(N^2)$, for conventional BEM, to $O(N)$ using the fast multipole solution method, where N is the number of equations [49]. The computer memory requirements have also been greatly reduced using the fast multiple method through the use of iterative solvers that do not require the storing of the entire matrix. Lui. et. al [49] used RVEs with up to 5832 fibers and over ten million degrees of freedom to find the elastic moduli of short and long fiber composites with aligned and random orientations. The method of Lui et. al [49] allows for an elastic matrix, but is still limited by the assumption of rigid fibers. Advanced boundary element methods have been recently developed to solve the more complicated problem of nonrigid fibers [50]. Chen and Liu [50] developed a BEM code using quadratic elements to model short fiber composites with an elastic matrix and fiber, thus removing the limitations of earlier boundary element methods. The method was used to find the effective modulus of composites with short fibers and spherical inclusions. However, Chen and Liu [50] were limited to models with only a few thousand elements or several tens of fibers due to the use of a conventional BEM solution approach.

CHAPTER 3

FINITE ELEMENT MODEL

A uniform mesh finite element method will be developed and used for elastic property prediction of continuous and short fiber composites. This method uses a regular array of parallelepiped elements for the finite element calculations, thus eliminating the problems associated with geometry and mesh creation. The model differs from others used in literature, in that an increased number of Guass points are used when calculating the stiffness matrix in order to provide the spatial refinement needed for representing the fiber/matrix microstructure. The Guass points are then assigned the material properties of the matrix if the Gauss point lies within the matrix or the material properties of the fiber if the Guass point lies within a fiber. The solution is refined by increasing the number of Gauss points instead of the number of elements. Therefore, the number of degrees of freedom are greatly reduced and very complex models can be run on a desktop computer with minimal memory requirements. This chapter presents the derivation and implementation of the custom element.

3.1 Finite Element Derivation

The finite element equations can be derived using Hamilton's principle, which states [51]

$$\int_{t_1}^{t_2} \delta L dt = 0 \tag{3.1}$$

where δ is the variational operator. The Lagrangian, L, is the given by [51]

$$L = T - \Pi_p \tag{3.2}$$

where T is the kinetic energy and Π_p is the potential energy of a system. For a static elastic body the kinetic energy is equal to zero and the potential energy is equal to [51]

$$\Pi_p = \Pi - W_p \tag{3.3}$$

where Π is the strain energy and W_p is the work done by external forces. The strain energy and work done by external forces can be expressed respectively as [51]

$$\Pi = \frac{1}{2}\int_V \boldsymbol{\varepsilon}^T \boldsymbol{\sigma} dV \tag{3.4}$$

and

$$W_p = \int_V \mathbf{b}^{\mathbf{T}}\mathbf{U} dV + \int_S \mathbf{t}^{\mathbf{T}}\mathbf{U} dS \tag{3.5}$$

where $\boldsymbol{\varepsilon}$ is the strain vector, $\boldsymbol{\sigma}$ is the stress vector, $\mathbf{b}$ is the body force vector, $\mathbf{U}$ is the displacement vector, $\mathbf{t}$ is a vector of surface tractions, V is the volume of the body, and S is the surface of the body. Hooke's law provides a relationship between stress and strain through the following

$$\boldsymbol{\sigma} = [C]\boldsymbol{\varepsilon} \tag{3.6}$$

If the individual constituents of the composite are assumed to be isotropic, then the material stiffness tensor $[C]$ is given by [52]

$$[C] = \frac{1}{E}\begin{bmatrix} 1 & -\nu & -\nu & 0 & 0 & 0 \\ -\nu & 1 & -\nu & 0 & 0 & 0 \\ -\nu & -\nu & 1 & 0 & 0 & 0 \\ 0 & 0 & 0 & 2(1+\nu) & 0 & 0 \\ 0 & 0 & 0 & 0 & 2(1+\nu) & 0 \\ 0 & 0 & 0 & 0 & 0 & 2(1+\nu) \end{bmatrix}^{-1} \tag{3.7}$$

where E is the Young's Modulus and ν is the Poisson's ratio of the material. Combining equations 3.4 and 3.6 and applying the variational operator yields

$$\begin{aligned} \delta\Pi &= \int_V \frac{1}{2}\delta\boldsymbol{\varepsilon}^T[C]\boldsymbol{\varepsilon} + \frac{1}{2}\boldsymbol{\varepsilon}^T[C]\delta\boldsymbol{\varepsilon}dV \\ &= \int_V \frac{1}{2}\delta\boldsymbol{\varepsilon}^T[C]\boldsymbol{\varepsilon} + \frac{1}{2}\delta\boldsymbol{\varepsilon}^T[C]^T\boldsymbol{\varepsilon}dV \\ &= \int_V \delta\boldsymbol{\varepsilon}^T[C]\boldsymbol{\varepsilon}dV \end{aligned} \tag{3.8}$$

Applying the variational operator to W_p yields

$$\delta W_p = \int_V \mathbf{b}^\mathbf{T}\delta\mathbf{U}dV + \int_S \mathbf{t}^\mathbf{T}\delta\mathbf{U}dS \tag{3.9}$$

Combining equations 3.1,3.2,3.3,3.8,3.9 results in the following expression

$$\int_{t_1}^{t_2}\int_V -\delta\boldsymbol{\varepsilon}^T[\mathbf{C}]\boldsymbol{\varepsilon} + \mathbf{b}^\mathbf{T}\delta\mathbf{U}dV + \int_S \mathbf{t}^\mathbf{T}\delta\mathbf{U}dSdt = 0 \tag{3.10}$$

Next, the domain V is divided into N_e finite elements. The displacement vector $\mathbf{U}$ over the element domain V_e becomes

$$\mathbf{U} = \begin{bmatrix} N_1 & 0 & 0 & N_2 & \dots & 0 \\ 0 & N_1 & 0 & N_2 & \dots & 0 \\ 0 & 0 & N_1 & N_2 & \dots & N_8 \end{bmatrix} \begin{bmatrix} u_1 \\ v_1 \\ w_1 \\ u_2 \\ \vdots \\ w_8 \end{bmatrix} = [N]\mathbf{d}^{(\mathbf{e})} \tag{3.11}$$

where $\mathbf{d}^{(e)}$ is the elemental displacement vector and $[N]$ is the shape function matrix.

The components of $[N]$ for the 8-noded solid element in figure 3.1 are given by [52]

$$\begin{aligned}
N_1 &= \tfrac{1}{8}(1-\xi)(1-\eta)(1-\zeta) \\
N_2 &= \tfrac{1}{8}(1+\xi)(1-\eta)(1-\zeta) \\
N_3 &= \tfrac{1}{8}(1+\xi)(1+\eta)(1-\zeta) \\
N_4 &= \tfrac{1}{8}(1-\xi)(1+\eta)(1-\zeta) \\
N_5 &= \tfrac{1}{8}(1-\xi)(1-\eta)(1+\zeta) \\
N_6 &= \tfrac{1}{8}(1+\xi)(1-\eta)(1+\zeta) \\
N_7 &= \tfrac{1}{8}(1+\xi)(1+\eta)(1+\zeta) \\
N_8 &= \tfrac{1}{8}(1-\xi)(1+\eta)(1+\zeta)
\end{aligned} \tag{3.12}$$

where ξ,ν and ζ are natural coordinates and $-1 \leq \xi, \eta, \zeta \leq 1$.

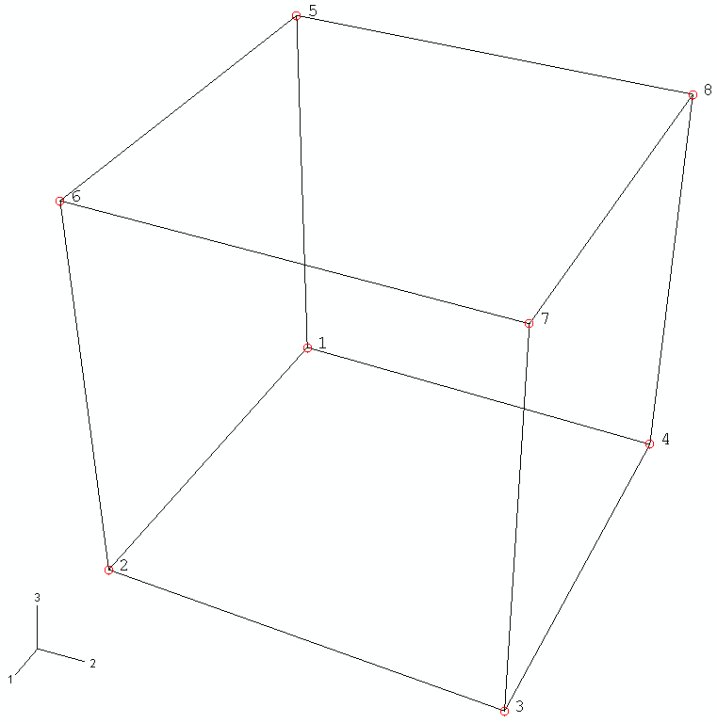

Figure 3.1: 8-noded solid element

For a uniform array of rectangular elements, the physical coordinates are related

to the natural coordinates through the following:

$$\begin{aligned} x &= \bar{x} + \xi \frac{l_x}{2} \\ y &= \bar{x} + \eta \frac{l_y}{2} \\ z &= \bar{x} + \zeta \frac{l_z}{2} \end{aligned} \tag{3.13}$$

where $\bar{x}, \bar{y}$ and $\bar{z}$ are the coordinates of the centroid of the element and l_x,l_y and l_z are the lengths of the x,y and z edges of the rectangular elements. The infinitesimal physical coordinates dx,dy,and dz are then related to the infinitesimal natural coordinates $d\xi$,$d\eta$, and $d\zeta$ through the following [52]

$$\begin{aligned} dx &= \frac{\partial x}{\partial \xi} d\xi = \frac{l_x}{2} d\xi \\ dy &= \frac{\partial y}{\partial \eta} d\xi = \frac{l_y}{2} d\eta \\ dz &= \frac{\partial z}{\partial \zeta} d\xi = \frac{l_z}{2} d\zeta \end{aligned} \tag{3.14}$$

The infinitesimal elemental volume, $dV^{(e)}$ then becomes

$$dV^{(e)} = dxdydz = \frac{l_x}{2}\frac{l_y}{2}\frac{l_z}{2} d\xi d\eta d\zeta \tag{3.15}$$

The strain vector $\boldsymbol{\varepsilon}$ can then be written as [52]

$$\boldsymbol{\varepsilon} = \begin{Bmatrix} \varepsilon_{xx} \\ \varepsilon_{yy} \\ \varepsilon_{zz} \\ \gamma_{xy} \\ \gamma_{yz} \\ \gamma_{xz} \end{Bmatrix} = \begin{bmatrix} \frac{\partial u}{\partial x} \\ \frac{\partial v}{\partial y} \\ \frac{\partial w}{\partial z} \\ \frac{\partial u}{\partial y} + \frac{\partial v}{\partial x} \\ \frac{\partial v}{\partial z} + \frac{\partial w}{\partial y} \\ \frac{\partial w}{\partial x} + \frac{\partial u}{\partial z} \end{bmatrix} = \begin{bmatrix} \frac{\partial}{\partial x} & 0 & 0 \\ 0 & \frac{\partial}{\partial y} & 0 \\ 0 & 0 & \frac{\partial}{\partial z} \\ \frac{\partial}{\partial y} & \frac{\partial}{\partial x} & 0 \\ 0 & \frac{\partial}{\partial z} & \frac{\partial}{\partial y} \\ \frac{\partial}{\partial z} & \frac{\partial}{\partial x} & 0 \end{bmatrix} \begin{Bmatrix} u \\ v \\ w \end{Bmatrix} = [B]\mathbf{d^{(e)}} \tag{3.16}$$

where the $[B]$ matrix in the element domain is given by [52]

$$[B] \;=\; [[B_1][B_2]\ldots[B_8]] \tag{3.17}$$

where

$$[B_i] = \begin{bmatrix} \frac{2}{l_x}\frac{\partial N_i}{\partial \xi} & 0 & 0 \\ 0 & \frac{2}{l_y}\frac{\partial N_i}{\partial \eta} & 0 \\ 0 & 0 & \frac{2}{l_z}\frac{\partial N_i}{\partial \zeta} \\ \frac{2}{l_y}\frac{\partial N_i}{\partial \eta} & \frac{2}{l_z}\frac{\partial N_i}{\partial \xi} & 0 \\ 0 & \frac{2}{l_z}\frac{\partial N_i}{\partial \zeta} & \frac{2}{l_y}\frac{\partial N_i}{\partial \eta} \\ \frac{2}{l_z}\frac{\partial N_i}{\partial \zeta} & 0 & \frac{2}{l_x}\frac{\partial N_i}{\partial \xi} \end{bmatrix}, i = 1, 8 \tag{3.18}$$

Combining equations 3.10,3.11,3.16 and summing over all the elements we obtain

$$\sum_{e=1}^{N_e} \int_{t_1}^{t_2} \int_V \delta \mathbf{d}^{(e)^T} [B][C][B]\mathbf{d}^{(e)} - \delta \mathbf{d}^{(e)^T} \mathbf{b}^T [N] dV^{(e)} \tag{3.19}$$

$$- \int_S^{(e)} \delta \mathbf{d}^{(e)^T} \mathbf{t}^T [N] dS^{(e)} dt = 0 \tag{3.20}$$

Next, we define the elemental stiffness matrix, $[K^{(e)}]$, and force vector, $\mathbf{P}^{(e)}$ as

$$[K^{(e)}] = \int_{V^{(e)}} [B]^T [C][B] dV^{(e)} \tag{3.21}$$

$$\mathbf{P^{(e)}} = \int_{V^{(e)}} \mathbf{b^T}[N] dV^{(e)} + \int_S \mathbf{t^T}[N] dS^{(e)} \tag{3.22}$$

Combining 3.19,3.21,3.22 we obtain the following

$$\sum_{e=1}^{N_e} \int_{t_1}^{t_2} \delta \mathbf{d^{(e)^T}} \left([\mathbf{K^{(e)}}]\mathbf{d^{(e)}} - \mathbf{P^{(e)}} \right) dt = 0 \tag{3.23}$$

Since $\delta \mathbf{d^{(e)^T}}$ is an arbitrary vector, the expression in the brackets must equal zero and the matrix equation becomes

$$[\mathbf{K}]\mathbf{D} = \mathbf{P} \tag{3.24}$$

where [**K**] is the assembled global stiffness matrix, **D** is the assembled global displacement vector, and **P** is the assembled global force vector given by

$$[K] = \sum_{e=1}^{N_e} [K^{(e)}] \tag{3.25}$$

$$\mathbf{P} = \sum_{e=1}^{N_e} \mathbf{P}^{(e)} \tag{3.26}$$

$$\mathbf{D} = \sum_{e=1}^{N_e} \mathbf{d}^{(e)} \tag{3.27}$$

where summation implies an assembly or expansion of the elemental matrices to form the global matrices. After combining 3.21,3.15, $[K^{(e)}]$ can be evaluated numerically using Gauss-Legendre quadrature with N_{gp} gauss points, ξ_i, η_i, ζ_i, and weights, W_i, through the following

$$[\mathbf{K^{(e)}}] = \int_{V^{(e)}} [B]^T [C][B] \frac{l_x}{2}\frac{l_y}{2}\frac{l_z}{2} d\xi d\eta d\zeta \tag{3.28}$$

$$= \sum_{n=1}^{N_{gp}} \sum_{m=1}^{N_{gp}} \sum_{l=1}^{N_{gp}} [B_{(\xi_n,\eta_m,\zeta_l)}]^T [C_{(\xi_n,\eta_m,\zeta_l)}][B_{(\xi_n,\eta_m,\zeta_l)}] \tfrac{l_x}{2}\tfrac{l_y}{2}\tfrac{l_z}{2} W_l W_m W_n \tag{3.29}$$

3.2 Correction Factor

The main difference between the uniform mesh method and conventional finite elements is that an element in the uniform mesh method may contain both fiber and matrix while in the conventional method each element contains only one material. Therefore, a "hybrid" uniform mesh element must be able to account for the differences in strain in the two materials in order to accurately predict the effective properties.

3.2.1 One-Dimensional Analysis

One dimensional spring or bar elements are employed to investigate the transverse modulus of the composite. This is done by finding the effective modulus of two conventional bar elements in series, one representing the matrix and the other representing a fiber. The effective modulus of two conventional elements in series can be derived from the fact that the forces exerted on each bar are equivalent:

$$F = \frac{E_m A}{L_m} u_1 = \frac{E_f A}{L_f} u_2 = \frac{E_{eff} A}{L_{eff}} (u_1 + u_2) \tag{3.30}$$

where L_{eff} and E_{eff} are the effective length and Young's Modulus. The lengths of the fiber and matrix, L_f and L_m, are related to the effective length and fiber length fraction, β, as follows

$$L_{eff} = L_f + L_m \tag{3.31}$$

$$\beta = \frac{L_f}{L_{eff}} \tag{3.32}$$

$$L_f = \beta L_{eff} \tag{3.33}$$

$$L_m = (1 - \beta) L_{eff} \tag{3.34}$$

Combining equations 3.30 and 3.31 yields

$$\begin{aligned} \frac{E_f A}{\beta L_{eff}} u_2 &= \frac{E_m A}{(1-\beta) L_{eff}} u_1 \\ u_2 &= \frac{E_m \beta}{E_f (1-\beta)} u_1 \end{aligned} \tag{3.35}$$

Substituting equation 3.35 into equation 3.30 results in an expression for the effective modulus in terms of the fiber length fraction β

$$E_{eff} = \frac{E_m E_f}{E_m \beta + E_f (1 - \beta)} \tag{3.36}$$

The displacement for a one-dimensional linear bar element will be a linear function of x as shown in figure 3.2, where the axial strain, ε is equivalent to the slope of the displacement.

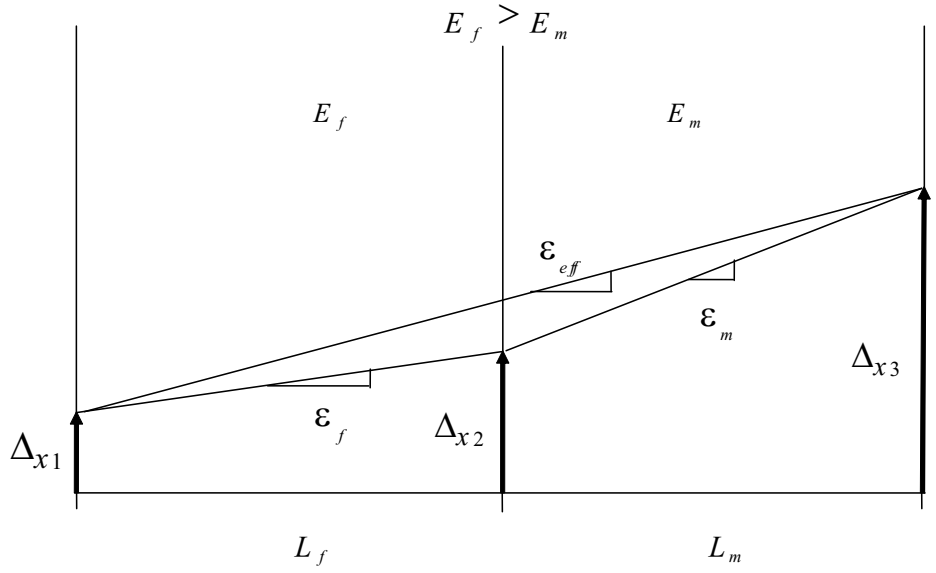

Figure 3.2: Displacement diagram using 2 conventional elements and 1 hybrid element

For two bar elements in series, the strain over the matrix ε_m is greater than the strain over the fiber ε_f. However, when a single element is used over the same region, the strain is constant over the entire element, ε_{eff}. Equation 3.30 can be written in terms of the strain as

$$F = E_f A\varepsilon_f = E_m A\varepsilon_m = E_{eff} A\varepsilon_{eff} \tag{3.37}$$

therefore

$$\frac{\varepsilon_m}{\varepsilon_{eff}} = E_{eff}/E_m \tag{3.38}$$

$$\frac{\varepsilon_f}{\varepsilon_{eff}} = E_{eff}/E_f \tag{3.39}$$

This equation provides a relationship between the strain over the uniform mesh element, and the strains over the conventional fiber and matrix elements.

The strain is equal to the strain-displacement matrix [B] times the elemental displacement vector as shown in equation 3.16. Therefore, in order to account for various strain values within a single hybrid element, a correction factor is applied to the strain-displacement matrix:

$$[B] = \alpha[B] \tag{3.40}$$

where the correction factor α is computed from equations 3.38 and 3.39. If the Gauss point lies within the matrix the correction factor is equal to:

$$\alpha = \frac{E_f}{E_m\beta + E_f(1-\beta)} \tag{3.41}$$

and if the Gauss point lies within the fiber the correction factor is equal to

$$\alpha = \frac{E_m}{E_m\beta + E_f(1-\beta)} \tag{3.42}$$

3.2.2 Three-Dimensional Analysis

The uniform mesh method in this thesis will use custom three-dimensional linear 8-node elements. The displacement over a conventional tri-linear element is defined by equation 3.12. Therefore, in order to apply the one-dimensional correction factor in 3 dimensions, the fiber length fraction in each of the three coordinate directions must be found. At each Gauss point, all other Gauss points will be checked in the x,y, and z directions and a fiber length fraction β_x,β_y and β_z will be obtained in each direction

using the following equations

$$\beta_\xi = \frac{\sum^{N_{gp}} W'_\xi}{\sum^{N_{gp}} W_\xi} \tag{3.43}$$

$$\beta_\eta = \frac{\sum^{N_{gp}} W'_\eta}{\sum^{N_{gp}} W_\eta} \tag{3.44}$$

$$\beta_\zeta = \frac{\sum^{N_{gp}} W'_\zeta}{\sum^{N_{gp}} W_\zeta} \tag{3.45}$$

where W' is the Gauss weight of each Gauss point that lies within a fiber. This is illustrated in two dimensions in figure 3.3. The figure represents a two-dimensional element with ten Gauss points in each direction. The blue x's are Gauss points that lie with fiber and the red circles are Gauss points that lie with matrix. From figure 3.3, it is shown that the fiber length fractions at the current Gauss point would be $\beta_\xi = 0$ and $\beta_\eta = 0.5$.

Correction factors for the x,y, and z directions α_ξ, α_ν and α_ζ are obtained at each Gauss point, where α_ξ is calculated using β_ξ, α_η is calculated using β_η, and α_ζ is calculated using β_ζ. The correction factors are then applied to the strain-displacement matrix, [B]

$$[B] \quad = \quad [[B_1][B_2]\dots[B_8]] \tag{3.46}$$

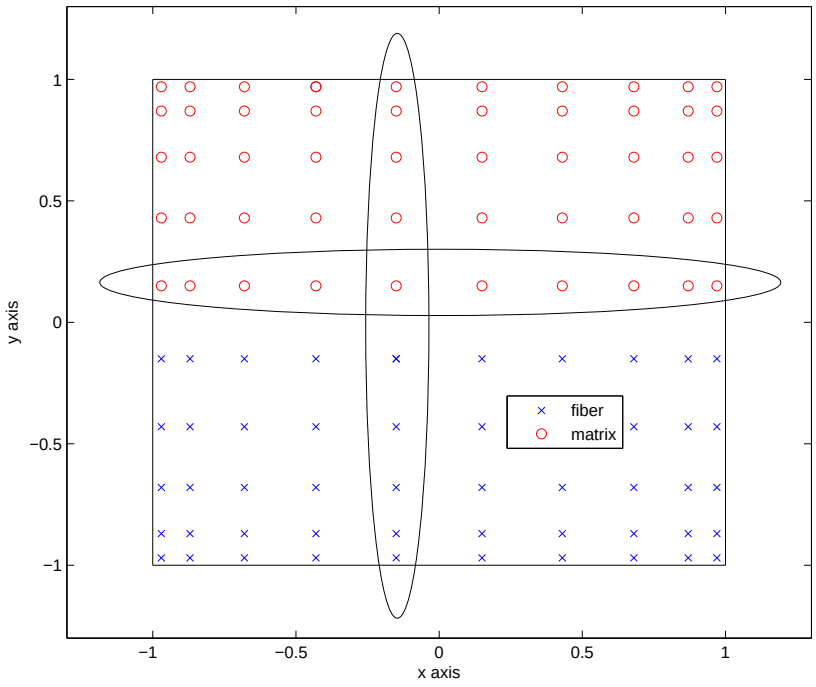

Figure 3.3: Calculation of the fiber length fraction

where

$$[B_i] = \begin{bmatrix} \frac{2}{l_x}\alpha_\xi\frac{\partial N_i}{\partial \xi} & 0 & 0 \\ 0 & \frac{2}{l_y}\alpha_\eta\frac{\partial N_i}{\partial \eta} & 0 \\ 0 & 0 & \frac{2}{l_z}\alpha_\zeta\frac{\partial N_i}{\partial \zeta} \\ \frac{2}{l_y}\alpha_\eta\frac{\partial N_i}{\partial \eta} & \frac{2}{l_z}\alpha_\xi\frac{\partial N_i}{\partial \xi} & 0 \\ 0 & \frac{2}{l_z}\alpha_\zeta\frac{\partial N_i}{\partial \zeta} & \frac{2}{l_y}\alpha_\eta\frac{\partial N_i}{\partial \eta} \\ \frac{2}{l_z}\alpha_\zeta\frac{\partial N_i}{\partial \zeta} & 0 & \frac{2}{l_x}\alpha_\xi\frac{\partial N_i}{\partial \xi} \end{bmatrix}, i = 1, 8 \qquad (3.47)$$

3.3 Periodic Boundary Conditions

Our uniform mesh method will assume the composite has a periodic structure and the average elastic properties of the composite can be found by modeling a representative volume element (RVE). Hori and Nemet-Nasser [53] have shown the the effective elastic properties vary depending on the boundary conditions applied to an RVE. Bounds for the effective moduli can be found by applying uniform traction or uniform displacement boundary conditions, where uniform traction results in a lower bound and uniform displacement results in an upper bound [53]. This is a direct result of the bounds produced by the Voigt constant strain assumption and Reuss constant stress assumption discussed previously. The uniform strain and traction boundary conditions are also sensitive to the size of the unit cell [36, 54] and approach the actual value as the size of the RVE increases. Several authors [1, 29] have also shown for longitudinal and transverse shear loading case, uniform displacement boundary conditions in which the boundary remains plane, represent an over constrained case and overestimate the effective shear moduli. Xia et. al. [29] have also shown that uniform displacement boundary conditions for an RVE with sides l_x,l_y and l_z in the x,y and z directions respectively, may violate the following stress and strain periodicity conditions [29]

$$\sigma(x, y, z) = \sigma(x + l_x, y + l_y, z + l_z) \tag{3.48}$$

$$\varepsilon(x, y, z) = \varepsilon(x + l_x, y + l_y, z + l_z) \tag{3.49}$$

Therefore, uniform displacement boundary conditions are not appropriate for the analysis of a periodic RVE.

Appropriate periodic boundary conditions must ensure each RVE has the same deformation mode such that there is no separation or overlap between adjacent RVE's [29]. These conditions are met by the following displacement field [29]

$$u_i = \bar{\varepsilon}_{ik} x_k + u_i^* \tag{3.50}$$

where u_i is the i^{th} component of the displacement vector, $\bar{\varepsilon}_{ik}$ is the average strain tensor, x_k is the k^{th} component of the coordinate vector, and u_i^* is the i^{th} component of the periodic displacement vector and is generally unknown. Note that the indices $i, j, k \in \{1, 2, 3\}$, and repeated indices imply summation in the usual manner. For parallelepiped RVEs the displacements on opposite boundary surfaces are written as [29]

$$u_i^{j+} = \bar{\varepsilon}_{ik} x_k^{j+} + u_i^* \tag{3.51}$$

$$u_i^{j-} = \bar{\varepsilon}_{ik} x_k^{j-} + u_i^* \tag{3.52}$$

where $j+$ and $j-$ refer to the positive and negative x_j boundary surfaces respectively. Subtracting the above equations yields [29]

$$u_i^{j+} - u_i^{j-} = \bar{\varepsilon}_{ik}(x_k^{j+} - x_k^{j+}) = c_i^j \tag{3.53}$$

where c_i^j is a constant corresponding to the average deformation of the RVE. Therefore, this equation specifies the difference in displacement between corresponding points on opposite boundary surfaces. Note that the displacement is still a function of the coordinates and therefore does not specify that the boundary surfaces remain plane [29]. This boundary condition will ensure that there is no seperation or overlap beween adjacent RVEs and satisfy stress and strain periodicity.

3.4 Finite Element Implementation

As mentioned earlier, ABAQUS 6.5 will be used to illustrate the uniform mesh method described above with a custom parallelepiped element for predicting the properties of short fiber composites. In order to run linear analysis in ABAQUS, the user must first generate an input file that contains: the nodal coordinates, element connectivity, material assignment, boundary conditions, and specify the required output. A Fortran subroutine is used to generate a regular array of parallepiped elements as shown in figure 3.4.

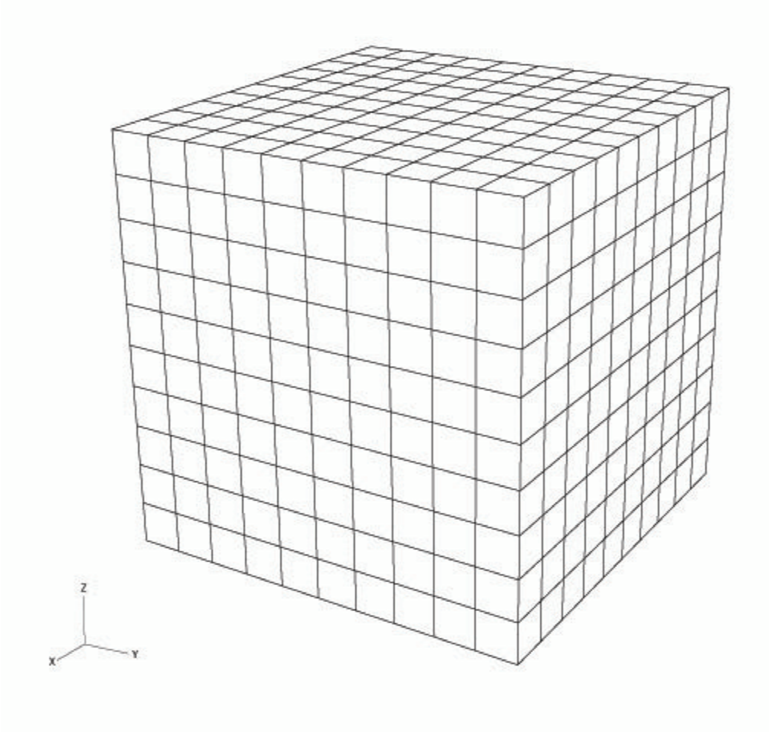

Figure 3.4: Uniform Mesh

The uniform mesh does not define the boundaries of the fibers and greatly simplifies the meshing process. The mesh is defined by the number of elements in the x,y and

z directions and the length of the element in each direction.

The boundary conditions given in equation 3.53 are then applied to the model. Equation 3.53 relates the displacements of corresponding points on opposite boundary surfaces. Therefore, the x_2 and x_3 coordinates must be the same for a pair of nodes on the positive and negative x_1 boundary surfaces. Similarly, the x_1 and x_3 coordinates must be the same for the x_2 boundary nodes, and the x_1 and x_2 coordinates must be the same for the x_3 boundary nodes. This requirement on the node placement makes the uniform mesh method ideal for the application of the periodic boundary conditions. Conversely, it is nearly impossible to fully apply the periodic boundary conditions on a complex part containing an irregular mesh. Next, text files containing the mesh and fiber data must be generated. The mesh file simply contains the number of elements in each direction, the number of Gauss points to be used for the elemental stiffness matrix calculation, and the dimensions of the model.

The fibers are assumed to be cylinders of constant length and diameter as shown in figure 3.5. Therefore, the orientation of a fiber is defined by the unit vector, $p(\theta, \phi)$ [20]

$$\mathbf{p}(\theta, \phi) = \left\{ \begin{array}{c} \sin\theta\cos\phi \\ \sin\theta\sin\phi \\ cos\theta \end{array} \right\} \tag{3.54}$$

where θ is the angle between the fiber and the x_3 axis and ϕ is the angle between the fiber and the x_1 axis as shown in figure 3.6. The spatial distribution of a fiber is defined by the coordinates of its centroid. Thus, the fibers are completely defined in the fiber file by specifying: the number of fibers, the aspect ratio and length of the

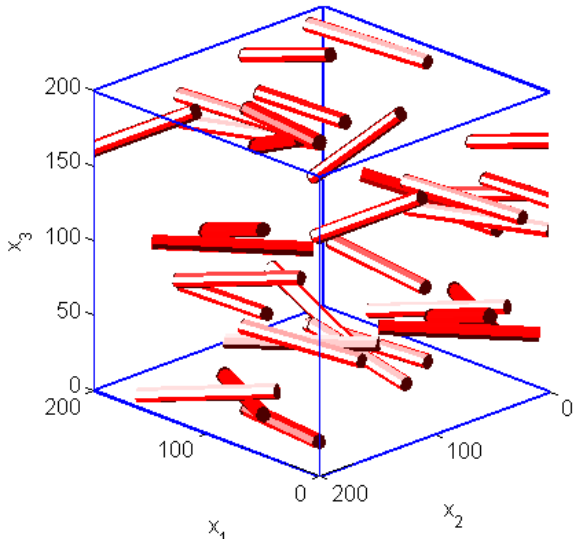

Figure 3.5: Short fibers with constant length and diameter

fibers, the centroid coordinates of each fiber, and the θ and ϕ angles of each fiber.

The elemental matrix equations were written into a user defined element subroutine, or UEL, within ABAQUS 6.5. The UEL subroutine is written in Fortran code and allows the user to develop custom elements not found in the ABAQUS element library. ABAQUS makes a call to the subroutine at the beginning and end of every iteration for every element. The current elemental nodal displacement vector, nodal coordinates, and the specified material properties are passed into the subroutine and the elemental stiffness matrix and force vector must be calculated and output to ABAQUS. ABAQUS then assembles the global stiffness matrix and force vector and solves the finite element equation 3.24.

Files may be opened and closed at the beginning of the analysis through the use of a user external database subroutine. The mesh and fiber files are opened using the user external database UEXTERNALDB in order to read in the mesh and fiber

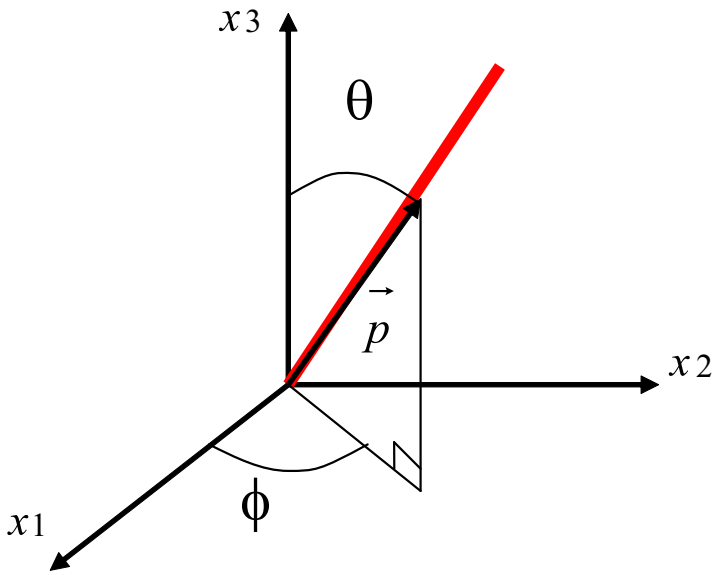

Figure 3.6: The fiber angles θ and ϕ and unit vector $p(\theta, \phi)$

data. Once the fiber data has been obtained, a subroutine is used to loop over all the elements and determine whether each Gauss point lies within the matrix or a fiber. This is done by first converting the Gauss point to the global coordinate system using equation 3.13. The vector from the fiber centroid to the Gauss point $\mathbf{D}_{gp}$ is used to calculate distance between the Gauss point and the fiber centroid d_{gp} and projected onto the fiber to find the longitudinal distance d_l

$$\mathbf{D}_{gp} = \left\{ \begin{array}{c} X - FX \\ Y - FY \\ Z - FZ \end{array} \right\} \tag{3.55}$$

$$d_{gp} = \sqrt{\mathbf{D_{gp}}^T \mathbf{D_{gp}}} \tag{3.56}$$

$$d_l = \mathbf{D}_{gp}^T \mathbf{p} \tag{3.57}$$

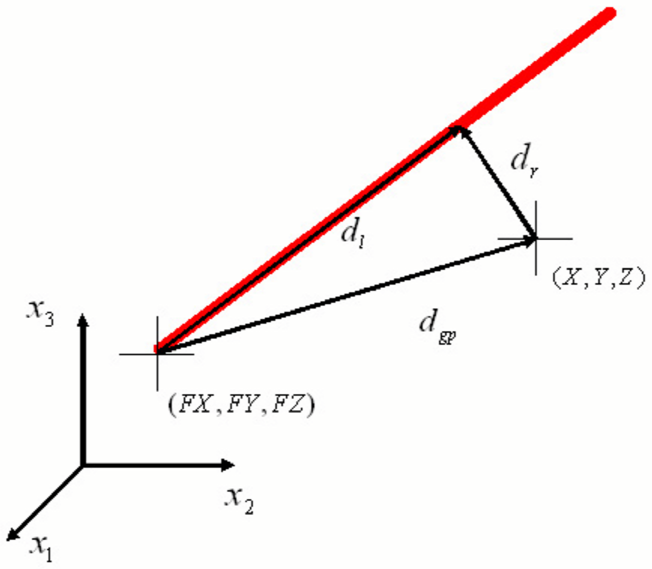

Figure 3.7: Geometry of the Gauss point and fiber

where X, Y, Z are the coordinates of the Gauss point and FX, FY, FZ are the coordinates of the fiber centroid as shown in figure 3.7.

The radial distance between the Gauss point and the fiber, d_r, is then calculated

$$d_r = \sqrt{d_{gp}^2 - d_l^2} \tag{3.58}$$

The following conditions can then be used to determine whether the Gauss point lies within a fiber

$$\begin{aligned} d_l &\leq \frac{L}{2} \\ d_r &\leq R \end{aligned} \tag{3.59}$$

where L is the length of the fiber and R is the radius of the fiber. If both conditions are met then the Gauss point lies within a fiber. Otherwise, the Gauss point lies within the matrix. These equations are calculated for each fiber.

The volume fraction, v_f, is then calculated as follows

$$v_f = \frac{\sum^{N} v_f^e}{N} \tag{3.60}$$

where N is the number of elements and v_f^e is the volume fraction of a single element given by

$$v_f^e = \frac{1}{8} \sum^{N_{gp}} \sum^{N_{gp}} \sum^{N_{gp}} W'_\xi W'_\eta W'_\zeta \tag{3.61}$$

where $W'_\xi, W'_\eta, W'_\zeta$ are the Gauss weights corresponding to the Gauss points that lie within a fiber. Equation 3.60 represents the volume fraction in the uniform mesh model. If this volume fraction is different than the actual volume fraction of the composite within a specified limit, then the number of Gauss points needs to be increased to more accurately determine the fiber boundaries.

Once all of the Gauss points have been assigned to fiber or matrix and the volume fraction has been determined, then the elemental stiffness matrix and force vector are calculated. The elemental stiffness matrix is evaluated using equation 3.28. The Young's modulus and Poisson's ratio used in the calculation of the stiffness matrix given in equation 3.7 are dependent upon whether the current Gauss point has been assigned to the matrix or fiber. If the Gauss point lies within the matrix then the matrix Young's modulus and Poisson's ratio are used and if it lies with a fiber then the fiber properties are used. The location of the Gauss point also determines the value of the correction factor. If the Gauss point lies within matrix the correction factor is evaluated using equation 3.41 and if the Gauss point lies within fiber the correction factor is evaluated using equation 3.42. Since the current elemental displacement

vector is passed into the subroutine, the elemental force vector can be found by simply multiplying the elemental stiffness matrix with the displacement vector as shown in equation 3.24.

The UEL procedure must be modified slightly in order to plot the element connectivity as well as the stress, strain, and other parameters using ABAQUS. Since the uniform mesh method uses a modified linear eight node brick element, the connectivity of the elements can only be plotted by overlaying the uniform mesh with a conventional eight node brick element C3D8 used by ABAQUS. The same nodes and connectivity are used for both sets of elements so that the ABAQUS elements accurately show the UEL deformation. The ABAQUS elements must be assigned a very small value for the Young's modulus so that they do not effect the UEL calculations. The UVARM subroutine in ABAQUS allows the user to plot calculated variables at the Gauss points of the conventional elements. However, since the ABAQUS and uniform mesh elements do not have the same number of Gauss points, only average element parameters may be plotted. The average strain and stress over the element are calculated as:

$$\bar{\boldsymbol{\varepsilon}}^{(e)} = \sum_{n=1}^{N_{gp}} \sum_{m=1}^{N_{gp}} \sum_{l=1}^{N_{gp}} [B(\xi_n, \eta_m, \zeta_l)] \mathbf{d}^{(e)} \frac{l_x}{2} \frac{l_y}{2} \frac{l_z}{2} W_l W_m W_n \tag{3.62}$$

$$\bar{\boldsymbol{\sigma}}^{(e)} = \sum_{n=1}^{N_{gp}} \sum_{m=1}^{N_{gp}} \sum_{l=1}^{N_{gp}} [C][B(\xi_n, \eta_m, \zeta_l)] \mathbf{d}^{(e)} \frac{l_x}{2} \frac{l_y}{2} \frac{l_z}{2} W_l W_m W_n \tag{3.63}$$

where $\mathbf{d}^{(e)}$ is the elemental displacement vector passed into the UEL subroutine by ABAQUS. The volume fraction of each element can also be plotted using equation 3.61.

CHAPTER 4

ELASTIC PROPERTY PREDICTION

The uniform mesh method and periodic boundary conditions were derived in the previous chapter. In this chapter, the method for obtaining the effective properties from the finite element results and two micromechanical models will be presented. The effective properties obtained using the uniform mesh method will be compared with a simple composite consisting of two conventional elements in series in order to validate the solution process and the application of the correction factor.

4.1 Effective Elastic Properties

The effective elastic properties can be found once the average stress and strain are known through Hooke's Law as shown in equation 3.6. The average strain is defined as

$$\bar{\varepsilon}_{ij} = \frac{1}{V}\int_V \varepsilon_{ij} dV \tag{4.1}$$

where V is the volume of the RVE. The strain tensor can be written in terms of displacement as:

$$\varepsilon_{ij} = \frac{1}{2}(u_{i,j} + u_{j,i}) \tag{4.2}$$

where $u_{i,j}$ implies differentiation of u_i with respect to x_j. The average strain is related to the boundary displacements using equation 4.2 and the Gauss Theorem as [1]

$$\bar{\varepsilon}_{ij} = \frac{1}{2V}\int_S (u_i n_j + u_j n_i) dS \tag{4.3}$$

where n_j is the j^{th} component of the unit normal to the boundary surface S of the RVE. For a parallelepiped in which the boundary faces surfaces are normal to the coordinate axes, the normal will have only one non-zero component and equation 4.3 can be reduced to the following [29]

$$\begin{aligned}
\bar{\varepsilon}_{ij} &= \frac{1}{2V}\left[\int_{S_j}(u_i^{j+}-u_i^{j-})dS+\int_{S_i}(u_j^{i+}-u_j^{i-})dS\right] \\
&= \frac{1}{2V}(c_i^j S_j + c_j^i S_i) \\
&= \frac{c_i^j l_x l_k + c_j^i l_j l_k}{2 l_i l_j l_k} \\
&= \frac{1}{2}\frac{c_i^j l_i + c_j^i l_j}{l_i l_j}
\end{aligned} \tag{4.4}$$

where l_i refers to the length of the RVE in the x_i direction, and c_i^j is the constant defining the periodic boundary condition given in equation 3.53. Therefore, the average strain is simply found from the dimensions of the RVE and the applied boundary conditions.

Similarly, the average stress is defined as

$$\bar{\sigma}_{ij} = \frac{1}{V}\int_V \sigma_{ij} dV \tag{4.5}$$

In the absence of body forces the equations of equilibrium are

$$\sigma_{ij,j} = 0 \tag{4.6}$$

Using the equilibrium equation it can be shown that [55]

$$\begin{aligned}
(\sigma_{ik}x_j)_{,k} &= \sigma_{ik,k}x_j + \sigma_{ij}x_{j,k} \\
&= \sigma_{ij}\delta_{jk} \\
&= \sigma_{ij}
\end{aligned} \tag{4.7}$$

Therefore, combining equations 4.5,4.7 and using Gauss theorem yields

$$\bar{\sigma}_{ij} = \frac{1}{V}\int_S \sigma_{ik} x_j n_k \, dS \tag{4.8}$$

Due to periodicity, the stress at two corresponding points on opposite surfaces must be equal. Similar to the derivation of equation 4.4, the average stress can be reduced to [29]

$$\begin{aligned} \bar{\sigma}_{ij} &= \frac{1}{S}\left[\int_{S_m^+} \sigma_{im}^+ x_j^+ - \int_{S_m^-} \sigma_{im}^- x_j^-\right] \\ &= \frac{1}{V}\int_{S_m^+} \sigma_{im}^+ (x_j^+ - x_j^-) dS \end{aligned} \tag{4.9}$$

When $m \neq j$, the coordinates $x_j^+ = x_j^-$, and when $m = j$, $x_j^+ - x_j^- = l_j$, therefore [29]

$$\bar{\sigma}_{ij} = \frac{l_j}{V}\int_{S_j} \sigma_{ij} dS = \frac{R_{ij}}{S_j} \tag{4.10}$$

where R_{ij} is the sum of the reactions forces on the boundary face S_j and there is no summation over j.

Once the average stress and strain have been obtained, the effective elastic properties are evaluated from

$$\bar{\boldsymbol{\sigma}} = [\bar{C}]\bar{\boldsymbol{\varepsilon}} \tag{4.11}$$

where $[\bar{C}]$ is the average or effective stiffness matrix of the composite, $\bar{\boldsymbol{\sigma}}$ is the effective stress vector, and $\bar{\boldsymbol{\varepsilon}}$ is the effective strain vector. For an orthotropic composite, the average stiffness tensor is related to the average material properties through the

following

$$[\bar{C}] = \begin{bmatrix} 1/\bar{E}_{11} & -\nu_{21}/\bar{E}_{22} & -\bar{\nu}_{31}/\bar{E}_{33} & 0 & 0 & 0 \\ -\bar{\nu}_{12}/\bar{E}_{11} & 1/\bar{E}_{22} & -\bar{\nu}_{32}/\bar{E}_{33} & 0 & 0 & 0 \\ -\bar{\nu}_{13}/\bar{E}_{11} & -\bar{\nu}_{23}/\bar{E}_{22} & 1/\bar{E}_{33} & 0 & 0 & 0 \\ 0 & 0 & 0 & 1/\bar{G}_{12} & 0 & 0 \\ 0 & 0 & 0 & 0 & 1/\bar{G}_{23} & 0 \\ 0 & 0 & 0 & 0 & 0 & 1/\bar{G}_{13} \end{bmatrix}^{-1} \tag{4.12}$$

From equation 4.12 it is shown that for an orthotropic material there are nine independent material properties ($E_{11}, E_{22}, E_{33}, \nu_{12}, \nu_{23}, \nu_{13}, G_{12}, G_{23}, G_{13}$). Therefore, nine independent equations are needed to solve for the nine independent material properties. The nine equations are obtained from six independent strain conditions defined by six sets of deformation constants, c_i^j:

$$\text{set } 1 : c_1^1 = 0.05 l_x, \text{ all other } c_i^j = 0 \tag{4.13}$$

$$\text{set } 2 : c_2^2 = 0.05 l_y, \text{ all other } c_i^j = 0 \tag{4.14}$$

$$\text{set } 3 : c_3^3 = 0.05 l_z, \text{ all other } c_i^j = 0 \tag{4.15}$$

$$\text{set } 4 : c_1^2 = 0.025 l_y,\ c_2^1 = 0.025 l_x, \text{ all other } c_i^j = 0 \tag{4.16}$$

$$\text{set } 5 : c_2^3 = 0.025 l_z,\ c_3^2 = 0.025 l_y, \text{ all other } c_i^j = 0 \tag{4.17}$$

$$\text{set } 6 : c_1^3 = 0.025 l_z,\ c_3^1 = 0.025 l_x, \text{ all other } c_i^j = 0 \tag{4.18}$$

The six strain sets represent three uniaxial extension conditions and three pure shear conditions. From the three uniaxial extension conditions nine nontrivial equations will be obtained, only six of which are independent, and from the three pure shear conditions the three remaining independent equations will be obtained.

To ensure the effective stiffness matrix is of the form in equation 3.7, Lagrange multipliers are used when solving equation 3.6 to impose the necessary symmetry

constraints. This is done by first forming average stress and strain matrices from the average stress and strain vectors obtained from the six finite element runs so that equation 3.6 becomes:

$$[\sigma] = [\mathbf{C}][\varepsilon] \tag{4.19}$$

By multiplying both sides of equation 4.19 by the transpose of the average strain matrix $[\varepsilon]^{\mathbf{T}}$ the following unconstrained least squares equation is obtained:

$$[\varepsilon]^T[\sigma] = [\mathbf{C}][\varepsilon]^T[\varepsilon] \tag{4.20}$$

Equation 4.20 can then be expanded as follows:

$$\begin{bmatrix} \varepsilon_{ik}^T\sigma_{k1} \\ \varepsilon_{ik}^T\sigma_{k2} \\ \vdots \\ \varepsilon_{ik}^T\sigma_{k6} \end{bmatrix}_{36\times1} = \begin{bmatrix} \varepsilon_{ik}^T\varepsilon_{kj} & 0_{ij} & 0_{ij} & 0_{ij} & 0_{ij} & 0_{ij} \\ 0_{ij} & \varepsilon_{ik}^T\varepsilon_{kj} & 0_{ij} & 0_{ij} & 0_{ij} & 0_{ij} \\ 0_{ij} & 0_{ij} & \varepsilon_{ik}^T\varepsilon_{kj} & 0_{ij} & 0_{ij} & 0_{ij} \\ 0_{ij} & 0_{ij} & 0_{ij} & \varepsilon_{ik}^T\varepsilon_{kj} & 0_{ij} & 0_{ij} \\ 0_{ij} & 0_{ij} & 0_{ij} & 0_{ij} & \varepsilon_{ik}^T\varepsilon_{kj} & 0_{ij} \\ 0_{ij} & 0_{ij} & 0_{ij} & 0_{ij} & 0_{ij} & \varepsilon_{ik}^T\varepsilon_{kj} \end{bmatrix}_{36\times36} \begin{bmatrix} C_{11} \\ C_{12} \\ C_{13} \\ \vdots \\ C_{66} \end{bmatrix}_{36\times1} \tag{4.21}$$

or

$$\mathbf{b} \;=\; [\mathbf{A}]\mathbf{C} \tag{4.22}$$

where i and j are the components of the stress and strain matrices and $i, j \in 1, 2, .., 6$.

The least squares form is needed when the system is overdetermined. For example, this occurs when predicting transversely isotropic and isotropic stiffness matrices in which there are fewer than nine independent properties.

The 6×6 orthotropic stiffness matrix contains x non-zero constants. Due to symmetry the number of constants is reduced to 9 as described above. Therefore, 27

constraints must be applied to the solution process. These constraint equations are combined with equation 4.22 as follows [56]

$$\left[\begin{array}{c}\mathbf{b}\\\hline\mathbf{0}\end{array}\right]_{63\times1} = \left[\begin{array}{c|c}[\mathbf{A}] & [X]'\\\hline[X] & [0]\end{array}\right]_{63\times63} \left[\begin{array}{c}\mathbf{C}\\\hline\boldsymbol{\lambda}\end{array}\right]_{63\times1} \tag{4.23}$$

(4.24)

where $\boldsymbol{\lambda}$ is a vector of lagrange multipliers, and $[X]$ is a matrix of symmetry and zero constraints. Therefore, the modified $\mathbf{C}$ vector can be found as follows

$$\left[\begin{array}{c}\mathbf{C}\\\hline\lambda\end{array}\right]_{63\times1} = \left[\begin{array}{c|c}[\mathbf{A}] & [\mathbf{X}]'\\\hline[\mathbf{X}] & [\mathbf{0}]\end{array}\right]^{-1}_{63\times63} \left[\begin{array}{c}\mathbf{b}\\\hline\mathbf{0}\end{array}\right]_{63\times1} \tag{4.25}$$

The regression correlation coefficient is then calculated to determine the quality of the least squares solution. The regression coefficient R is given by

$$R_i = \sqrt{\frac{s_i^1 - s_i^2}{s_i^1}} \tag{4.26}$$

where s_i^1 and s_i^2 are given by:

$$s_i^1 = \sum_{j=1}^{n} (\bar{\sigma}_{ji} - \sigma_i^m)^2 \tag{4.27}$$

$$s_i^2 = \sum_{j=1}^{n} (\bar{\sigma}_{ji} - (C_{jk}\varepsilon_{ki}^T)^T)^2 \tag{4.28}$$

The mean stress vector, σ_i^m, is defined as

$$\sigma_i^m = \frac{1}{n}\sum_{j=1}^{n} \bar{\sigma}_{ij} \tag{4.29}$$

4.2 Micromechanical Models

The Halpin-Tsai and Tandon-Weng models have been widely used in literature and will be used for comparison with the finite element results. The Halpin-Tsai equations for the elastic constants are given by [5]

$$\frac{P}{P_m} = \frac{1+\zeta\eta v_f}{1-\eta v_f} \tag{4.30}$$

$$\eta = \frac{(P_f/P_m)-1}{(P_f/P_m)+1} \tag{4.31}$$

$$\nu_{12} = \nu_f v_f + \nu_m(1-v_f) \tag{4.32}$$

$$\nu_{23} = -1 + \frac{E_{22}}{2G_{23}} \tag{4.33}$$

where P represents any one of the moduli, P_m and P_f are the corresponding moduli of the matrix and fiber. The parameter ζ is dependent upon the moduli being calculated as shown in table 4.1.

P	P_f	P_m	ζ
E_{11}	E_f	E_m	$2(\mathrm{l/d})$
E_{22}	E_f	E_m	2
G_{12}	G_f	G_m	$1+40v_f^{10}$
G_{23}	G_f	G_m	$\frac{K_m/G_m}{K_m/G_m+2}$

Table 4.1: Halpin-Tsai parameters used for short fiber calculations [1]

The value of ζ_{G12} proposed by Hewitt and Malherbe [8] is used. The bulk modulus of the matrix, K_m, needed for ζ_{G23} is found from:

$$K_m = \frac{E_m}{3(1-2\nu_m)} \tag{4.34}$$

The Tandon-Weng equations are given by the following [4, 14]:

$$
\begin{aligned}
E_{11} &= \frac{E_m}{1 + v_f(A_1 + 2v_m A_2)/A} && (4.35)\\
E_{22} &= \frac{E_m}{1 + v_f[-2v_m A_3 + (1 - v_m)A_4 + (1 + v_m)A_5 A]/2A} && (4.36)\\
G_{12} &= \frac{G_m}{\frac{\mu_m}{\mu_f - \mu_m} + 2(1 - v_f)S_{1212}} && (4.37)\\
G_{12} &= \frac{G_m}{\frac{\mu_m}{\mu_f - \mu_m} + 2(1 - v_f)S_{2323}} && (4.38)\\
\nu_{12} &= \frac{\nu_m A - v_f(A_3 - \nu_m A_4)}{A + v_f(A_1 + 2\nu_m A_2)} && (4.39)\\
\nu_{23} &= -1 + \frac{E_{22}}{2G_{23}} && (4.40)
\end{aligned}
$$

The equation for ν_{12} was derived by Tucker and Liang [4] and provides an alternative to the iterative equation for ν_{12} given by Tandon and Weng. The constants A_i are found using equations 4.41

$$
\begin{aligned}
A_1 &= D1(B_4 + B_5) - 2B_2\\
A_2 &= (1 + D1)B_2 - (B_4 + B_5)\\
A_3 &= B_1 - D_1 B_3 && (4.41)\\
A_4 &= (1 + D_1)B_1 - 2B_3\\
A_5 &= (1 - D_1)/(B_4 - B_5)\\
A &= 2B_2 B_3 - B_1(B_4 + B_5)
\end{aligned}
$$

The constants D_i and B_i are found from the following

$$B_1 = v_f D_1 + D_2 + (1 - v_f)(D_1 S_{1111} + 2S_{2211}) \quad (4.42)$$

$$B_2 = v_f + D_3 + (1 - v_f)(D_1 S_{1122} + S_{2222} + S_{2233}) \quad (4.43)$$

$$B_3 = v_f + D_3 + (1 - v_f)(S_{1111} + (1 + D_1)S_{2211}) \quad (4.44)$$

$$B_4 = v_f D_1 + D_2 + (1 - v_f)(S_{1122} + D_1 S_{2222} + S_{2233}) \quad (4.45)$$

$$B_5 = v_f + D_3 + (1 - v_f)(S_{1122} + S_{2222} + D_1 S_{2233}) \quad (4.46)$$

$$D_1 = 1 + 2(\mu_f - \mu_m)/(\lambda_f - \lambda_m) \quad (4.47)$$

$$D_2 = (\lambda_m + 2\mu_m)/(\lambda_f - \lambda_m) \quad (4.48)$$

$$D_3 = \lambda_m/(\lambda_f - \lambda_m) \quad (4.49)$$

where μ_m, μ_f and λ_m, λ_f are Lame's constants for the matrix and fiber. Lame's constants are related to the elastic constants using equations 4.50 and 4.51

$$\lambda = \frac{E\nu}{(1 + \nu)(1 - 2\nu)} \quad (4.50)$$

$$\mu = \frac{E}{2(1 + v)} \quad (4.51)$$

S_{ijkl} are components of Eshelby's tensor for a fiber-like spheriodal inclusion and are

given by:

$$
\begin{aligned}
S_{1111} &= \frac{1}{2(1-\nu_m)}\left\{1-2\nu_m+\frac{3\alpha^2-1}{\alpha^2-1}-\left[1-2\nu_m+\frac{3\alpha^2}{\alpha^2-1}\right]g\right\} \\
S_{2222} &= S_{3333}=\frac{3}{8(1-\nu_m)}\frac{\alpha^2}{\alpha^2-1}+\frac{1}{4(1-\nu_m}\left[1-2\nu_m-\frac{9}{4(\alpha^2-1)}\right]g \\
S_{2233} &= S_{3322}=\frac{1}{4(1-\nu_m)}\left\{\frac{\alpha^2}{2(\alpha^2-1)}-\left[1-2\nu_m+\frac{3}{4(\alpha^2-1)}\right]g\right\} \\
S_{2211} &= S_{3322}=-\frac{1}{1(1-\nu_m)}\frac{\alpha^2}{\alpha^2-1}+\frac{1}{4(1-\nu_m}\left\{\frac{3\alpha^2}{\alpha^2-1}-(1-2\nu_m)\right\}g \\
S_{1122} &= S_{1133}=-\frac{1}{2(1-\nu_m}\left[1-2\nu_m-\frac{1}{\alpha^2-1}\right]+\frac{1}{2(1-\nu_m}\left[1-2\nu_m-\frac{3}{2(\alpha^2-1)}\right]g \\
S_{2323} &= S_{3232}=\frac{1}{4(1-\nu_m)}\left\{\frac{\alpha^2}{2(\alpha^2-1)}+\left[1-2\nu_m-\frac{3}{4(\alpha^2-1)}\right]g\right\} \\
S_{1212} &= S_{1313}=\frac{1}{4(1-\nu_m)}\left\{1-2\nu_m-\frac{\alpha^2+1}{\alpha^2-1}-\frac{1}{2}\left[1-2\nu_m+\frac{3(\alpha^2+1)}{\alpha^2-1}\right]g\right\}
\end{aligned}
\tag{4.52}
$$

where α is the aspect ratio, and g is given by

$$
g=\frac{\alpha}{(\alpha^2-1)^{3/2}}\left\{\alpha(\alpha^2-1)^{1/2}-\cosh^{-1}\alpha\right\} \tag{4.53}
$$

4.3 Results

The method described above will be used to obtain the effective properties of a simple composite containing two conventional elements in series, one representing the fiber and the other representing the matrix. The results will be compared with the effective properties obtained using a single uniform mesh element with and without the correction factor. The analysis will be performed in both one-dimension and three-dimensions.

4.3.1 One-Dimensional Comparison

The stiffness matrix for the 1D bar element is given by:

$$[K^{(e)}] = \int_L [B]^T \, EA \, [B] \frac{L}{2} d\xi \tag{4.54}$$

$$\tag{4.55}$$

where A is the cross sectional area of the bar element and L is the length of the bar element. The strain-displacement matrix [B] for a linear one-dimensional element is equal to

$$[B] = \begin{bmatrix} \dfrac{-1}{L} \\ \\ \dfrac{1}{L} \end{bmatrix} \tag{4.56}$$

If E and A are constant, the stiffness matrix for the conventional element reduces to

$$[K^{(e)}] = \frac{EA}{L} \begin{bmatrix} 1 & -1 \\ -1 & 1 \end{bmatrix} \tag{4.57}$$

For the hybrid element, E is not constant and therefore equation 4.57 must be found using Gauss-Legendre quadrature where the value of E depends on whether the Gauss point lies within the matrix or fiber. After running the finite element analysis, the effective modulus can be found from the reaction force R and the strain ε through the following

$$E_{eff} = \frac{R}{A\varepsilon} \tag{4.58}$$

Figure 4.1 shows the effective modulus results for the two methods over a range of volume fractions.

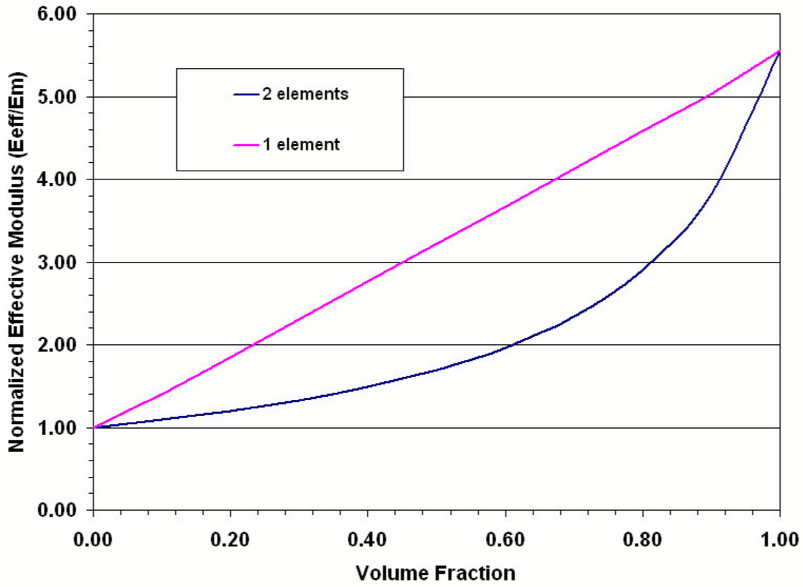

Figure 4.1: 1D spring results using 2 conventional elements and 1 uniform mesh element for $E_f/E_m = 5.55$

The ratio between the fiber modulus and the matrix modulus E_f/E_m was set equal to 5.55. The results are given as a ratio of the effective modulus to the matrix modulus E_{eff}/E_m. From the figure it can be seen that the hybrid element matches the conventional elements when the elements are both matrix, a volume fraction of zero, and when the elements are both both fiber, a volume fraction of one, as expected. However, the hybrid element does a very poor job of predicting the effective modulus for all other volume fractions. The error in the hybrid results increases as the ratio of the fiber and matrix moduli increases as shown in figure 4.2.

This is due to the fact that the hybrid element result tends to simply average the Young's modulus of the two materials, thus providing the rule-of-mixtures result for

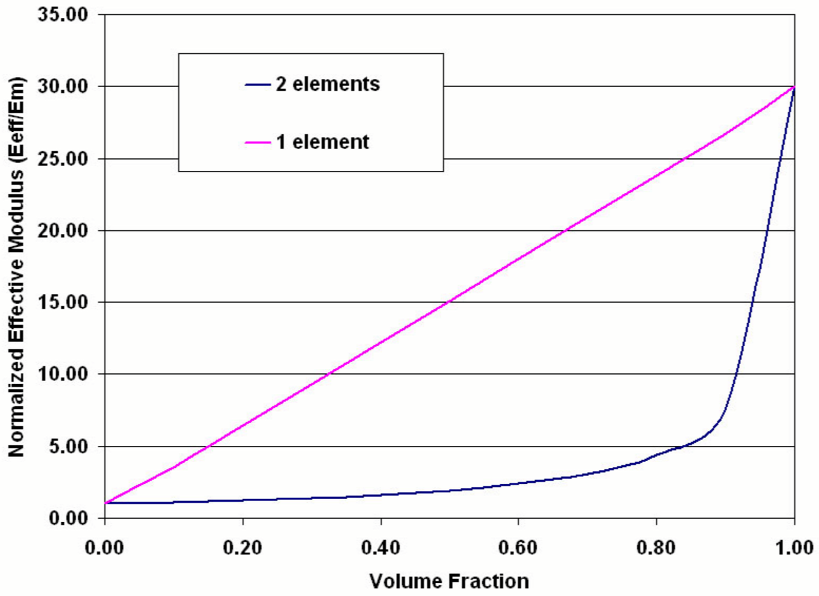

Figure 4.2: 1D spring results using 2 conventional elements and 1 uniform mesh element for $E_f/E_m = 30.0$

the effective modulus given below:

$$E_{eff} = v_f E_f + (1 - v_f) E_m \tag{4.59}$$

When the correction factors in equations 3.41 and 3.42 are used to compute $[B]$, values of E_{eff} using a single hybrid element exactly match the results using the conventional elements as shown in figures 4.3 and 4.4.

4.3.2 Three-Dimensional Comparison

The one-dimensional analysis showed that with the inclusion of a correction factor, the uniform mesh element could accurately predict the effective transverse modulus E_2. The ability of the uniform mesh element to accurately predict the remaining elastic constants will now be investigated. A single uniform mesh element will be

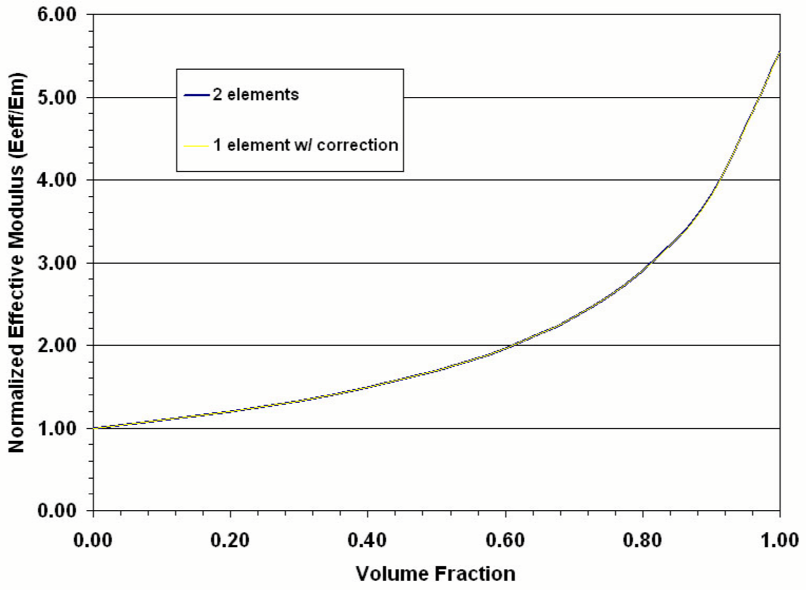

Figure 4.3: Results w/ correction factor for $E_f/E_m = 5.55$

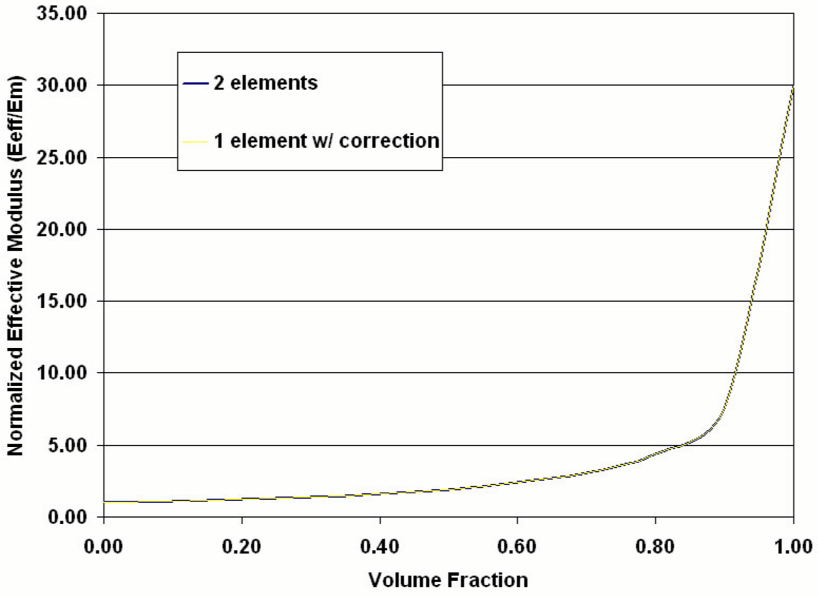

Figure 4.4: Results w/ correction factor for $E_f/E_m = 30.0$

compared with a simple composite consisting of two conventional 3D brick elements in series. Periodic boundary conditions were applied to the edges of the model and the effective properties were found from equations 4.4 and 4.13. The isotropic elastic properties for the matrix and fiber are given in Table 4.2.

$Material$	$E(GPa)$	ν
$Fiber$	379.3	0.1
$Matrix$	68.3	0.3

Table 4.2: Elastic properties of matrix and fiber

The effective composite will be transversely isotropic due to the geometry of the model. The same properties will be obtained in the x_1 and x_2 directions and only the results for the x_1 direction will be given. The results for effective longitudinal modulus, E_{11}, using the two conventional elements and the results for the hybrid element with and without the correction factor are shown in figure 4.5.

From the figure it can be seen that all the models result in the same prediction for E_{11}. This is due to the fact that the uniform mesh element has a length ratio of one in the x_1 direction at every Gauss point. Therefore, the uniform mesh element produces the same results with and without the correction factor. The uniform mesh element and conventional elements both predict an E_{11} modulus based on the rule-of-mixtures given in equation 4.59. The results for the E_{33} modulus are shown in figure 4.6.

The results for transverse modulus are similar to the one-dimensional bar results. The uniform mesh without the correction greatly overpredicts the modulus. The uniform mesh element with the correction accurately predicts E_{33} over the entire range of volume fractions. The results for the Poissons' ratios are given in figures 4.7

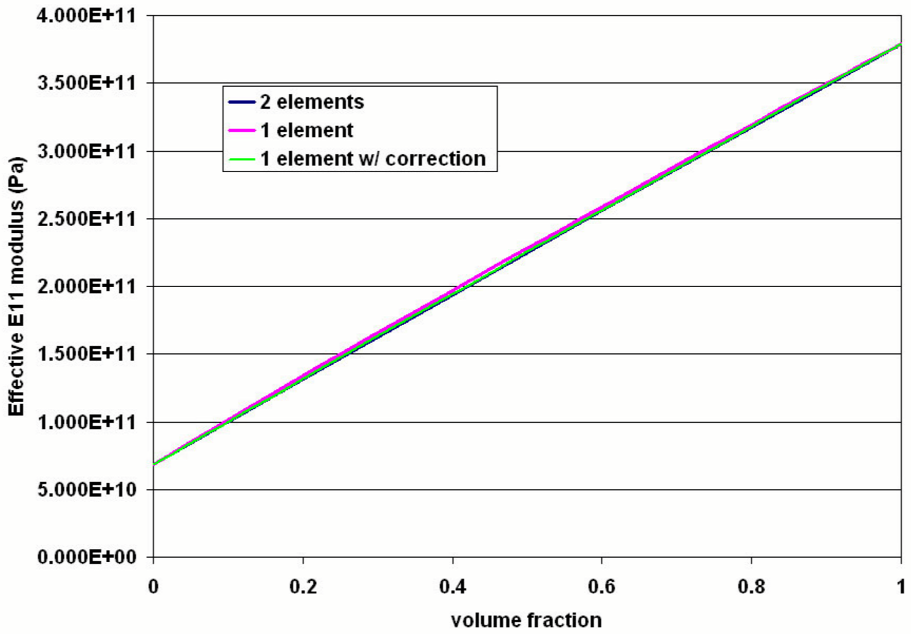

Figure 4.5: Effective E_{11} results

and 4.8.

The uniform mesh element slightly overpredicts ν_{12} and greatly underpredicts ν_{23}. However, with the correction, the uniform mesh element accurately predicts both Poisson's ratio over the entire range of volume fractions. Finally, the results for the shear moduli are given in figures 4.9 and 4.10.

All models provide the same predictions for G_{12}. However, uniform mesh element without the correction greatly overpredicts the G_{23} shear modulus with a maximum error over 100%. The uniform mesh prediction with the correction is better but still overpredicts G23 with a maximum error of approximately 30% occurring at a volume fraction of about 65%. Therefore, the uniform mesh element with correction accurately predicts all of the elastic constants except for the longitudinal shear modulus. A more accurate correction factor for the shear modulus needs to be developed in the

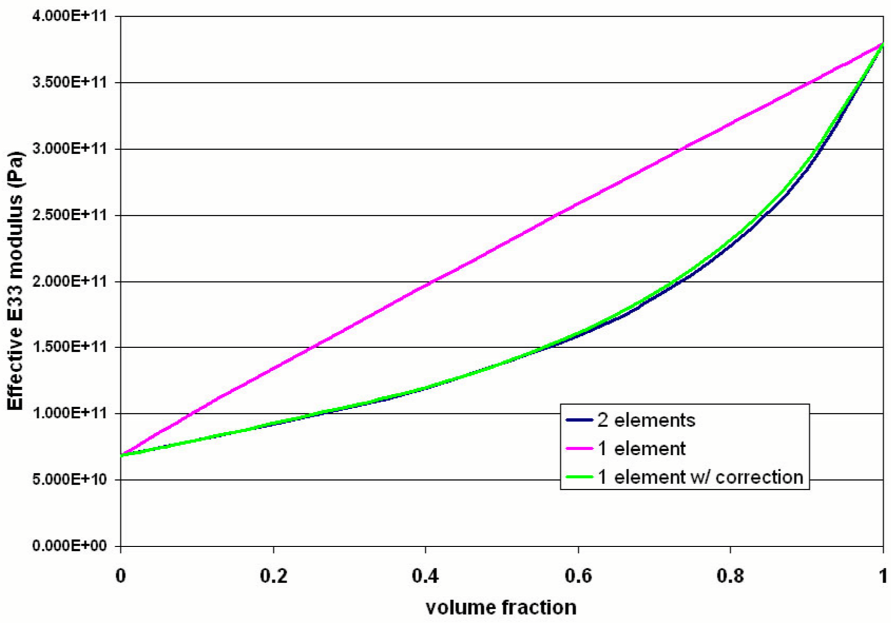

Figure 4.6: Effective E_{33} results

future. All results in future sections will be given using the uniform mesh element with correction.

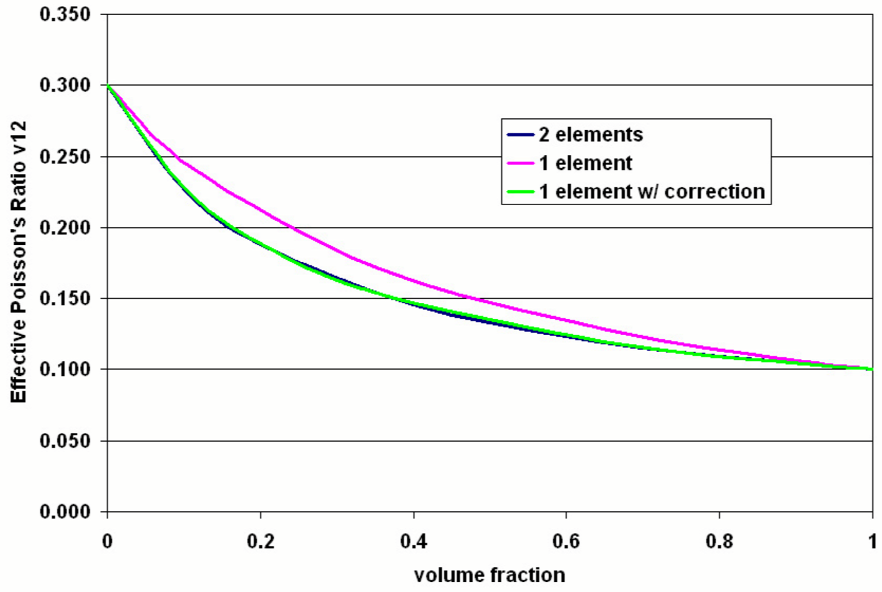

Figure 4.7: Effective ν_{12} results

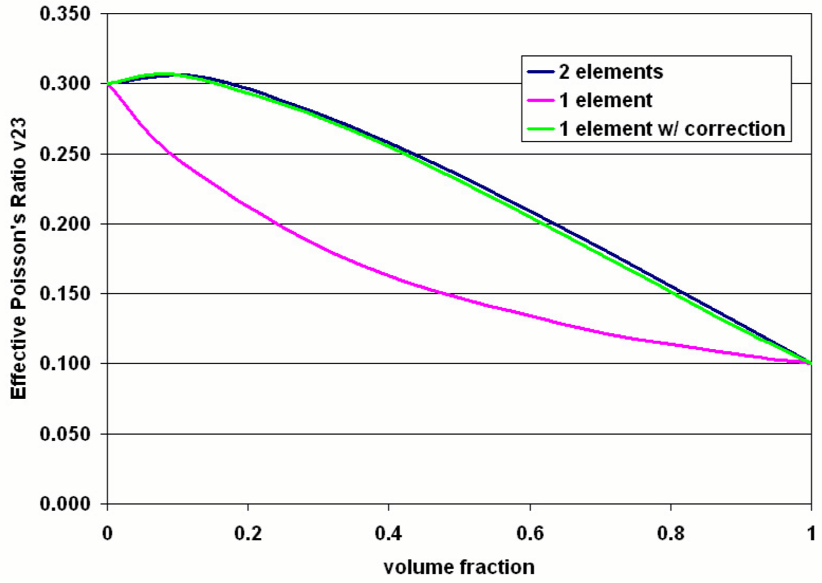

Figure 4.8: Effective ν_{23} results

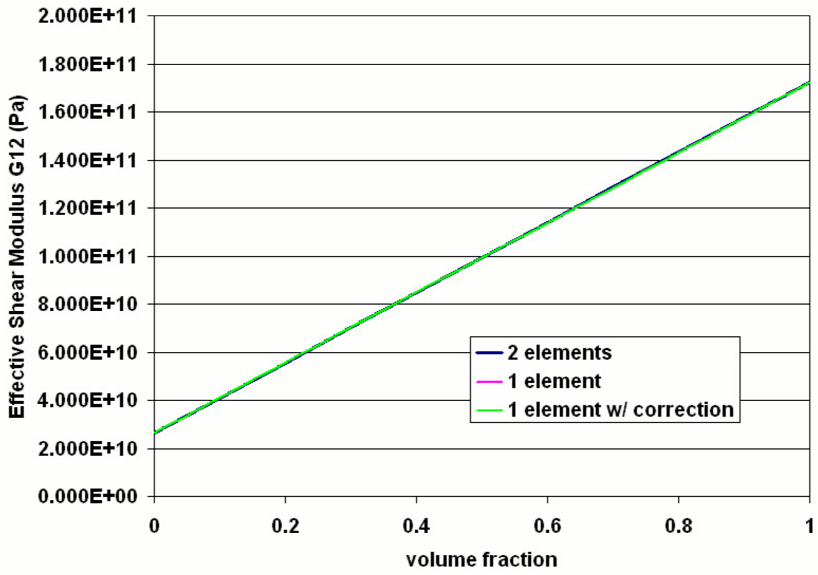

Figure 4.9: Effective G_{12} results

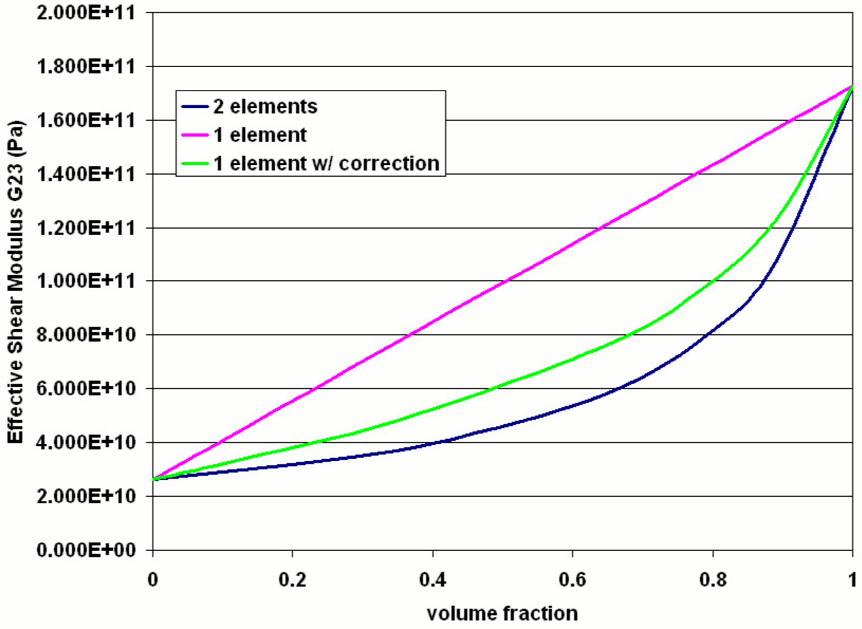

Figure 4.10: Effective G_{23} results

CHAPTER 5

SINGLE FIBER MODELS

In this chapter, the uniform mesh method will be used to predict the elastic properties of two single fiber models from literature. The first is a continuous fiber model used by Xia et al. [29] and the second is a short fiber model using using two different packing arrangements similar to that of Tucker and Liang [4]. The results of the uniform mesh method will be compared with the literature as well as a conventional finite element model developed in ABAQUS 6.5. For the short fiber models, the results will also be compared with the Halpin-Tsai and Tandon-Weng micromechanical models.

5.1 Continuous Fiber Comparison

Xia et al. [29] used a single fiber RVE to model a unidirectional continuous fiber composite laminate consisting of an aluminum matrix and boron fibers. The results of Xia et al. will be compared with a conventional finite element model and a uniform mesh model. A conventional finite element model was developed in ABAQUS in order to validate the periodic boundary conditions and effective property calculations developed in Chapter 2. The conventional and uniform finite element meshes is shown in figure 5.1. The conventional mesh consists of 1640 linear eight node elements and the uniform mesh consists of 1000 custom eight node elements.

Notice, that the two meshes are periodic and that the planar nodal coordinates are equal for nodes on opposite boundaries. More specifically, the y and z coordinates are equivalent for nodes on the positive and negative x boundaries and similar arguments

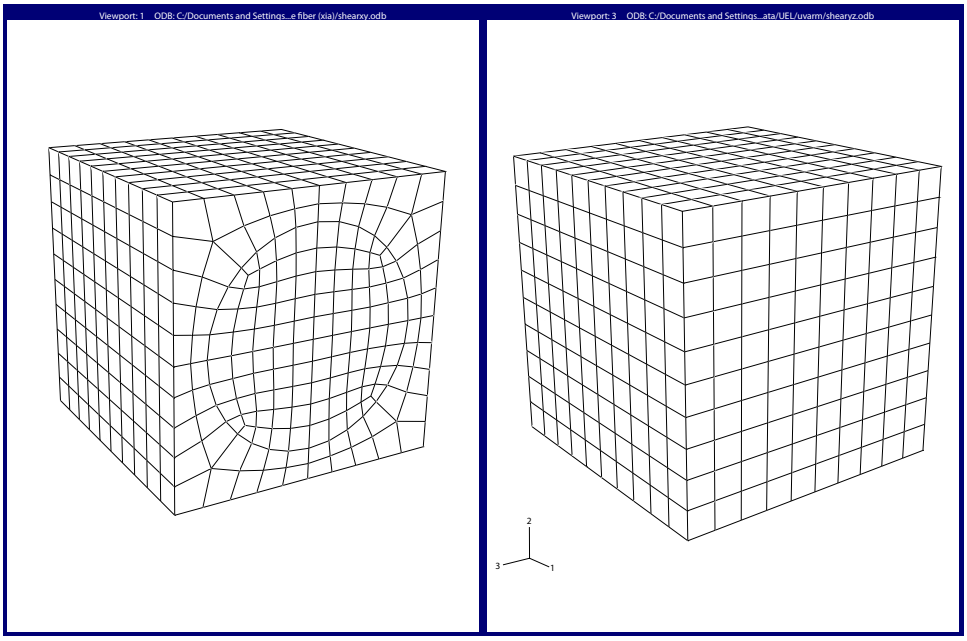

Figure 5.1: a)Conventional and b)uniform meshes for the continuous fiber model

can be made for nodes on the y and z boundaries. As described in Chapter 2, this is required for the periodic boundary conditions. However, even for this simple fiber model, it was very difficult to obtain an appropriate mesh. This is overcome by the uniform mesh method that simply uses a regular array of elements.

The material properties used in the model are given in table 5.1 and $v_f = 0.47$.

$Material$	$E(GPa)$	ν
$Boron$	379.3	0.1
$Aluminum$	68.3	0.3

Table 5.1: Elastic properties of matrix and fiber [1]

As described in Chapter 3, the effective properties are found by applying six independent strain conditions through the periodic boundary conditions. Due to the geometry of the model, similar stress and strain results are obtained for the x_2 and

x_3 directions. Therefore, the stress and strain contour plots will only be given for the x_1 and x_3 strain conditions.

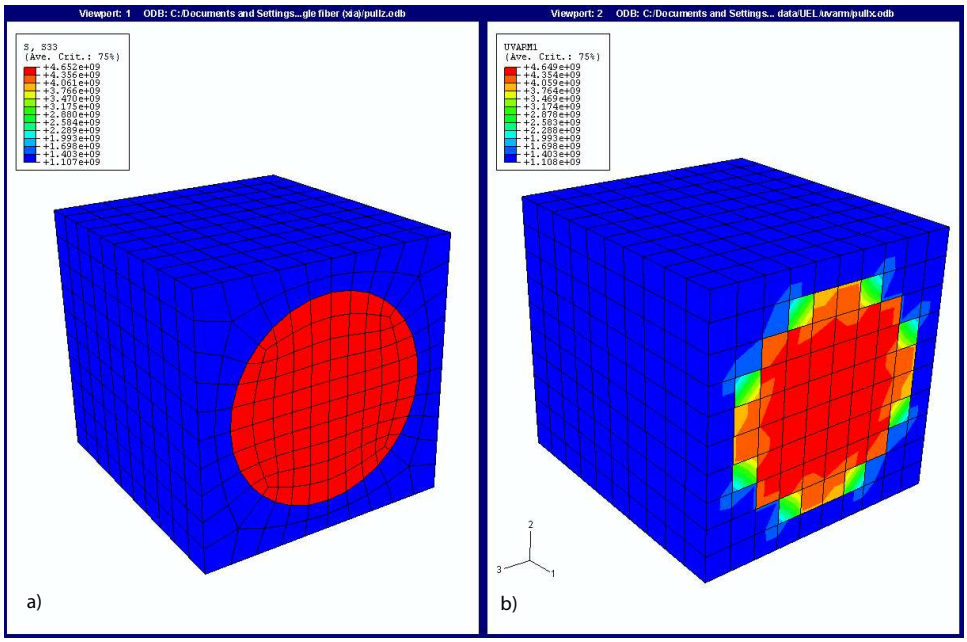

Figure 5.2: σ_{11} contour plots for a)conventional and b)uniform mesh continuous fiber models

The stress contour results for the axial strain condition are given in figures 5.2,5.3. These figures show that the axial strain condition results in boundaries that remain planer during deformation. This is due to the fact that the boundaries of the single fiber RVE in figure 5.1 are planes of symmetry for the axial strain conditions. It is also shown that transverse stresses are induced in the RVE during the axial stain. In order to ensure no overlap between neighboring RVE's, zero relative displacement between transverse boundaries is specified. Without the zero relative displacement conditions, necking would occur around the edges of the fiber, resulting in separation between adjacent RVEs.

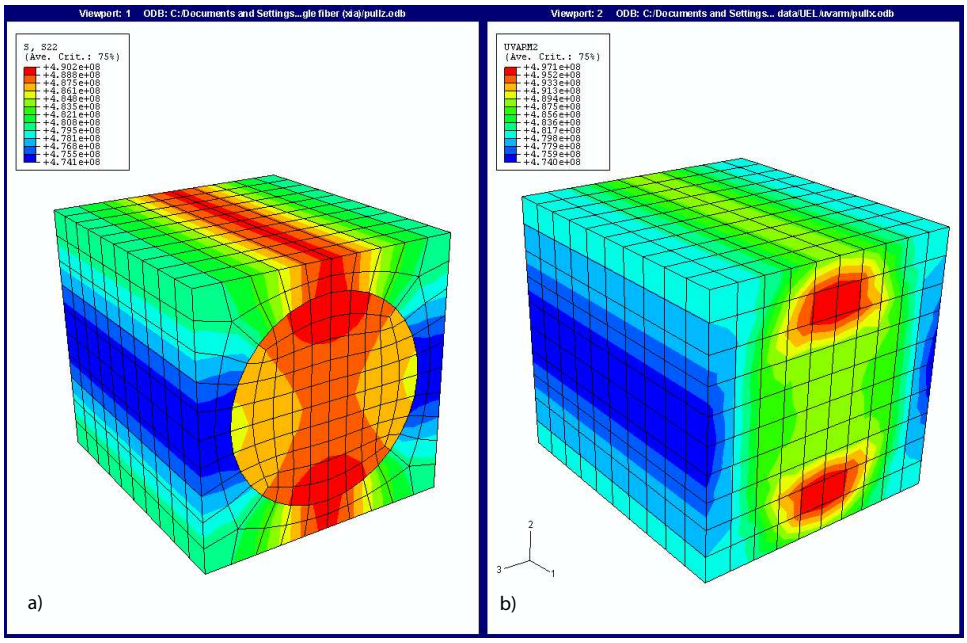

Figure 5.3: σ_{22} contour plots for a)conventional and b)uniform mesh continuous fiber models

The stress and strain for the longitudinal and transverse shear conditions are plotted in figures 5.4-5.7. The deformations appearing in these figures illustrate that the periodic boundary conditions do satisfy the stress and strain periodicity conditions of equation 3.50 in that the stress and strain are equal on opposite boundary conditions. From figures 5.4 through 5.7 it can also be seen that for the shear conditions, the boundaries do not remain plane.

The results for the effective properties of the composite are given in table 5.2 along with the results from Xia et al. [29] and Sun and Vaidya [1]. The results from the uniform mesh method are given using 6, 8, and 10 gauss points per element. From the table it is shown that the conventional element results are in agreement with the literature, thus validating the periodic boundary conditions and solution

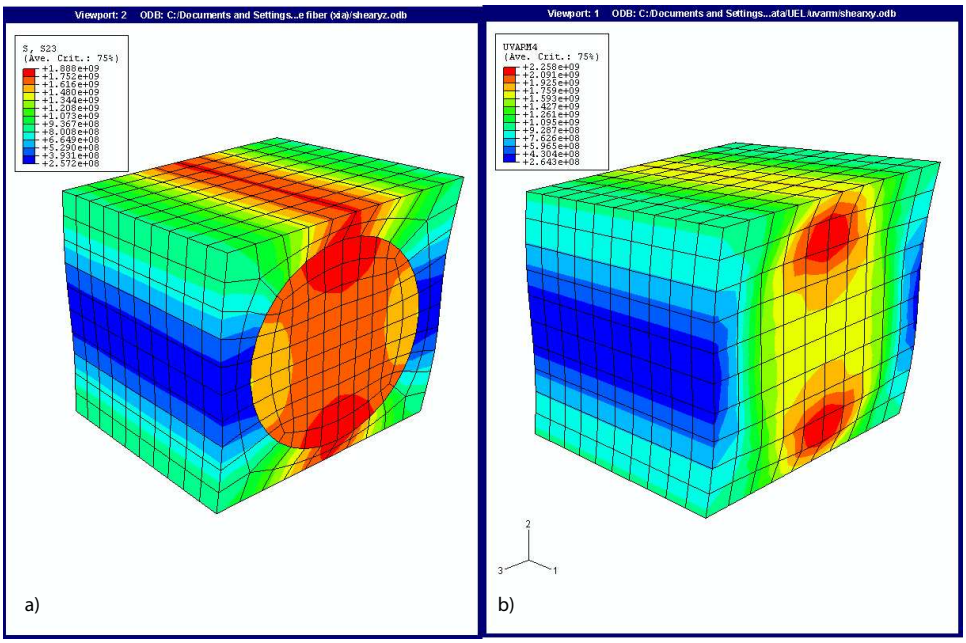

Figure 5.4: σ_{12} contour plots for a)conventional and b)uniform mesh continuous fiber models

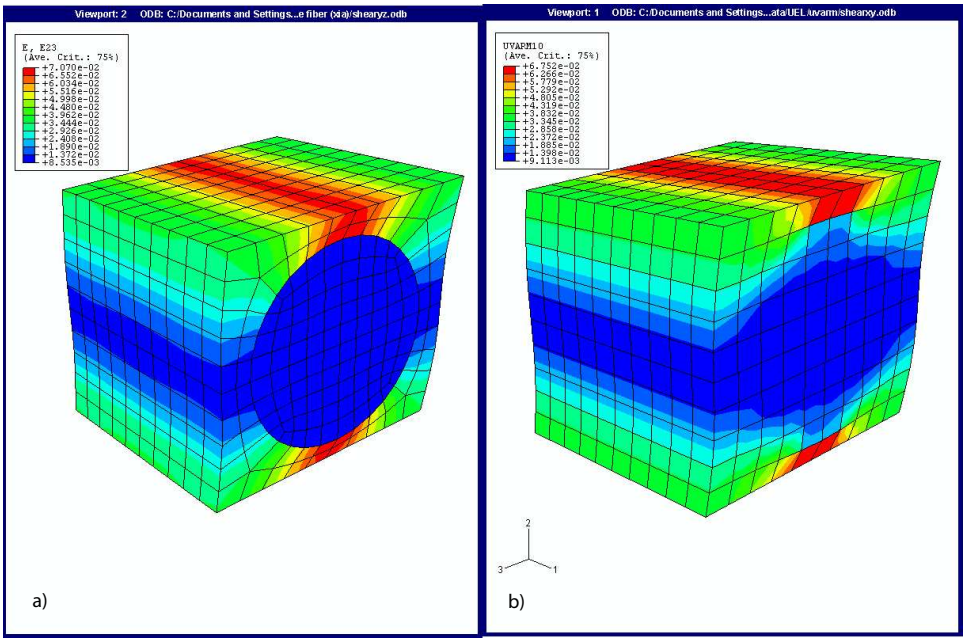

Figure 5.5: ε_{12} contour plots for a)conventional and b)uniform mesh continuous fiber models

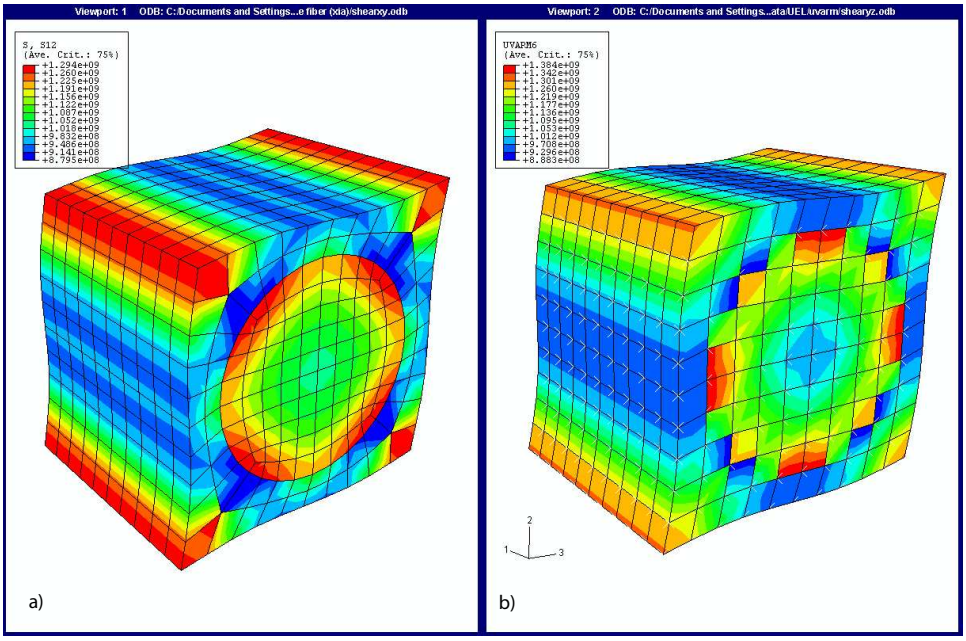

Figure 5.6: $\sigma 23$ contour plots for a)conventional and b)uniform mesh continuous fiber models

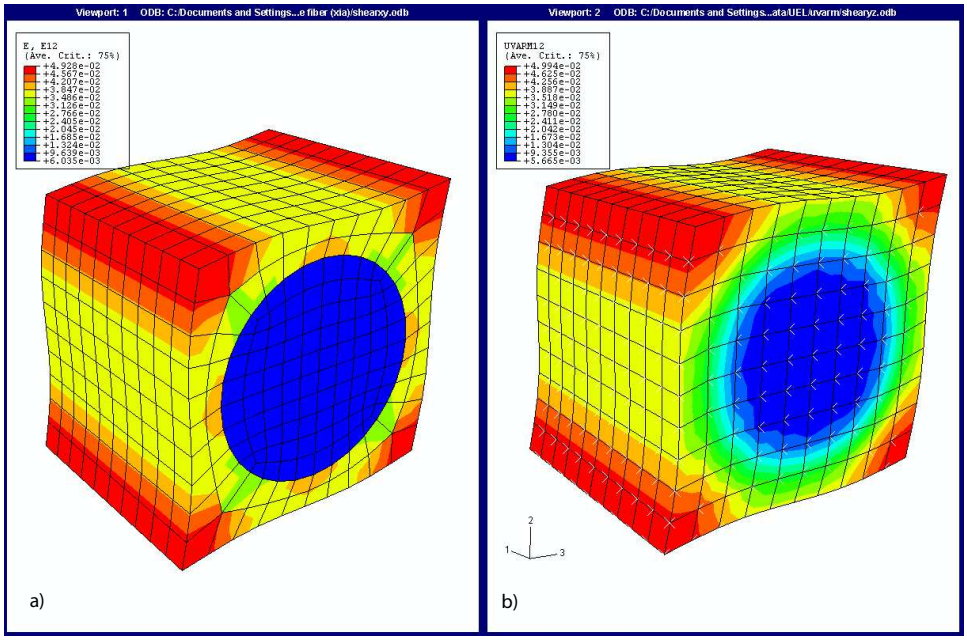

Figure 5.7: ε_{23} contour plots for a) conventional and b) uniform mesh continuous fiber models

process. The uniform mesh method results are slightly higher than the conventional mesh results but the error remains within a few percent. The error also decreases with an increasing number of gauss points as expected. The uniform mesh method provides a reasonable result for the transverse shear modulus G_{12}. Although hybrid elements will overpredict G_{12}, a relatively fine mesh was used for the current analysis, thus only a small percent of the total elements contained both fiber and matrix.

Elastic constants	*Xia et al.*	*Sun and Vaidya*	*Conventional mesh*	*Uniform mesh 6gp*	*Uniform mesh 8gp*	*Uniform mesh 10gp*
$E_{11}\,(GPa)$	214	215	214.4	216.1	215.5	215.9
$E_{22}\,(GPa)$	143	144	143.7	147	144.9	146.7
$G_{12}\,(GPa)$	54.2	57.2	53.9	56.4	57.4	56.3
$G_{23}\,(GPa)$	45.7	45.9	45.4	45.6	46	45.6
ν_{12}	0.195	0.19	0.195	0.194	0.196	0.194
ν_{23}	0.253	0.29	0.253	0.244	0.238	0.244

Table 5.2: Effective elastic property results for the continuous fiber model

5.2 Short Fiber Comparison

Tucker and Liang [4] used a single short fiber RVE to model short fiber composites with several different packing arrangements over a range of aspect ratios and compared them with numerous micromechanical models. The regular and staggered packing arrangements were chosen and conventional and uniform mesh models were developed for an aspect ratio of 8. These models will then be compared with the results of Tucker and Liang as well as the Halpin-Tsai and Tandon-Weng micromechanical models. The conventional and uniform meshes for the regular and staggered packing arrays are shown in figures 5.8 and 5.9 respectively.

Although Tucker and Liang [4] used a one-quarter model for the regular array, a full model is used in this analysis in order to apply the periodic boundary conditions. The periodic boundary conditions will make it possible to calculate the effective shear moduli which were not calculated by Tucker and Liang for a regular array. A one-quarter model is used on the staggered array and symmetry boundary conditions are applied as was done by Tucker and Liang. Therefore, the shear moduli will not be calculated for the staggered array. The symmetry boundary conditions are given in

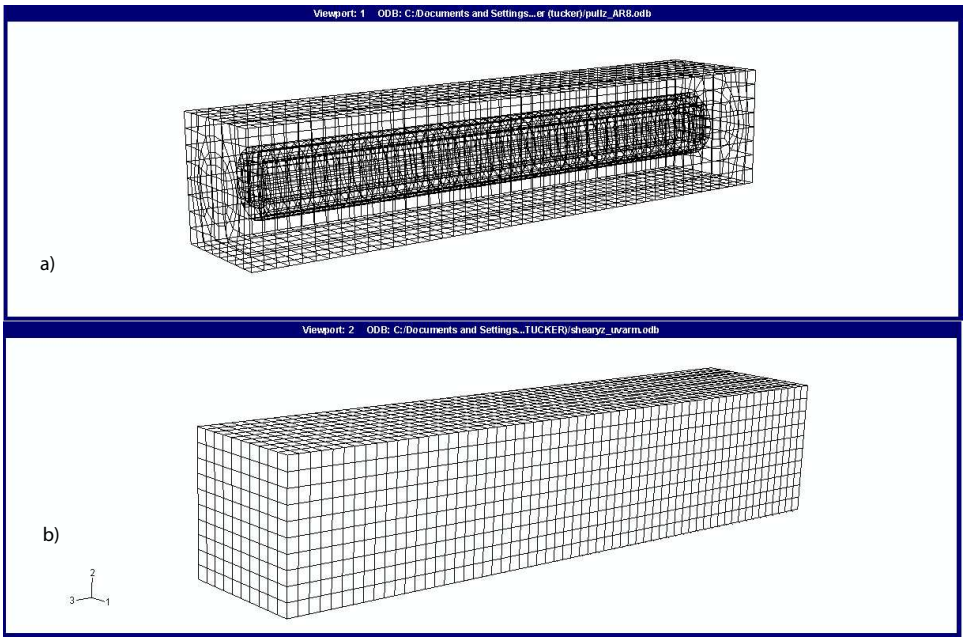

Figure 5.8: a)Conventional and b)uniform meshes for the regular short fiber model

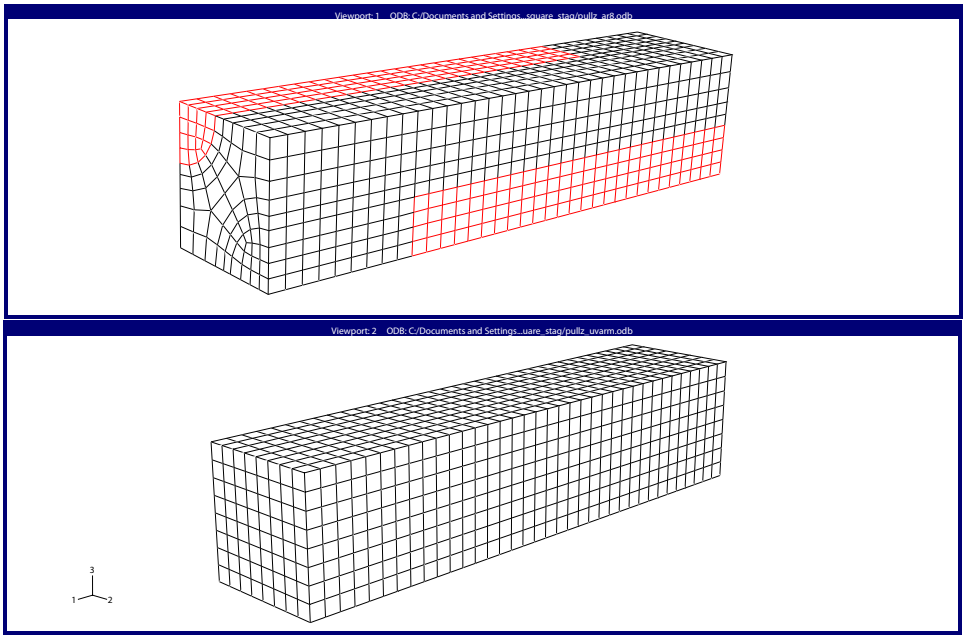

Figure 5.9: a)Conventional and b)uniform meshes for the staggered short fiber model

equation 5.1.

$$
\begin{aligned}
\text{set 1}: \quad & u(0,l_y,l_z)=0 \;\; v(l_x,0,l_z)=0 \;\; w(l_x,l_y,0)=0 \\
& u(l_x,l_y,l_z)=0.05l_x \;\; v(l_x,l_x,l_z)=0 \;\; w(l_x,l_y,l_z)=0 \\
\text{set 2}: \quad & u(0,l_y,l_z)=0 \;\; v(l_x,0,l_z)=0 \;\; w(l_x,l_y,0)=0 \\
& u(l_x,l_y,l_z)=0 \;\; v(l_x,l_x,l_z)=0.05l_y \;\; w(l_x,l_y,l_z)=0 \\
\text{set 3}: \quad & u(0,l_y,l_z)=0 \;\; v(l_x,0,l_z)=0 \;\; w(l_x,l_y,0)=0 \\
& u(l_x,l_y,l_z)=0 \;\; v(l_x,l_x,l_z)=0 \;\; w(l_x,l_y,l_z)=0.05l_z
\end{aligned}
\tag{5.1}
$$

The material properties used in the models are given in table 5.3 at a volume fraction $v_f = 0.2$ and aspect ratio $l/d = 8$.

$Material$	$E(GPa)$	ν
$Fiber$	300	0.2
$Matrix$	10	0.38

Table 5.3: Elastic properties of matrix and fiber for single short fiber model

The contour plots for the longitudinal strain case for the two models are given in figures 5.10,5.11,5.12 and 5.13 and longitudinal shear results for the regular array are given in figures 5.14 and 5.15. From the figures, it can be seen that stress and strain periodicity is again satisfied and the boundaries do not remain plane during shear. Figures 5.10-5.13 also show the effect of the fiber array on the stress and strain. The stress and strain fields are fairly uniform over the fiber in the regular array. For the staggered array, the stress and strain are at a minimum at the center where the fibers are staggered and the stress and strain increase in the regions where the fibers are not staggered as expected.

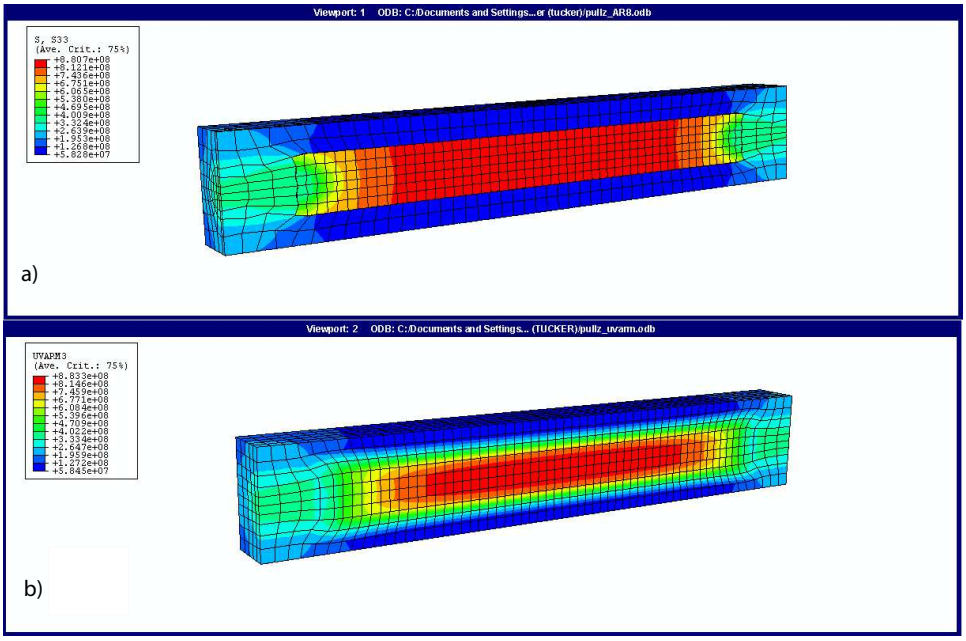

Figure 5.10: σ_{11} results for the regular array under longitudinal strain using a a) conventional and b) uniform mesh

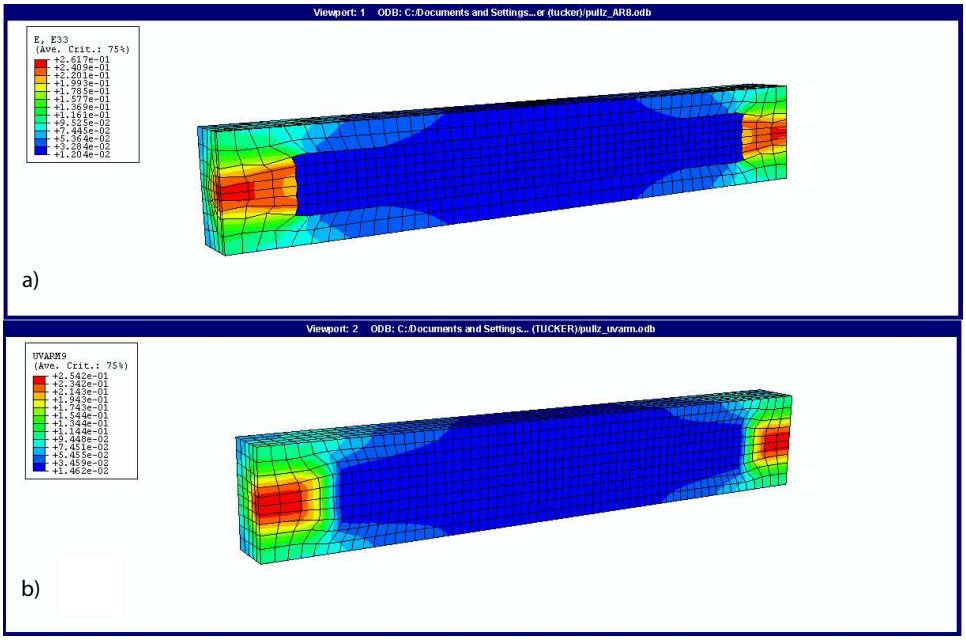

Figure 5.11: ε_{11} results for the a)regular array under longitudinal strain using a a) conventional and b) uniform mesh

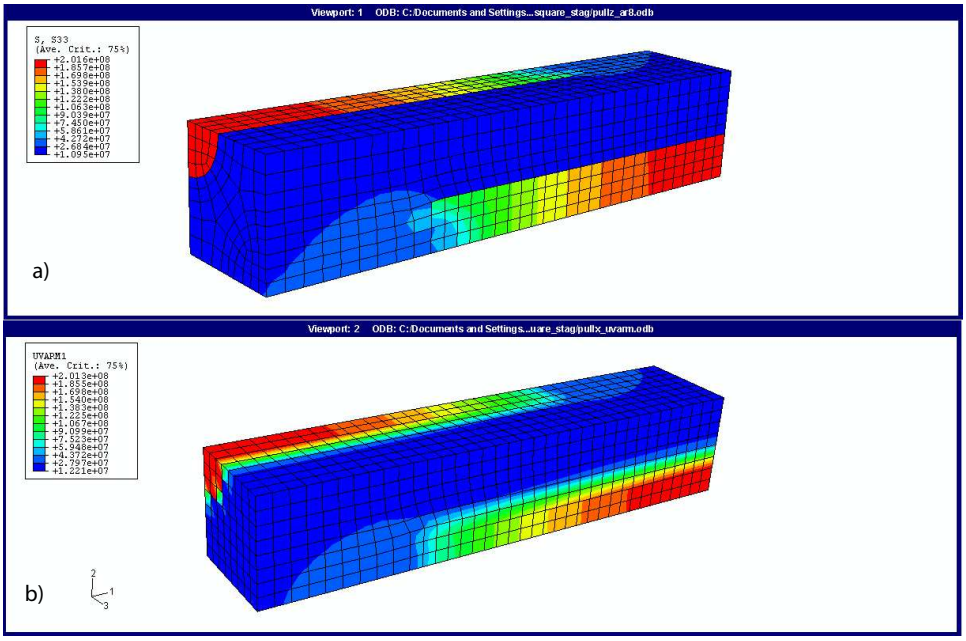

Figure 5.12: σ_{11} results for the staggered array under longitudinal strain using a a) conventional and b) uniform mesh

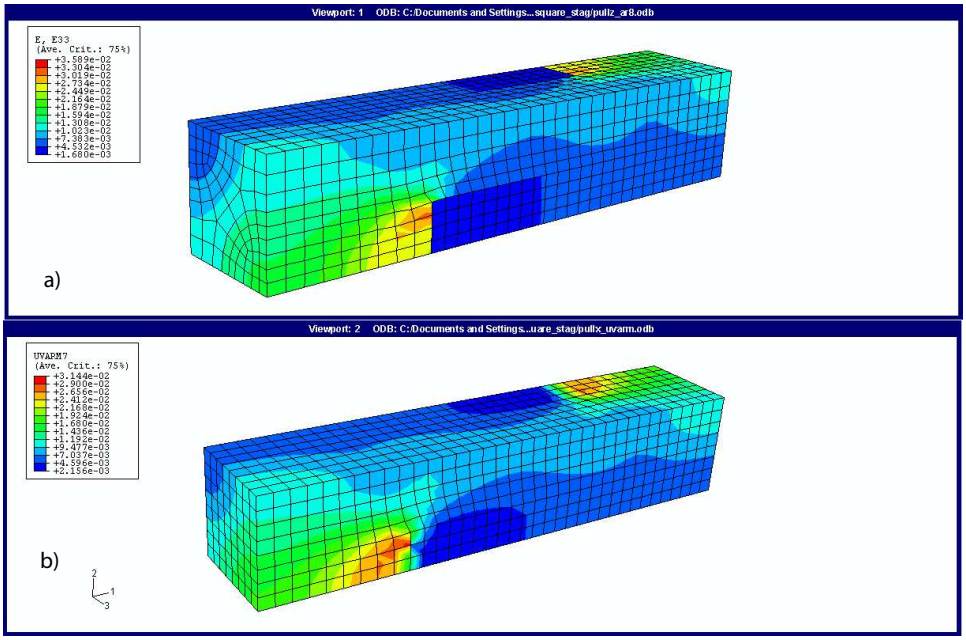

Figure 5.13: ε_{11} results for the staggered array under longitudinal strain using a a) conventional and b) uniform mesh

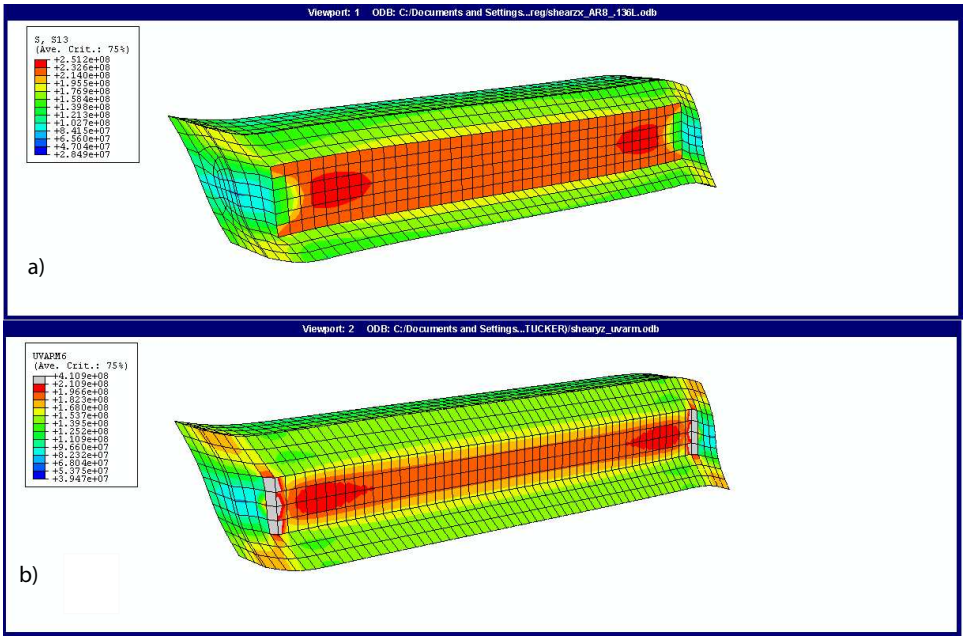

Figure 5.14: σ_{12} results for the staggered array under shear strain using a a) conventional and b) uniform mesh

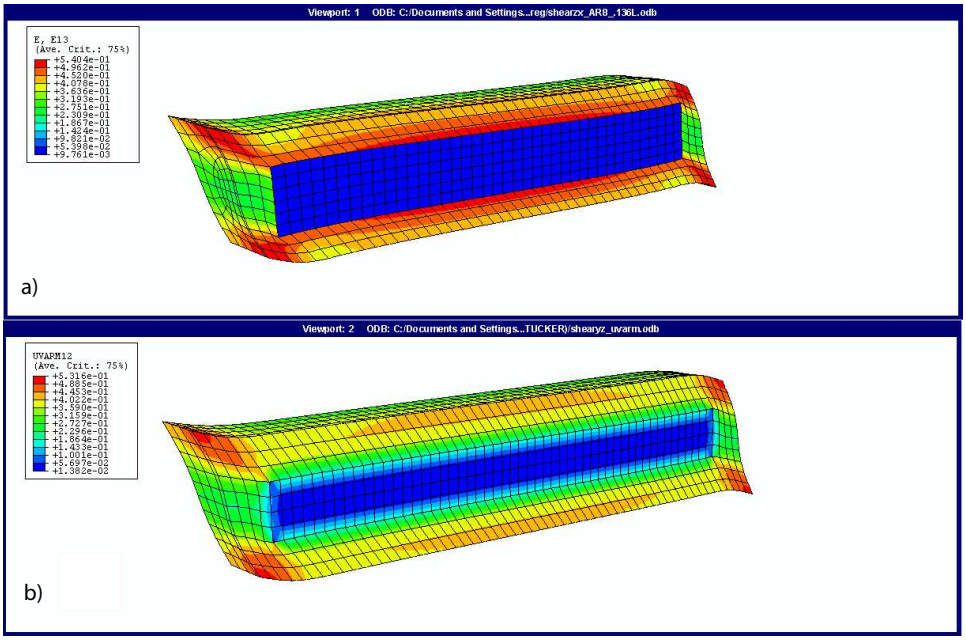

Figure 5.15: ε_{12} results for the staggered array under shear strain using a a) conventional and b) uniform mesh

The effective property results for the two models are given in tables 5.4 and 5.5 along with the results of Tucker and Liang [4]. The effective properties calculated using the Halpin-Tsai and Tandon-Weng micromechanical models are also given. All the results are given assuming the fiber is aligned with the x_1 direction.

Elastic constants	*Tucker & Liang*	*Halpin Tsai*	*Tandon Weng*	*Conv. mesh*	*Uniform mesh 6gp*	*Uniform mesh 8gp*	*Uniform mesh 10gp*
E_{11}/E_m	4.2	3.45	3.37	3.97	4.11	4.06	4.04
E_{22}/E_m	1.55	1.66	1.51	1.62	1.72	1.67	1.67
G_{12}/E_m	n/a	0.53	0.54	0.53	0.55	0.54	0.53
G_{23}/E_m	n/a	0.50	0.51	0.49	0.48	0.48	0.48
ν_{12}	0.335	0.344	0.362	0.338	0.333	0.338	0.338
ν_{23}	0.48	0.652	0.49	0.487	0.467	0.471	0.471

Table 5.4: Effective property results for the regular packing array

Elastic constants	*Tucker & Liang*	*Halpin Tsai*	*Tandon Weng*	*Conv. mesh*	*Uniform mesh 6gp*	*Uniform mesh 8gp*
E_{11}/E_m	4.2	3.45	3.37	4.07	4.18	4.19
E_{22}/E_m	1.5	1.66	1.51	1.51	1.56	1.56
G_{12}/E_m	n/a	0.53	0.54	n/a	n/a	n/a
G_{23}/E_m	n/a	0.50	0.51	n/a	n/a	n/a
ν_{12}	0.345	0.344	0.362	0.347	0.343	0.343
ν_{23}	0.52	0.652	0.49	0.522	0.513	0.515

Table 5.5: Effective property results for the staggered packing array

Table 5.4 shows that the conventional mesh provides results for E_{11} slightly lower than those givein in Tucker and Liang [4] and results for E_{22} that are slightly higher. The results using the uniform mesh and 6 gauss points are slightly higher than the conventional mesh. The largest error occurs in the prediction for E_{22} and is approximately 6%. By increasing the number of gauss points to 8, the uniform mesh results approach that of the conventional mesh and the error for E_{22} is reduced to around

3%. The Halpin-Tsai and Tandon-Weng micromechanical models underpredict E_{11}. The Halpin-Tsai prediction for E_{22} is close to that using the conventional and uniform meshes, while the Tandon-Weng prediction for E_{22} is close to the Tucker and Liang result. Both models provide similar results for the shear moduli and are in close agreement with the conventional and uniform mesh results. The Halpin-Tsai and Tandon-Weng models slightly overpredict ν_{12} with Halpin-Tsai providing the better prediction. The Tandon-Weng model provides a very good prediction for ν_{23} while the Halpin-Tsai result for ν_{23} is over 30% higher than the other models.

Table 5.5 gives the results using the staggered array. The conventional and uniform mesh results are in very good agreement with the Tucker and Liang results for the staggered array. Table 5.5 shows that the packing array does have an effect on the effective properties of the composite. Tucker and Liang's results for the Poisson's ratios increase slightly for the staggered array. The conventional and uniform mesh results also predict a slight increase in the Poisson's ratios as well as E_{11}. The conventional and uniform mesh results also show a slight decrease in E_{22}. Note that the Halpin-Tsai and Tandon-Weng results are independent of the packing arrangement due to their inability to account for the spatial distribution of the fibers. It also worth noting that all of the models predict a transverse Poisson's ratio ν_{23} greater than 0.5. Although the Poisson's ratio for isotropic materials must be less than 0.5, the Poisson's ratios for orthotropic materials may exceed this value and the limiting values are dependent upon the ratio of the Young's moduli [57].

5.3 Uniform Mesh Convergence Analysis

A convergence analysis of the uniform mesh elements was run by predicting the effective properties of a multiple fiber composite model using an increasing number of elements and gauss points. By investigating the convergence of the uniform mesh elements, the maximum element size and minimum number of gauss points needed to obtain reliable results can be determined. The multiple fiber model was created by forming a 5x5 array of continuous fiber RVEs as shown in figure 5.16. Since the RVE is periodic and periodic boundary conditions are used, the effective properties of the 5x5 array of continuous fibers will be equivalent to the effective properties of the single RVE given in table 5.2.

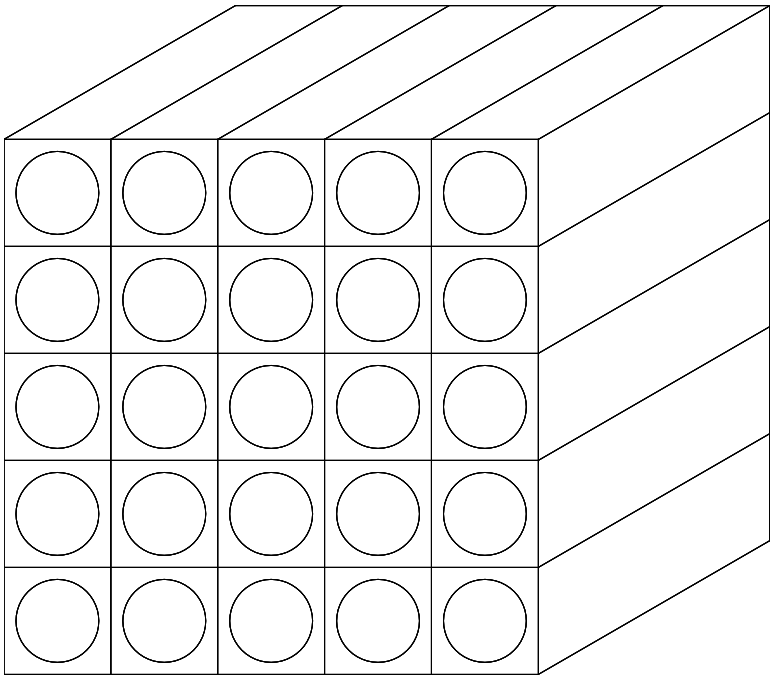

Figure 5.16: Continuous fiber model used in the convergence analysis

The continuous fiber composite was modeled with 2,3,5,6 and 7 uniform mesh

elements in each direction using between 2 and 20 Gauss points. The results for the effective properties are given in figures 5.17-5.22. The total number of elements used and the size of the element relative to the fiber diameter are given in the figures.

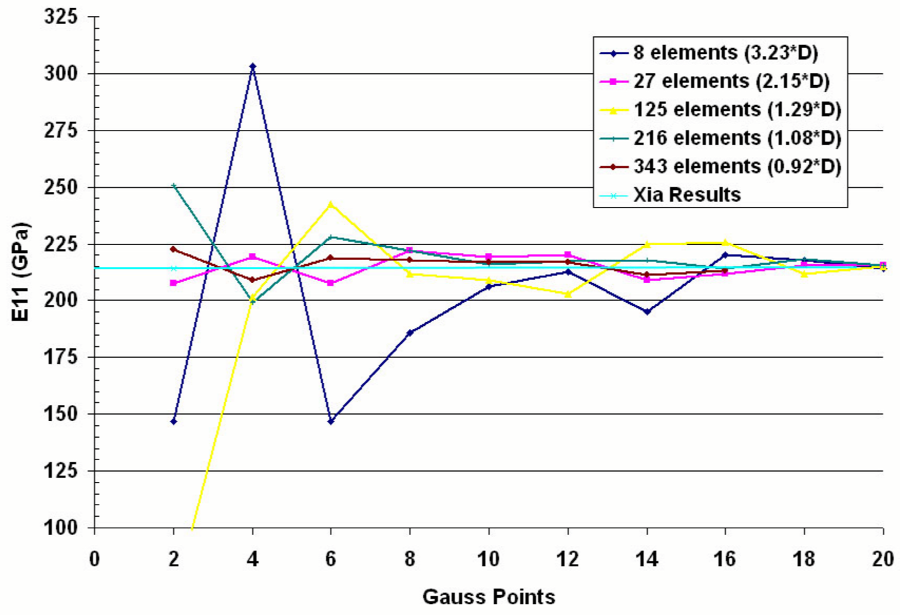

Figure 5.17: E_{11} convergence

The figures show the uniform mesh results oscillate about the actual solution. The effective properties are highly dependent upon the volume fraction of the composite. The uniform mesh method determines the volume fraction based on the number of Gauss points that lie within the fiber and is given in equations 3.60 and 3.61. Varying the number of Gauss points changes the total number of Gauss points that lie within fiber, resulting in a change in the volume fraction. Since the Gauss points are not uniformly distributed across the element, an increase in the number of Gauss points could lead to a decrease in the volume fraction and the opposite is also true. This causes the oscillations in the effective properties shown in the figures. However,

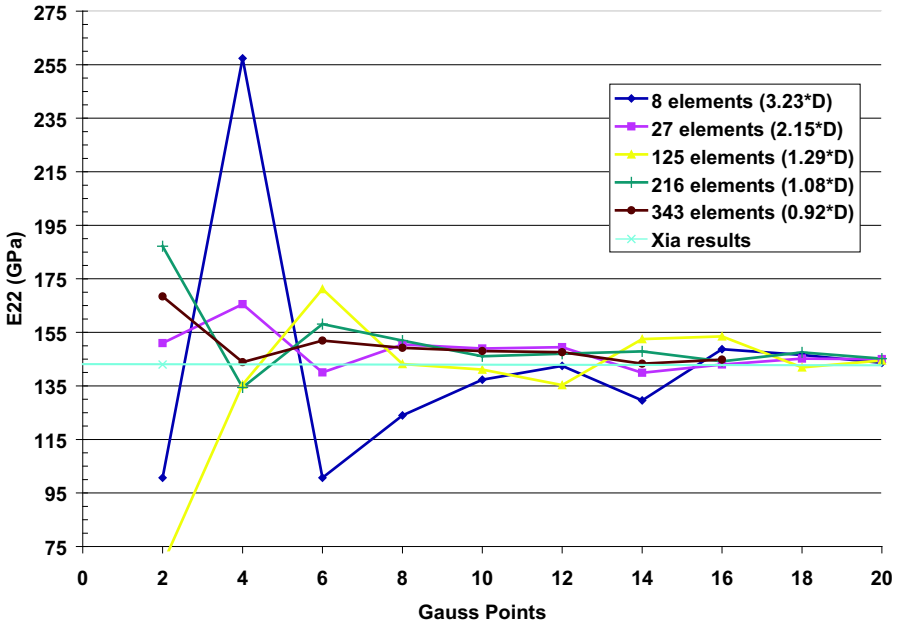

Figure 5.18: E_{22} convergence

by increasing the number of Gauss points and elements, the volume fraction will eventually approach the actual volume fraction and the solution will converge. All of the effective properties converge to the actual solution except G_{12} which converges to a value slightly higher than the actual. This was expected due to the correction factors inability to accurately predict the longitudinal modulus.

Figures 5.17-5.22 show that either a large number of elements with few Gauss points can be used or a large number of Gauss points with few elements. Increasing the number of elements increases the amount of computer memory needed to run the analysis, but increasing the number of Gauss points greatly increases the computational time. The amount of computational time needed to run an analysis is plotted versus the number of elements and Gauss points in figure 5.23.

Figure 5.23 shows that the number of Gauss points has a greater effect on the

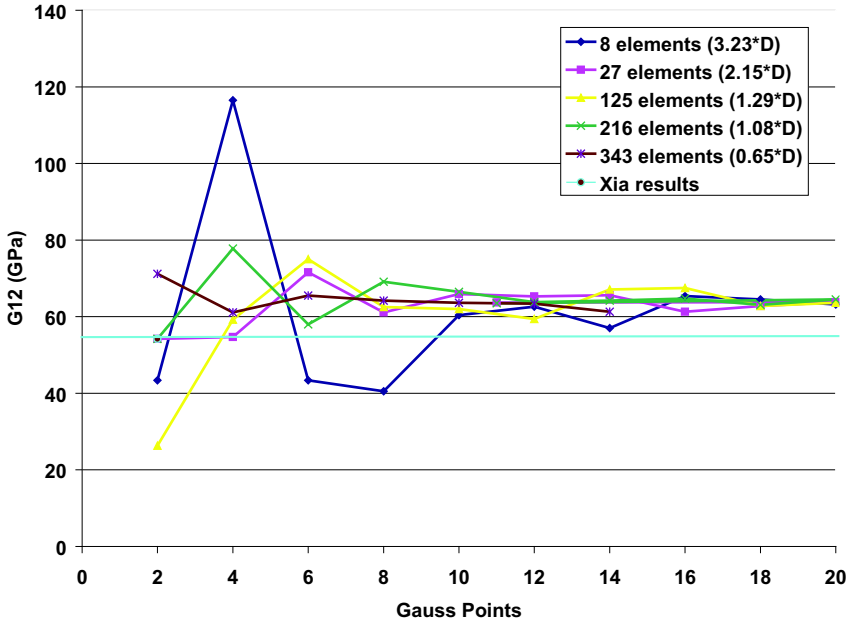

Figure 5.19: G_{12} convergence

computational time than the number of elements. The computational time shows approximately a linear dependence on the number of elements. Therefore, doubling the number of elements approximately doubles the computational time. However, increasing the number of Gauss points from 6 to 10 approximately triples the computational time. Therefore, the number of Gauss points should be kept to a minimum. From figures 5.17,5.18,5.19,5.20,5.21 and 5.22 it is seen that when the element is approximately the size of the fiber, the solution remains within a few percent of the actual when using 8 or more Gauss points.

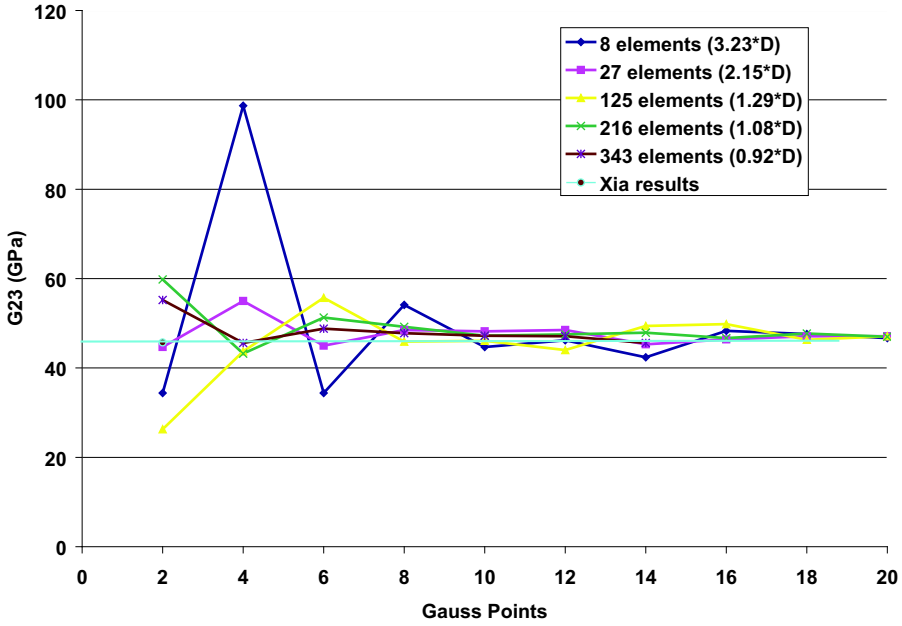

Figure 5.20: G_{23} convergence

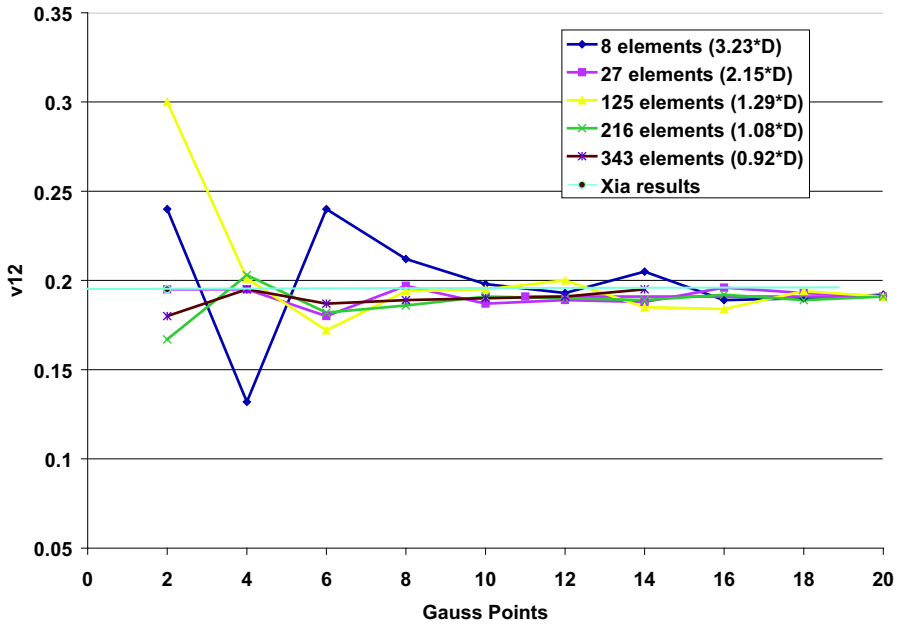

Figure 5.21: ν_{12} convergence

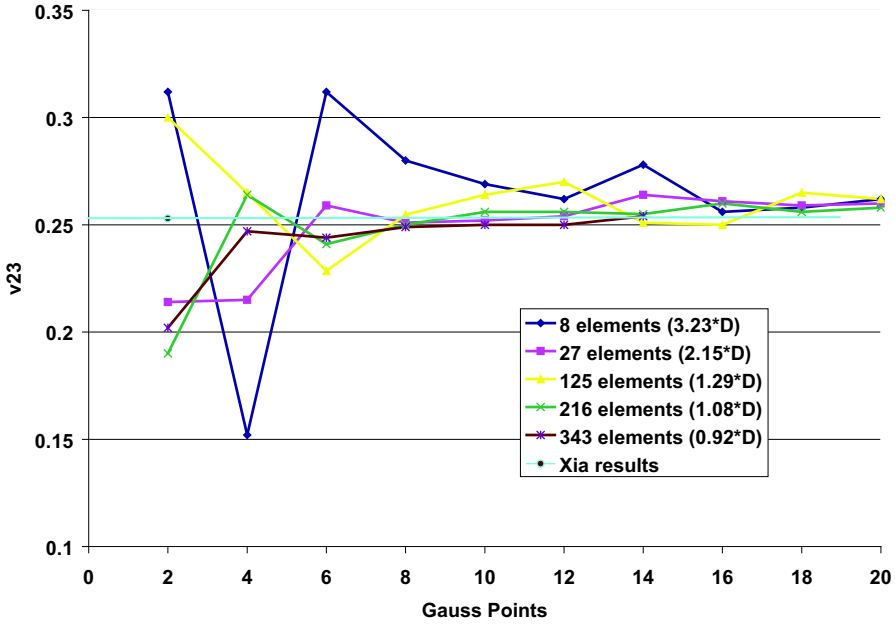

Figure 5.22: ν_{23} convergence

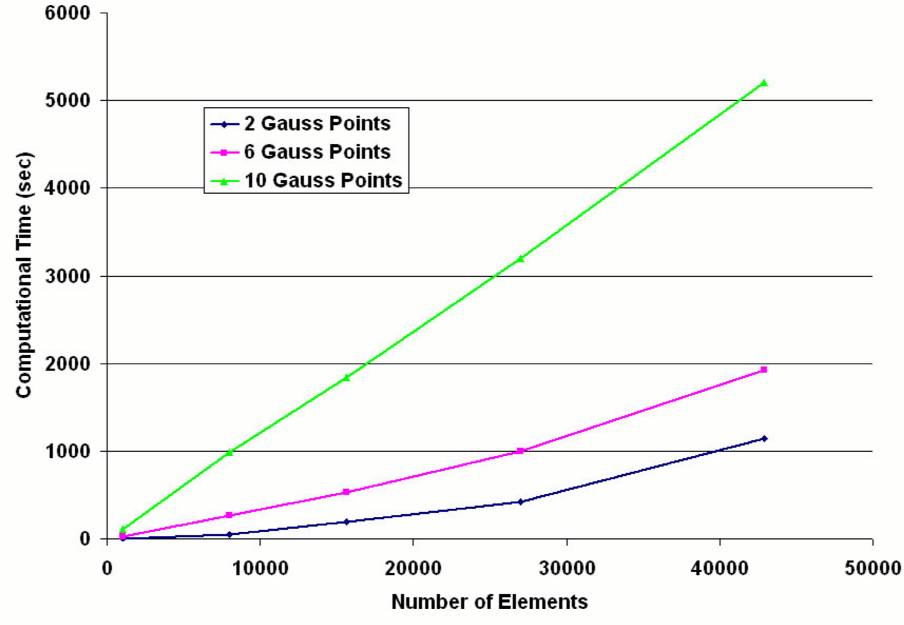

Figure 5.23: Computational time

CHAPTER 6

MULTIPLE FIBER MODELS

The single fiber models are limited because they can only be used to model fully aligned composites with a uniform array of fibers. However, real injected molded composites will always contain a certain degree of misalignment and the fibers are randomly dispersed throughout the matrix. Therefore, multiple fiber RVE's must be used to account for the fiber orientation and arrangement of real composites. In this chapter, a composite with an assumed fiber orientation distribution function will be modeled over a range of fiber volume fractions using the finite element method and the results will be compared with an orientation averaging scheme.

6.1 Fiber Orientation

In order to model the orientation of a real injection molded composite, a way of characterizing the orientation must first be specified. If one assumes the fibers are rigid cylinders, uniform in length and diameter, and that the fibers are spatially uniform, then the orientation of a single fiber is defined by the angles ϕ and θ as shown in figure 3.6 [20]. The orientation state at a point in the composite can be characterized in terms angles by a probability distribution function $\psi(\theta, \phi)$ or in terms of the fiber unit vector, $\bar{p}$ as $\psi(\bar{p})$, where $\bar{p}$ is given in equation 3.54 [20]. A more convenient way of representing the fiber orientation is through orientation tensors, $a_{ij..}$, which are defined as

$$a_{ij..} = \oint p_i p_j .. \psi(\bar{p}) d\bar{p} \tag{6.1}$$

As described in Chap. 2, the effective properties of a misaligned composite can be found through a two step homogenization procedure [20–22] as shown in figure 6.1. This is done by first decomposing the composite into a set of fully aligned cells

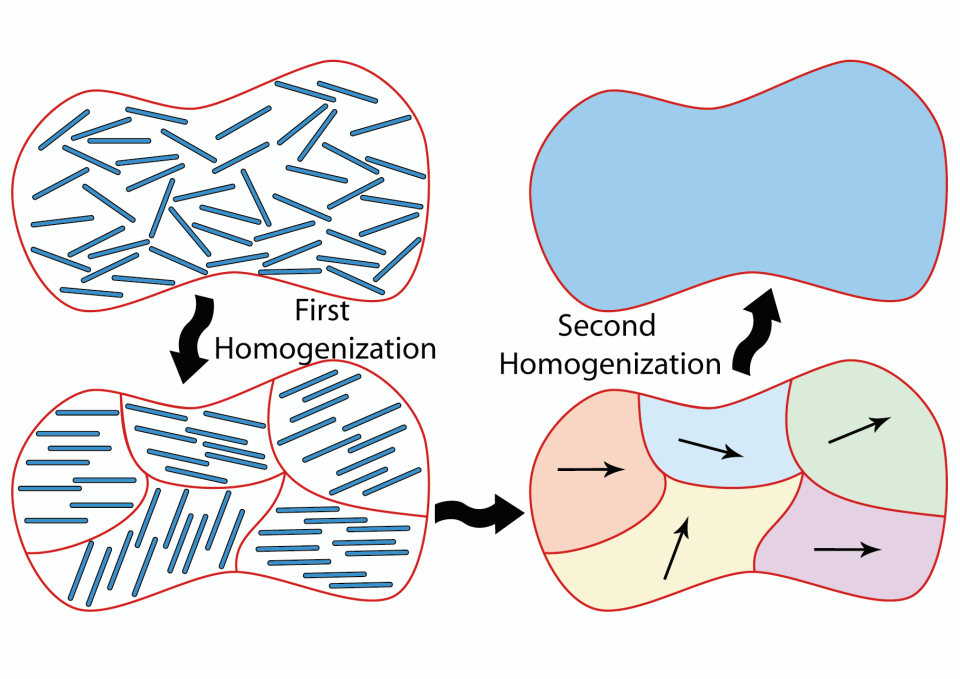

Figure 6.1: Two step homogenization procedure taken from Jack and Smith [2]

or aggregates containing the same volume fraction as the composite. Each aggregate is then homogenized using an appropriate micromechanical model discussed in Chap. 2. The second step involves homogenizing the aggregates into a single anisotropic material by performing an orientation average. The second step is done assuming a distribution of stress and strains between the aggregates.

Advani and Tucker [20] derived an orientation average of the effective stiffness

tensor, $\langle C_{ijkl} \rangle$, in terms of the second and fourth order orientation tensors as:

$$\langle C_{ijkl} \rangle = B_1 a_{ijkl} + B_2(a_{ij}\delta_{kl} + a_{kl}\delta_{ij}) + B_3(a_{ik}\delta_{jl} + a_{il}\delta_{jk} + a_{jk}\delta_{il} + a_{jl}\delta_{ik}) + B_4(\delta_{ij}\delta_{kl}) + B_5(\delta_{ik}\delta_{jl} + \delta_{il}\delta_{jk}) \quad (6.2)$$

where the constants, B_i, are related to the unidirectional stiffness components, C'_{ij}, through the following [20]

$$\begin{aligned} B_1 &= C'_{11} + C'_{22} - 2C'_{12} - 4C_{66} \\ B_2 &= C'_{12} - C'_{23} \\ B_3 &= C'_{66} + 1/2(C'_{23} - C'_{22}) \\ B_4 &= C'_{23} \\ B_5 &= 1/2(C'_{22} - C'_{23}) \end{aligned} \quad (6.3)$$

Expressions for $\langle C_{ijkl} \rangle$ have also been derived by first rotating the homogenized stiffness tensor of a single aggregate in the local coordinate system to the global composite coordinate system using the following expression [21]

$$C^{(n)}_{ijkl} = Q_{qi}(\theta_n, \phi_n) Q_{rj}(\theta_n, \phi_n) Q_{sk}(\theta_n, \phi_n) Q_{tl}(\theta_n, \phi_n) C'_{qrst} \quad (6.4)$$

where $\mathbf{Q}(\theta, \phi)$ is the rotation tensor and is given by

$$\mathbf{Q}(\theta, \phi) = \begin{bmatrix} \sin\theta cos\phi & \sin\theta\sin\phi & \cos\theta \\ -\sin\phi & \cos\phi & 0 \\ -\cos\theta\cos\phi & -\cos\theta\sin\phi & \sin\theta \end{bmatrix} \quad (6.5)$$

Assuming constant strain between the aggregates, the mean effective stiffness tensor, m_{ijkl} can be found by summing the stiffness of the rotated aggregates [2]

$$m_{ijkl} = \frac{1}{N} \sum_{n=1}^{N} \left(Q_{qi}(\theta_n, \phi_n) Q_{rj}(\theta_n, \phi_n) Q_{sk}(\theta_n, \phi_n) Q_{tl}(\theta_n, \phi_n) C'_{qrst} \right) \quad (6.6)$$

where N is the number of units or aggregates. Jack and Smith [2] have shown that as $N \rightarrow \infty$ then the mean, m_{ijkl}, approaches the orientation average

$$\langle C_{ijkl} \rangle = \oint Q_{qi}(\theta_n, \phi_n) Q_{rj}(\theta_n, \phi_n) Q_{sk}(\theta_n, \phi_n) Q_{tl}(\theta_n, \phi_n) C'_{qrst} \psi(\theta, \phi) dS \qquad (6.7)$$

6.1.1 Monte Carlo Algorithm

The fiber angles were obtained using a Monte Carlo algorithm to generate random angle pairs (θ_n, ϕ_n) sampled from a given orientation distribution function. An Accept-Reject Generation Algorithm is used in order to ensure the random angle pairs accurately represent the fiber orientation distribution function as was done by Jack and Smith [2]. Once the fiber angles have been generated, they are then randomly placed inside a periodic box. A Monte Carlo algorithm was also used for the fiber placement and a flowchart of the algorithm is shown in figure 6.2.

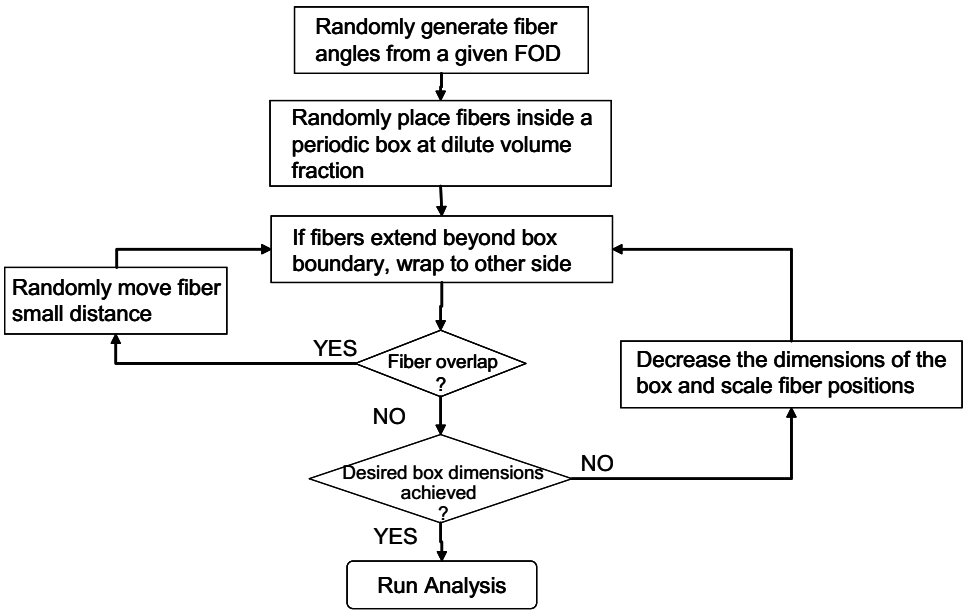

Figure 6.2: Monte Carlo algorithm

The fibers are initially placed inside a box at a very dilute volume fraction ($v_f < 0.1\%$) by randomly generating the centroid coordinates of each fiber using a uniform random number generator. A check is then performed to determine whether any of the fibers extend beyond the boundaries of the box. If a fiber does extend beyond the boundaries, a copy of the fiber is added by translating the original fiber a distance equal to the dimensions of the box. For example, if a fiber extends beyond the positive x face of the box, a copy added and placed a distance $x - l_x$ from the original fiber. If a fiber extends beyond more than one face, then multiple copies are made. This is done to ensure the box is periodic.

Next, the fibers are checked to ensure no overlap occurs. If a fiber overlaps another fiber, then the coordinates of the centroid of the fiber are randomly moved a small distance. Since the fiber has now moved it must be rechecked to determine whether it extends beyond the box boundaries and whether it overlaps any fibers. This process continues until no overlap occurs or the maximum number of iterations has been reached. If no overlap is achieved, then the box dimensions are decreased slightly,the fiber coordinates are scaled accordingly, and the process is repeated until the desired box dimensions are achieved. If the maximum number of iterations is achieved, then all the fibers are replaced inside the box at the dilute volume fraction and the entire process is repeated. This is done to ensure that an impossible fiber configuration is not obtained and to keep the algorithm constantly moving.

It was impossible to randomly place fibers without overlap for volume fractions greater than approximately 10 %. Therefore, models with larger volume fractions will possess a certain degree of overlap. As the box collapses, the volume fraction increases

because the number of fibers is held constant. In order to minimize the overlap for large volume fractions, the fibers were randomly moved to ensure no overlap up until the volume fraction inside the box exceeded 10%. Once the volume fraction exceeded 10%, the box was allowed to collapse to the desired dimensions without checking for overlap. This ensures that the fibers are spread out and in a desirable configuration before the box collapses to its final size. For a volume fraction of 30%, this method kept the overlap to less than 2%.

6.2 Results

For this analysis it is assumed the fiber distribution function is of the form [2]

$$\psi(\theta, \phi) = c\, sin^{2n}\theta cos^{2n}\phi \tag{6.8}$$

where c is a constant chosen to satisfy a normalization condition. The value of n determines the degree of fiber alignment in that as n increases, the the alignment of the fibers with the x_1 axis increases. In this example, the values for c and n are taken from Jack and Smith [2] where $n = 4$ resulting in $c = 9/4\pi$. The Monte Carlo algorithm was used to generate random angle pairs from the orientation distribution function in equation 6.8. The fibers were then placed in a periodic box and the effective stiffness was found using the uniform mesh method over a range of volume fractions. The material properties are the same as those used in the previous chapter and given in table 5.3. The aspect ratio for this example was $AR = 10$, the diameter of the fiber was $D = 10\mu m$ and the dimensions of the box were $l_x = l_y = l_z = 200\mu m$. Figure 6.3 shows a sample periodic box at a volume fraction of 5%.

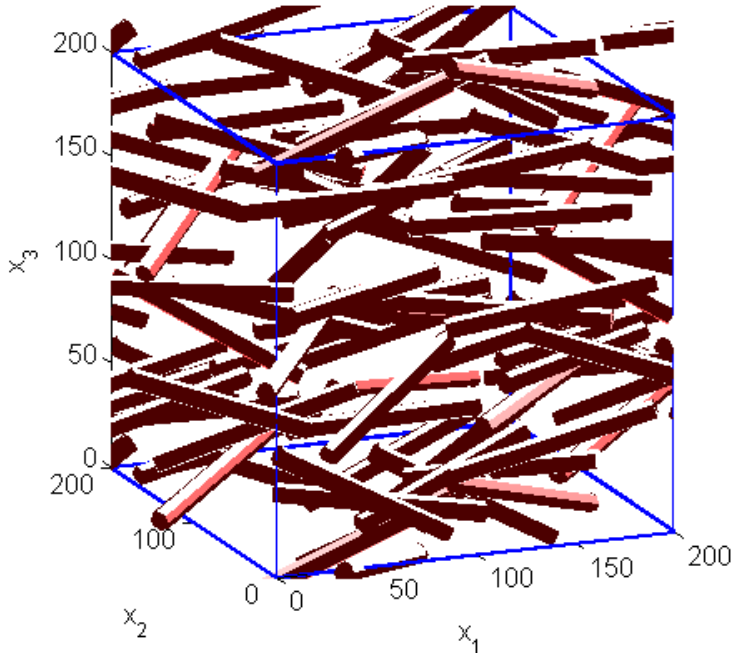

Figure 6.3: Sample periodic box with $v_f = 5\%$

Due to the random nature of the fiber placement and fiber orientation, 10 separate configurations were modeled at each volume fraction. The mean effective stiffness of the 10 configurations was found and the 95% confidence interval was calculated and presented as error bars, where the 95% confidence interval refers to the statistical reliability of the data using the given method. The mean and confidence interval are found through the following

$$[\bar{\mathbf{C}}]_{eff} = \frac{1}{N}\sum_{i=1}^{N}[\mathbf{C}]_{eff} \tag{6.9}$$

$$\left([\bar{\mathbf{C}}]_{eff} - t_{\alpha/2,N-1}\frac{\mathbf{s}}{\sqrt{N}}\right) \leq [\bar{\mathbf{C}}]_{eff} \leq \left([\bar{\mathbf{C}}]_{eff} + t_{\alpha/2,N-1}\frac{\mathbf{s}}{\sqrt{N}}\right) \tag{6.10}$$

where $t_{\alpha/2,N-1}$ is found from the student t table and the variance, s^2, is given by

$$\mathbf{s}^2 = \frac{1}{1-N}\sum_{i=1}^{N}[[C]_{eff}^{(i)} - [\bar{\mathbf{C}}]_{eff}]^2 \tag{6.11}$$

The results were compared with an orientation averaging scheme using both the Halpin-Tsai and Tandon-Weng micromechanical models for finding the unidirectional properties of the aligned aggregates. The orientation average was approximated using equation 6.9 for the angle pairs generated during the uniform mesh analysis. The mean and confidence interval of were also calculated for the orientation averages of the 10 configurations.

The composite with volume fraction $v_f = 0.10$ was modeled using 2 different element sizes and two sets of Gauss points in order to check for converge. The results are shown in table 6.1

Elastic constants	8000 *elem* 6*gp*	8000 *elem* 10*gp*	27000 *elem* 6*gp*	27000 *elem* 10*gp*	64000 *elem* 6*gp*
E_{11}/E_m	1.938	1.928	1.972	1.964	1.980
E_{22}/E_m	1.362	1.354	1.351	1.346	1.345
G_{12}/E_m	0.543	0.541	0.552	0.551	0.551
G_{23}/E_m	0.432	0.430	0.439	0.438	0.444
ν_{12}	0.363	0.364	0.369	0.369	0.373
ν_{23}	0.423	0.424	0.426	0.426	0.427

Table 6.1: Convergence analysis

The table shows that for a given number of elements there the solutions vary by less than 0.5% when using 6 and 10 Gauss points. It is also shown that the effective property results using 8000 elements and 27000 elements are within approximately 1.5% of each other. The results using 27000 elements and 64000 elements are within less than 1% and 4 of the 6 constants are within 0.5%. The calculated 95% confidence intervals are up to 1% of the mean. Therefore the results obtained using 27000 and 64000 elements are statistically indistinguishable. All of the results will be ran using

27000 elements and 6 Gauss points.

Several components of the mean effective stiffness matrix are shown in figures 6.4,6.5,6.6 and 6.7 and the mean mechanical properties are given in figures 6.8,6.9,6.10 and 6.11

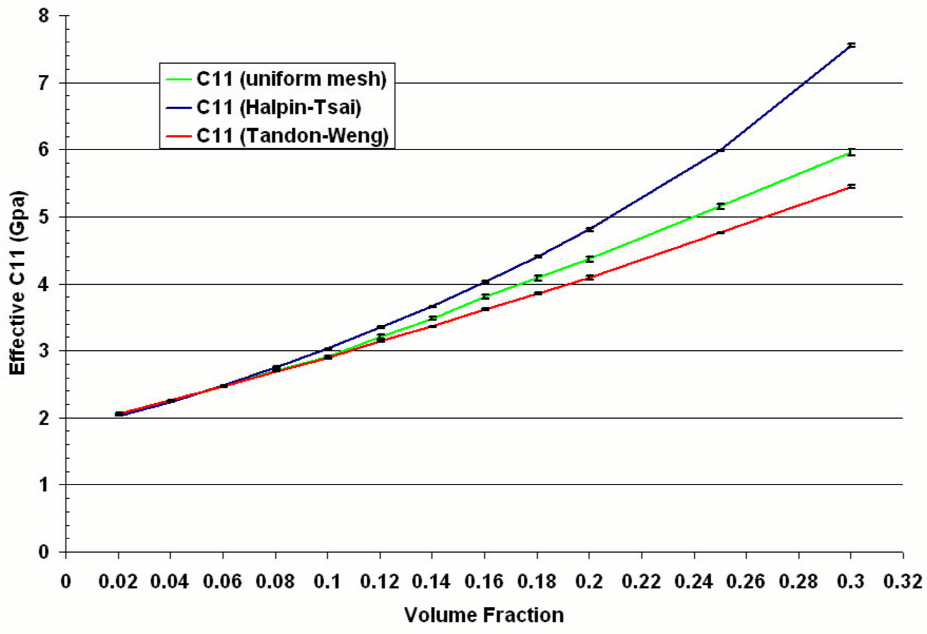

Figure 6.4: Mean C_{11} results

Figures 6.4 and 6.5 show that at low volume fractions, all of the models predict similar results for the effective stiffness components. However, as the volume fraction increases, the Halpin-Tsai model greatly overpredicts the other two models for C_{11} and C_{22}. At a volume fraction of 30%, the Halpin-Tsai result for C_{11} is approximately 39% stiffer than the Tandon-Weng result and 26% stiffer than the uniform mesh result. The Halpin-Tsai result for C_{22} is over 120% stiffer than the C_{22} results for the Tandon-Weng and uniform mesh models. The Tandon-Weng and uniform mesh results for C_{11} and C_{22} are in a good agreement over the entire range of volume fractions. At the

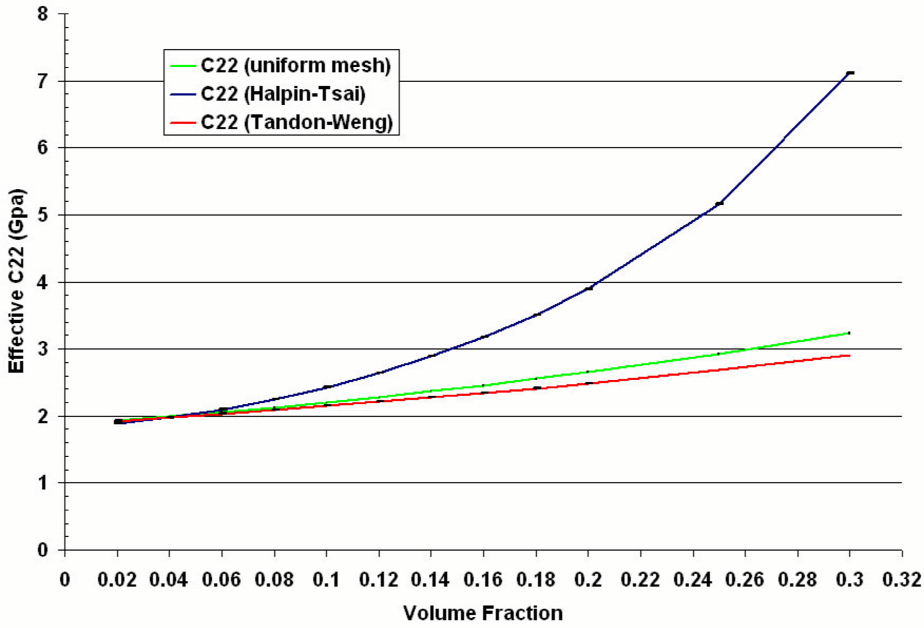

Figure 6.5: Mean C_{22} results

highest volume fraction the uniform mesh results for C_{11} and C_{22} are approximately 10% higher than the Tandon-Weng results. The large disparity in the Halpin-Tsai model is a result of its poor prediction for the transverse Poisson's ratio, ν_{23}, as shown in figure 6.11. For the transverse Poisson's ratio, the Halpin-Tsai model overpredicts the Tandon-Weng model by as much as 52% at the highest volume fraction. The uniform mesh result for ν_{23} remains with 13% of the Tandon-Weng result with the largest disparity occurring at the highest volume fraction. Both micromechanical give similar predictions for the longitudinal Poisson's ratio and Young's modulus, ν_{12} and E_{11} as shown in figures 6.10 and 6.8. The Halpin-Tsai result for E_{22} lies between the uniform mesh and Tandon-Weng results.

Tables 6.6 and 6.7 show that the Halpin-Tsai and Tandon-Weng models provide similar predictions for C_{44} and C_{55} over the entire range of volume fractions. These

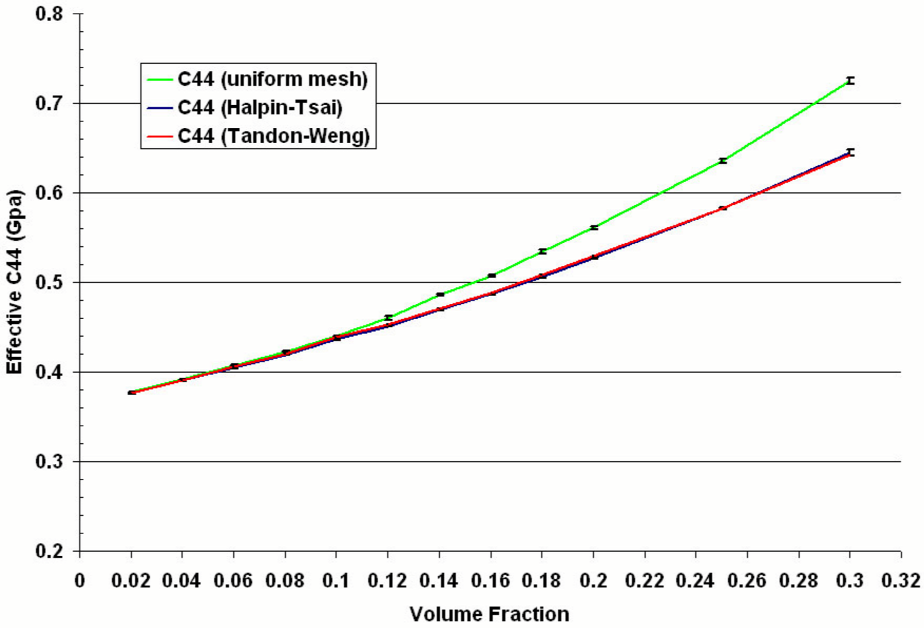

Figure 6.6: Mean C_{44} results

models give predictions for C_{44} slightly below those of the uniform mesh method at higher volume fractions with a maximum disparity of approximately 6%. The uniform mesh result for C_{55} is up to 15% stiffer than the micromechanical models. This is a result of the uniform mesh method's overprediction of the longitudinal modulus as discussed in the previous chapters.

The increasing disparity between the uniform mesh results and the orientation averaging results at higher volume fractions is a result of the basic assumptions inherent in the orientation averaging procedure. The orientation averaging assumes there is no interaction between fibers and only accounts for the fiber orientation. Therefore, the fiber separation and spatial arrangement are not accounted for. These factors are accounted for in the uniform mesh method. As the volume fraction increases the fiber interaction becomes increasingly important and a disparity between the two methods

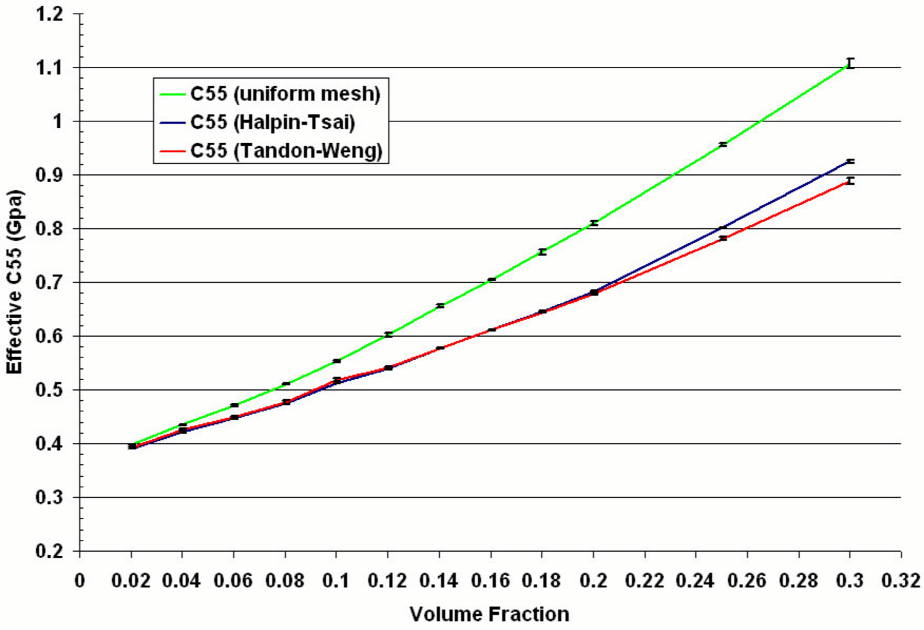

Figure 6.7: Mean C_{55} results

occurs.

The confidence intervals, shown as error bars in the figures, tend to increase with increasing volume fraction. Overall, the confidence intervals are very small since so many fibers were used in the model. There is also a slight jump in the confidence intervals for volume fractions greater than 12% due to the possibility of fiber overlap. However, even at the highest volume fraction, the confidence intervals are still within a few percent of the mean. Fiber overlap does not have a large effect on the effective properties in that the results appear to follow the same trend over the entire range of volume fractions. The transverse Poisson's ratio ν_{23} does peak around $10 - 12\%$ and then decrease but similar a trend is predicted by the Tandon-Weng model. This trend in the transverse Poisson's ratio over a range of volume fractions has also been noted in literature [11, 34].

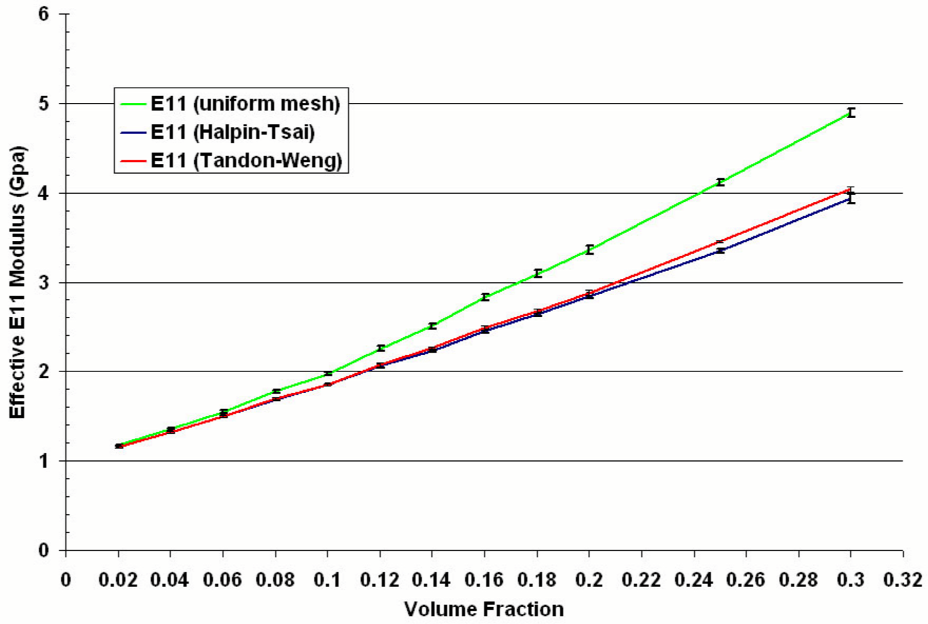

Figure 6.8: Mean E_{11} results

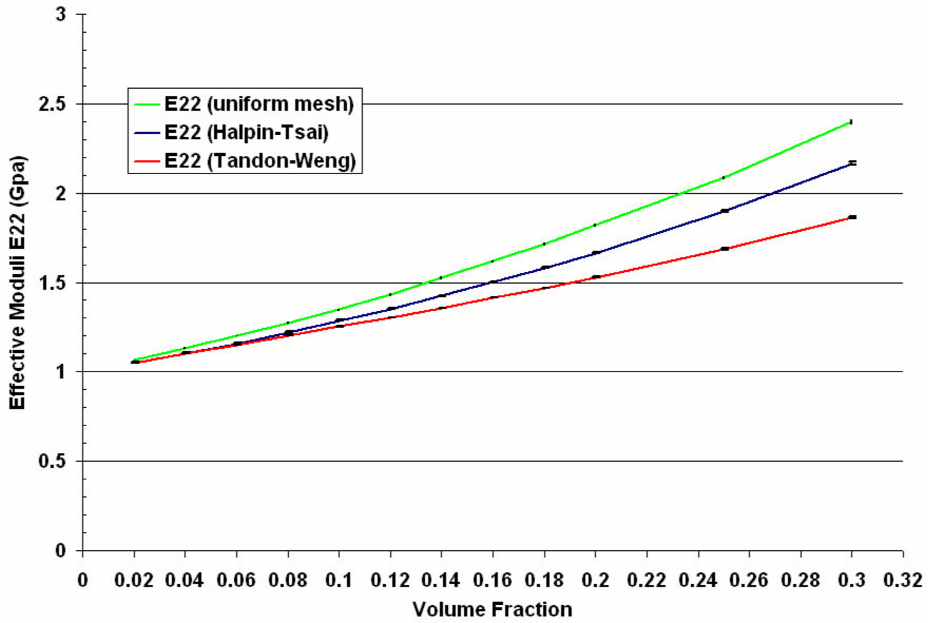

Figure 6.9: Mean E_{22} results

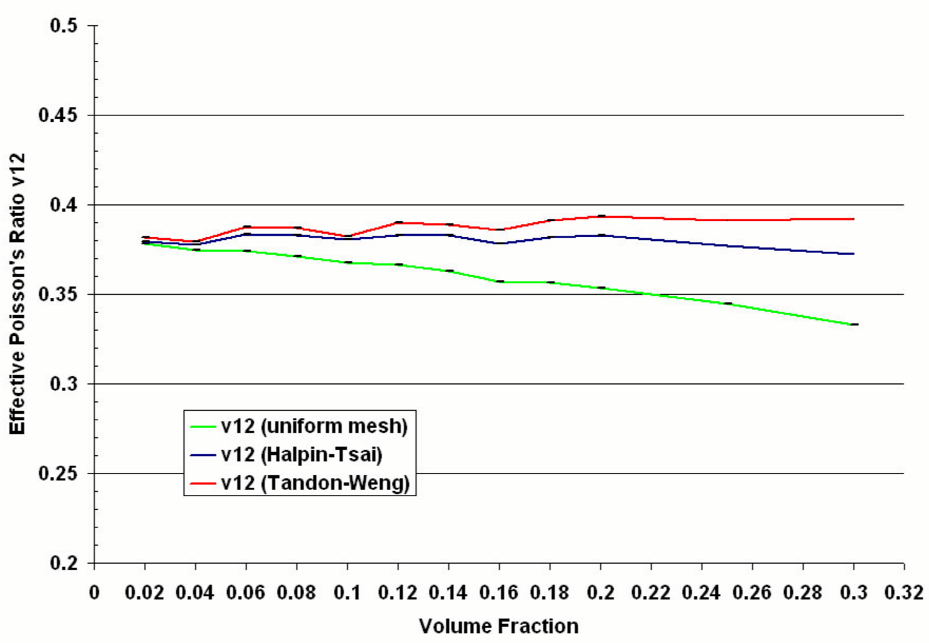

Figure 6.10: Mean ν_{12} results

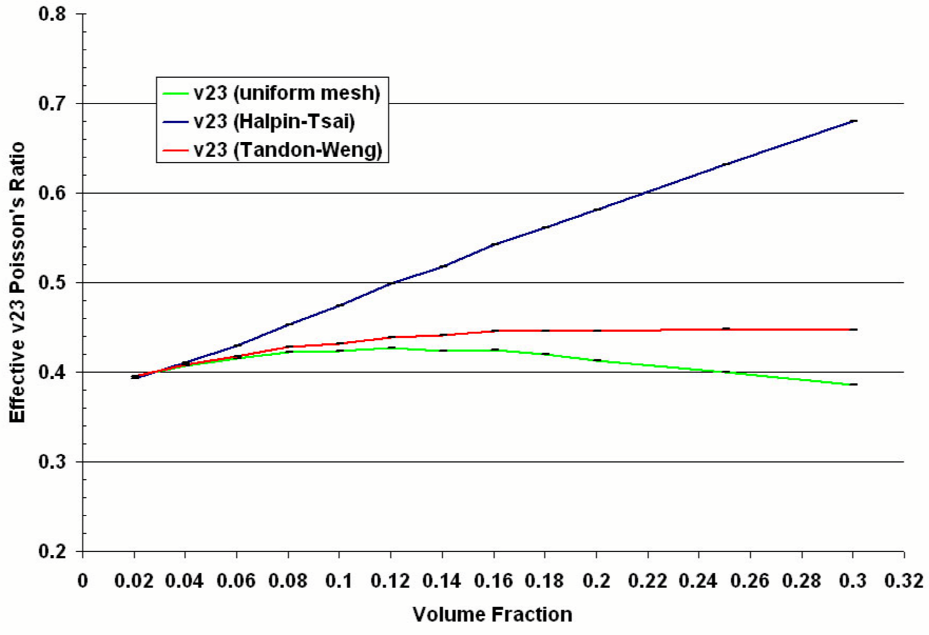

Figure 6.11: Mean ν_{23} results

CHAPTER 7

CONCLUSIONS AND RECOMMENDATIONS

The effective properties of composite materials are highly are dependent upon many different factors and highly variable. Therefore, developing cost effective, yet reliable, methods for determining the effective properties of composite materials remains an active area of research. Numerous analytical and empirical micromechanical models have been developed over the years, but they all make many assumptions about the microstructure of the composite and are therefore limited in their application. Numerical methods, such as finite elements and boundary elements, have seen increased composite modeling due to their flexibility in solving very complex problems. However, numerical models require that a high quality mesh be obtained over all the constituents in order provide accurate results. This remains a very difficult and time intensive task and after a quality mesh is obtained, the user must have sufficient computer memory in order to solve the problem.

A uniform mesh finite element method was developed in order to greatly simplify the meshing procedure and reduce the degrees of freedom of the model, thus reduce the computer memory requirements. The main difference between the uniform mesh method and conventional finite elements is that uniform mesh elements can contain more than one material. A correction factor was developed in order to account for the differences in the strain in the two materials within a single element. A single uniform mesh element was compared with two conventional finite elements and it was shown that with the addition of the correction factor, the uniform mesh element

could accurately predict all of the elastic constants except the transverse shear moduli. Although the inclusion of the correction factor decreased the error for the longitudinal shear moduli, the uniform mesh element provides a stiffer result than that of the conventional elements.

The uniform mesh element was then compared with a continuous and single fiber models from literature. The results of the uniform mesh method were in close agreement with the literature. The uniform mesh method was then used to predict the elastic constants of a composite with a given orientation distribution and the results were compared with an orientation averaging scheme using both the Halpin-Tsai and Tandon-Weng models over a range of volume fractions. A Monte-Carlo algorithm was written to provide random fiber angle pairs sampled from the fiber orientation distribution. The fibers were then randomly placed inside a periodic box. Up to a volume fraction of 10%, the fibers were placed such that no overlap occured. At volume fractions above 10%, a certain degree of overlap was unavoidable. It was found that all three methods provided similar results for the stiffness components at low volume fractions. However, the Halpin-Tsai was much stiffer than the uniform mesh and Tandon-Weng models at higher volume fractions. This was due to the Halpin-Tsai's poor predictions for the transverse Poisson's ratio. The uniform mesh and Tandon-Weng results were within 10% over the entire range of volume fractions. The disparity in the two models is most likely a result of the inability of the orientation averaging procedure to account for fiber interactions which become increasing important at higher volume fractions.

The following recommendations are made for future work:

- The correction factor needs to be adjusted in order to increase the accuracy of the longitudinal shear moduli prediction.

- A more efficient packing algorithm needs to be developed in order to obtain higher volume fractions without fiber overlap.

- Image analysis needs to be performed on a composite sample in order to experimentally determine the fiber orientation and length distributions. This information could then be used to seed the Monte Carlo algorithm in order to obtain a realistic uniform mesh model. The effective elastic constants of the uniform mesh model could then be compared with the experimentally obtained elastic constants

- The uniform mesh method needs to be adapted model to textile composites. Currently, the only two fibers angles are required for each fiber and all fibers are assumed to have the same length. For woven composites, a similar approach could be taken, in that only the orientations of the individual fiber tows would need to be specified and the fiber tows could be assumed infinite in length. However, for knitted fabric composites, both the orientation and curvature of the individual fiber tows would need to be specified. Since the curvature is not constant, the fiber tows would need to be divided into segments, and each segment would be defined by a separate curvature and orientation. These values would then be used to determine whether each Gauss point lies within a fiber tow or matrix.

- The elemental stiffness matrix calculations also need to be modified to incorporate fiber tows and fibers that are non-isotropic. This would involve rotating the local material stiffness matrix to the global coordinate system at Gauss points that lie within the non-isotropic fibers or fiber tows.

BIBLIOGRAPHY

[1] Sun, C.T. and R.S. Vaidya. Prediction of Composite Properties from a Representative Volume Element. *Composites Science and Technology*, 56:171–179, 1996.

[2] Jack, D.A. and D.E. Smith. Elastic Properties of Short-Fiber Polymer Composites, Derivation and Demonstration of Analytical Forms for Expectation and Variance from Orientation Tensors. *Journal of Composite Materials*, accepted, 2007.

[3] Advani, S.G. and E.M. Sozer. *Process Modeling in Composites Manufacturing*. Marcel Dekker, Inc., New York, NY, 2003.

[4] Tucker III, C.L. and E. Liang. Stiffness predictions for unidirectional short-fiber composites: Review and evaluation . *Composites Science and Technology*, 59:655–671, 1999.

[5] Halpin, J.C. and J.L. Kardos. The Halpin-Tsai Equations: A Review. *Polymer Engineering and Science*, 16(5):344–352, May 1976.

[6] Hill, R. Theory of Mechanical Properties of Fibre-Strengthened Materials: I Elastic Behavior. *J. Mech. Phys. Solids*, 4:280–282.

[7] Hermans, J.J. The elastic properties of fiber reinforced materials when the fibers are aligned. *Proc. Koninkl. Nederl. Akademie Van Wetenschappen-Amsterdam B*, 65:1–9.

[8] Hewitt, R.L. and M.C. de Malherbe. An Approximation for the Longitudinal Shear Modulus of Continuous Fibre Composites. *Journal of Composite Materials*, 59:655–671, 1999.

[9] Lewis, T.B. and L.E. Nielson. Dynamic Mechanical Properties of Particulate-Filled Composites. *Journal of Applied Polymer Science*, 14:1449–1471.

[10] Ingber, M.S. and T.D. Papathanasiou. A Parallel-Supercomputing Investigation of the Stiffness of Aligned, Short-Fiber Reinforced Composites Using the Boundary Element Method. *International Journal for Numerical Methods in Engineering*, 40:3477–3491, 1997.

[11] Gusev, A.A., P.J. Hine, and I.M. Ward. Fiber packig and elastic properties of a transversely random unidirectional glass/epoxy composite. *Composites Science and Technology*, 60:535–541, 2000.

[12] K Mori, T Tanaka. Average stress in matrix and average elastic energy of materials with misfitting inclusions. *Acta Metallurgica*, 21:571–574.

[13] Eshelby, J.D. The determination of the elastic field of an ellipsoidal inclusion, and related problems. *Proc. Roy. Soc. London A*, 241:376–396.

[14] Tandon, G.P. and G.J. Weng. The Effect of Aspect Ratio of Inclusions on the Elastic Properties of Unidirectionally Aligned Composites. *Polymer Composites*, 5(4):327–333, October 1984.

[15] Lusti, R.H., P.J. Hine, and A.A. Gusev. Direct numerical predictions for the elastic and thermoelastic properties of short fiber composites. *Composites Science and Technology*, 62:1927–1934, 2002.

[16] Gusev, A.A., H.R. Lusti, and P.J. Hine. Stiffness and Thermal Expansion of Short Fiber Composites with Fully Aligned Fibers. *Advanced Engineering Materials*, 4(12):927–930, 2002.

[17] Hashin, Z. and S. Shtrikman. A Variational Approach to the Theory of The Elastic Behavior of Muliphase Materials. *J. Mech. Phys. Solids*, 11:127–140.

[18] Willis, J.R. Counds and Self-consistent Estimates for the Overall Properties of Anisotropic Composites. *J. Mech. Phys. Solids*, 25:185–202.

[19] Lielens, G., P. Pirotte, A. Couniot, F. Dupret, and R. Keunings. Prediction of thermo-mechanical properties for compression moulded composites. *Composites Part A*, 29A:63–70, 1998.

[20] Advani, S.G. and C.L. Tucker III. The Use of Tensors to Describe and Predict Fiber Orientation in Short Fiber Composites. *J. Rheology* , 31:751, 1987.

[21] Ward, I.M. Optical and Mechanical Anisotropy in Crystalline Polymers. *Proc. Phys. Soc.*, 80:1176–1188, 1962.

[22] Camacho, C.W. and C.L. Tucker III. Stiffness and Thermal Expansion Predictions for Hybrid Short Fiber Composites. *Polymer Composites*, 11(4):229–239, 1990.

[23] Hine, P.J., H.R. Lusti, and A.A. Gusev. On the possiblity of reduced variable predictions for the thermoelastic properties of short fiber composites. *Composites Science and Technology*, 64:1081–1088, 2004.

[24] Naik, R.A. Failure Analysis of Woven and Braided Fabric Reinfored Composites. *Journal of Composite Materials*, 29(23):2334–2363, 1995.

[25] J. Vandeurzen, P.and Ivens and I. Verpoest. A Three-Dimensional Micromechanical Analysis of Woven-Fabric Composites: II. Elastic Analysis. *Composites Science and Technology*, 56:1317–1327, 1996.

[26] Gommers, B., I. Verpoest, and P. Van Houtte. The Mori-Tanaka Method Applied to Textile Composite Materials. *Acta Metallurgica*, 46(6):2223–2235, 1998.

[27] Gommers, B., I. Verpoest, and P. Van Houtte. Modelling the elastic properties of Knitted-fabric-reinforced composites. *Composites Science and Technology*, 56:685–694, 1996.

[28] Huysmans, G., I. Verpoest, and P. Van Houtte. A Poly-Inclusion Approach for the Elastic Modelling of Knitted Fabric Composites. *Acta Metallurgica*, 46(9):3003–3013, 1998.

[29] Xia, Z., Y. Zhang, and F. Ellyin. A unified periodical boundary conditions for representative volume elements of composites and applications. *Polymer Engineering and Science*, 40(8):1907–1921, April 2003.

[30] Li, S. On the Unit Cell for Micromechanical Analysis of Fibre-Reinforced Composites. *Proc. Roy. Soc. London A*, 455(1983), 1999.

[31] Drugan, W.J. and J.R. Willis. A Micromechanics-Based Nonlocal Constituative Equation and Estimates of Representative Volume Elements Size for Elastic Composites. *J. Mech. Phys. Solids*, 44(4):497–524, 1996.

[32] Gusev, A.A. A Fast Boundary Element Method for the Analysis of Fiber-Reinforced Composites Based on a Rigid-Inclusion Model. *J. Mech. Phys. Solids*, 45(9):1449–1459, 1997.

[33] Gusev, A.A. Numerical Identification of the Potential of Whisker and Platelet-Filled Polymers. *Macromolecules*, 34:3081–3093, 2001.

[34] Hine, P.J., H.R. Lusti, and A.A. Gusev. Numerical simulation of the effects of volume fraction, aspect ratio and fiber length distribution on the elastic and thermoelastic properties of short fiber composites. *Composites Science and Technology*, 62:1445–1453, 2002.

[35] Michel, J.C., H. Moulinec, and P. Suquet. Effective properties of composite materials with periodic microstructure: a computational approach. *Comput. Methods Appl. Engr.*, 172(1999), 1999.

[36] Jiang, M., K. Alzebdeh, I. Jasiuk, and M. Ostoja-Starzewski. Scale and boundary ocnditions effects in elastic properties of random composites. *Acta Mechanica*, 148:63–78, 2001.

[37] Gusev, A.A., M. Heggli, H.R. Lusti, and P.J. Hine. Orientation Averaging for Stiffness and Thermal Expansion of Short Fiber Composites. *Advanced Engineering Materials*, 4(12):931–933, 2002.

[38] Lusti, H.R. and A.A. Gusev. Finite element predictions for the thermoelastic properties of nanotube reinforced polymers. *Modelling and simulation in materials science and engineering*, 12:S107–S119, 2004.

[39] G. Lomov, S.V.and Huysmans, Y. Luo, R.S. Parnas, A. Prodromou, I. Verpoest, and F.R. Phelan. Textile composites: modelling strategies. *Composite: Part A*, 32:1379–1394, 2001.

[40] S. Whitcomb, J.and Kanthikannan and C. Shapman. Evaluation of homogenization for global/local stress analysis of textile composites. *Composite Structures*, 31:137–149, 1995.

[41] J. Kanthikannan, S.and Whitcomb and C. Shapman. Model technique for three-dimensional global/local stress analysis of plain weave composites. *Composite Structures*, 39:145–156, 1997.

[42] Xu, J., B.N. Cox, M.A. McGlockton, and W.C. Carter. A Binary Model of Textile Composites-II. The Elastic Regime. *Acta Metallurgica Mater.*, 43:3511–3524, 1995.

[43] W. Zeng, T.and Lin-zhi and G. Li-cheng. Mechanical analysis of 3D braided composites: a finite element model. *Composite Structures*, 64:399–404, 2004.

[44] Takano, N., Y. Uetsuji, Y. Kashiwagi, and Z. Masaru. Hierarchical modelling of textile composite materials and structures by the homogenization method. *Modlling Simul. Mater. Sci. Eng.*, 7:207–231, 1999.

[45] Peng, X. and J. Cao. A dual homogenization and finite element approach for material characterization of textile composites. *Composites: Part B*, 33:45–56, 2002.

[46] Papathanasiou, T.D. Stiffness Enhancement in Aligned, Short-Fiber Composites: A Computational and Experimental Investigation. *Composites Science and Technology*, 54:1–9, 1995.

[47] Papathanasiou:94, M.S. Inger, L.A. Mondy, and A.L. Graham. The Effective Elastic Modulus of Fiber-Reinforced Composites. *Journal of Composite Materials*, 28(4):289–303, 1994.

[48] Nashimura, N. Fast multipole accelerated boundary integral equation methods. *Appl. Mech. Rev.*, 55(4):299–324, 2002.

[49] Liu Y.J., Nishimura N, Otani Y, Takahashi T, Chen XL, and Munakata H. An advanced 3D boundary element method for characterizations of composite materials. *ASME J. Appl. Mech.*, 72:115–128, 2005.

[50] Chen X.L. and Y.J. Liu. An advanced 3D boundary element method for characterizations of composite materials. *Engineering Analysis with Boundary Elements*, 29:513–523, 2005.

[51] Rao, S.S. *The Finite Element Method in Engineering.* Elsevier Butterworth-Heinemann, Burlington, MA, 2005.

[52] Gosz, M.R. *Finite Element Method: Aplications in Solids, Structures, and Heat Transfre.* CRC Press, 2006.

[53] Nemat-Nassar, S. and M. Hori. *Micromechanics: Overall Properteis of Heterogeneous Materials*. Elsavier, 1999.

[54] Hollister, S.J. and N. Kikuchi. A comparison of homogenization and standard mechanics analyses for periodic porous composites. *Computational Mechanics*, 10:73–95, 1992.

[55] Aboudi, J. *Mechanics of Composite Materials: A Unified Micromechanical Approach*. Elsavier, 1991.

[56] D.S. Cook, R.D.and Malkus and R.J. Plesha, M.E. adn Witt. *Concepts and Applications of Finite Element Analysis*. John Wiley & Sons Inc., 2002.

[57] Jones, R.M. *Mechanics of Composite Materials*. Taylor & Francis, Inc., 1999.